2
Polymer-based and Polymer-filled Nanocomposites

Linda S. Schadler

2.1
Introduction

Polymer composites are important commercial materials with applications that include filled elastomers for damping, electrical insulators, thermal conductors, and high-performance composites for use in aircraft. Materials with synergistic properties are chosen to create composites with tailored properties; for example, high-modulus but brittle carbon fibers are added to low-modulus polymers to create a stiff, lightweight composite with some degree of toughness. In recent years, however, we have reached the limits of optimizing composite properties of traditional micrometer-scale composite fillers, because the properties achieved usually involve compromises. Stiffness is traded for toughness, or toughness is obtained at the cost of optical clarity. In addition, macroscopic defects due to regions of high or low volume fraction of filler often lead to breakdown or failure.

Recently, a large window of opportunity has opened to overcome the limitations of traditional micrometer-scale polymer composites – nanoscale filled polymer composites – in which the filler is <100 nm in at least one dimension (Figure 2.1). Although some nanofilled composites (carbon black [1] and fumed silica [2, 3] filled polymers) have been used for more than a century, research and development of nanofilled poly-

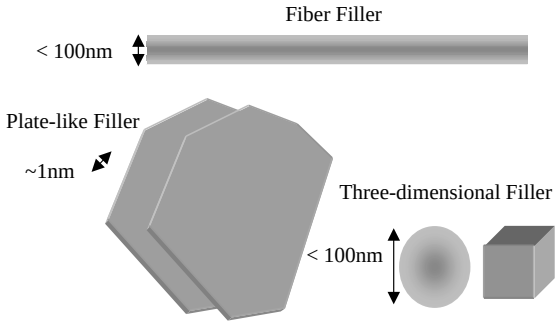

Fig. 2.1 Schematic of nanoscale fillers

Nanocomposite Science and Technology. Edited by P.M. Ajayan, L.S. Schadler, P.V. Braun

ISBN: 3-527-30359-6

mers has greatly increased in recent years, for several reasons. First, unprecedented combinations of properties have been observed in some polymer nanocomposites [4]. For example, the inclusion of equi-axed nanoparticles in thermoplastics, and particularly in semicrystalline thermoplastics, increases the yield stress, the tensile strength, and Young's modulus [5] compared to pure polymer. A volume fraction of only 0.04 mica-type silicates (MTS) in epoxy increases the modulus below the glass transition temperature by 58% and the modulus in the rubbery region by 450% [6]. In addition [7], the permeability of water in poly(e-caprolactone) decreases by an order of magnitude with the addition of 4.8% silicate by volume. Yano et al. [8] showed a 50% decrease in the permeability of polyimides at a 2% loading of MTS. Many of these nanocomposites are optically transparent and/or optically active.

A second reason for the large increase in research and development efforts was the 'discovery' of carbon nanotubes in the early 1990s [9]. Although more careful review has shown that nanotubes have been observed since the 1960s [10], it was only in the mid-1990s that they were made in the quantities required for property evaluation of composites. The properties of these carbon nanotubes, particularly strength and electrical properties, are significantly different from those of graphite and offer exciting possibilities for new composite materials.

Third, significant development in the chemical processing of nanoparticles and in the in situ processing of nanocomposites has led to unprecedented control over the morphology of such composites. It has also created an almost unlimited ability to control the interface between the matrix and the filler.

Thus, this is an exciting time to study nanocomposites, because of the unique combinations of properties that are achievable and because of the high potential for successful commercial development. Although the technical community has made advances in the processing of nanocomposites, we are just beginning to assemble the interdisciplinary teams required to understand, tailor, and optimize properties. We have at our fingertips, however, the ability to change the size, shape, volume fraction, interface, and degree of dispersion or aggregation. Thus, the opportunities may well become limitless when theory and experiment have assembled enough information to guide further development.

A relevant question addressed throughout this chapter is: What is unique to nanofillers compared to micrometer-scale traditional fillers, and how do the composites compare to their macroscopic counterparts? The most obvious difference is the small size of the fillers. For example, very small nanoparticles do not scatter light significantly, and thus it is possible to make composites with altered electrical or mechanical properties that retain their optical clarity. In addition, the small size means that the particles do not create large stress concentrations and thus do not compromise the ductility of the polymer. A similar concept applies for electrical breakdown strength.

The small size of nanofillers can also lead to unique properties of the particles themselves. For example, single-walled nanotubes are essentially molecules, free from defects, and have a modulus as high as 1 TPa and strengths that may be as high as 500 GPa. Single-crystal particles that are optically active, but are unmanageable on the macro scale can be combined in a polymer to achieve the optical gain of the material and the ease of processing afforded by the polymer.

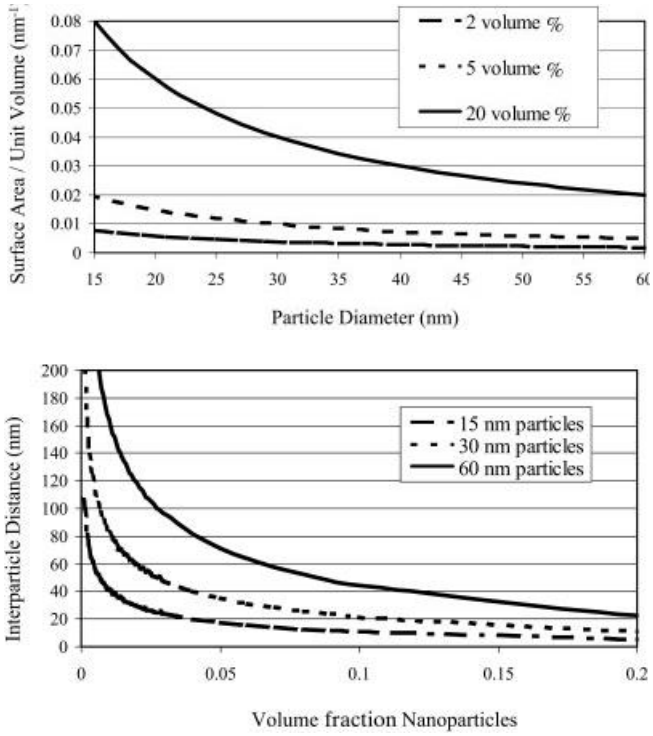

Fig. 2.2 (a) Surface area per unit volume vs. particle size for spherical particles that are ideally dispersed, and (b) interparticle distance for spherical particles that are ideally dispersed (Thanks to B.J. Ash for preparation of this figure)

In addition to the effect of size on particle properties, the small size of the fillers leads to an exceptionally large interfacial area in the composites. Figure 2.2a shows the surface area per unit volume as a function of particle size for spherical particles that are ideally dispersed. The increase in surface area below 100 nm is dramatic. The interface controls the degree of interaction between the filler and the polymer and thus controls the properties. Therefore, the greatest challenge in developing polymer nanocomposites may be learning to control the interface. Thus, it seems relevant to define the interfacial region and discuss its properties.

As defined in traditional composites, the interfacial region is the region beginning at the point in the fiber at which the properties differ from those of the bulk filler and ending at the point in the matrix at which the properties become equal to those of the bulk matrix [11]. It can be a region of altered chemistry, altered polymer chain mobility, altered degree of cure, and altered crystallinity. Interface size has been reported to be as small as 2 nm and as large as about 50 nm. Figure 2.2b shows interparticle spacing as a function of particle size for an ideally dispersed nanoparticle composite: at low volume fractions the entire matrix is essentially part of the interfacial region. For example, for 15-nm particles at a filler loading of 10 vol %, the interparticle spacing is

only 10 nm. Even if the interfacial region is only a few nanometers, very quickly the entire polymer matrix has a different behavior than the bulk. If the interfacial region is more extended, then the polymer matrix behavior can be altered at much smaller loadings. Therefore, by controlling the degree of interaction between the polymer and the nanofiller, the properties of the entire matrix can be controlled.

To implement the novel properties of nanocomposites, processing methods that lead to controlled particle size distribution, dispersion, and interfacial interactions are critical. Processing technologies for nanocomposites are different from those for composites with micrometer-scale fillers, and new developments in nanocomposite processing are among the reasons for their recent success.

This chapter highlights what we feel are important concepts for understanding and developing polymer nanocomposites. We start with a description of nanotube or nanofiber fillers, plate-like fillers, and equi-axed fillers. We then introduce the interfacial region and attempt to give a broad understanding of how to control it, without delving too deeply into the chemistry involved. This is followed by a section on the processing of composites. Finally, we describe some of the properties that have been achieved in nanofilled polymer composites.

2.2 Nanoscale Fillers

Nanoscale fillers come in many shapes and sizes. For ease of discussion, we have grouped nanofillers into three categories (Figure 2.1). Fiber or tube fillers have a diameter $<$100 nm and an aspect ratio of at least 100. The aspect ratios can be as high as 10^6 (carbon nanotubes). Plate-like nanofillers (Figure 2.1) are layered materials typically with a thickness on the order of 1 nm, but with an aspect ratio in the other two dimensions of at least 25. Three dimensional (3D) nanofillers are relatively equi-axed particles $<$100 nm in their largest dimension. This is a convenient way to discuss polymer nanocomposites, because the processing methods used and the properties achieved depend strongly on the geometry of the fillers.

2.2.1 Nanofiber or Nanotube Fillers

2.2.1.1 Carbon Nanotubes

Micrometer-size carbon tubes, which are similar in structure (but not in dimensions) to the recently discovered multi-walled carbon nanotubes, were first found in 1960 by Roger Bacon [12]. These nanosized, near-perfect whiskers (termed nanotubes) were first noticed and fully characterized in 1991 by Sumio Iijima [9] of NEC Corporation in Japan. He was investigating the surface of carbon electrodes used in an electric arc-discharge apparatus that had been used to make fullerenes. Several exciting developments have taken place in this field since then, and several books document recent progress [13].

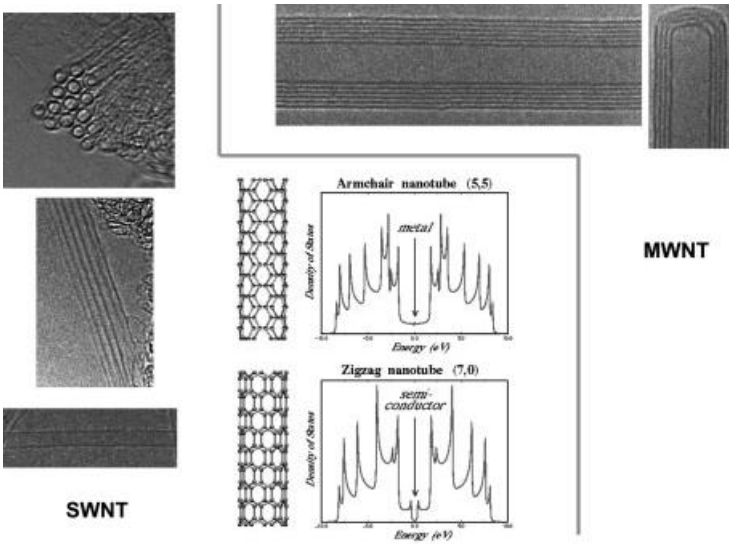

Fig. 2.3 (a) HRTEM image showing the SWNT in bundles, (b) HRTEM images of a MWNT along its length and at the end, (c) schematic showing two examples of the helicity that occurs, zigzag and armchair

The first nanotubes observed were multi-walled nanotubes (MWNT). MWNTs consist of two or more concentric cylindrical shells of graphene sheets coaxially arranged around a central hollow core with interlayer separation as in graphite (0.34 nm) [14]. In contrast, single-shell or single-walled nanotubes [15, 16] (SWNT) are made of single graphene (one layer of graphite) cylinders and have a very narrow size distribution (1 – 2 nm). Often many (tens) single-shell nanotubes pack into larger ropes. Figure 2.3 shows electron micrographs of SWNT and MWNT. Both types of nanotubes have the physical characteristics of solids and are microcrystals, although their diameters are close to molecular dimensions. In nanotubes, the hexagonal symmetry of the carbon atoms in planar graphene sheets is distorted, because the lattice is curved and must match along the edges (with dangling bonds) to make perfect cylinders. This leads to a helical arrangement of carbon atoms in the nanotube shells. Depending on the helicity and dimensions of the tubes, the electronic structure changes considerably [17, 18]. Hence, although graphite is a semi-metal, carbon nanotubes can be either metallic or semiconducting. Nanotubes are closed by fullerene-like end caps that contain topological defects (pentagons in a hexagonal lattice). The electronic character of the ends of these tubes differs from the cylindrical parts of the tubes and is more metallic, due to the presence of defects in these regions [19].

The discovery of nanotubes has complemented the excitement and activities associated with fullerenes [20]. Although fullerenes have fascinating physical properties, their relevance in the nanocomposite field is limited, so we shall restrict our discussion of carbon nanostructures to nanotubes.

Tab. 2.1 Theoretical and experimentally measured properties of carbon nanotubes.

Property	Nanotubes	Graphite
Lattice structure	(Cylindrical) hexagonal lattice helicity Nanotubes: ropes, tubes arranged in triangular lattice with lattice parameters of a = 1.7 nm, tube–tube distance = 0.315	Planar hexagonal, plane-to-plane distance c = 0.335
Specific gravity	0.8–1.8 g cc^{-1} (theoretical)	2.26 g cc^{-1}
Elastic modulus	~1 TPa for SWNT ~0.3–1 TPa for MWNT	1 Tpa (in-plane)
Strength	50–500 GPa for SWNT, 10–60 GPa for MWNT	
Resistivity	~5–50 micro-ohm-cm	50 (in-plane)
Thermal conductivity	3000 W $m^{-1}K^{-1}$ (theoretical)	3000 W $m^{-1}K^{-1}$ (in-plane) 6 W $m^{-1}K^{-1}$ (c axis)
Thermal expansion	Negligible (theoretical)	-1×10^{-6} K^{-1} (in-plane) 29×10^{-6} K^{-1} (c axis)
Oxidation in air	>700 °C	450–650 °C

The properties of carbon nanotubes are unique compared to other graphite fibers. Their structure remains distinctly different from that of traditional carbon fibers [21], which have been used industrially for several decades (e.g., as reinforcements in tennis rackets, airplane body parts, and batteries). Nanotubes represent the ideal, most perfect, ordered carbon fiber, the structure of which is entirely known at the atomic level. Table 2.1 shows measured and theoretical properties of both SWNT and MWNT. A nice review of the mechanics of nanotubes was recently published [22]. The mechanical properties reported in Table 2.1 were determined directly on nanotubes by using various methods of loading with an AFM. Salvetat et al. [23] were able to place SWNT ropes across a silicon bridge and bend them using an AFM tip. They found that the modulus decreased dramatically as the size of the bundle increased (Figure 2.4). Walters et al. [24] did a similar study and measured the complete stress–strain curve. The modulus of an SWNT rope, which, at this point for composites, is the relevant form of SWNT, was low at small strains and increased at higher strains. As further support of this, Wood et al. [25] found similar results with a more indirect measurement of the stress–strain curve. Because individual SWNTs are theorized to have a modulus as high as 1 TPa, this low modulus of larger ropes at low strains implies that slippage occurs between the individual nanotubes within the rope. The mechanics of this are not clear, but may be similar to that of rope mechanics [26]. If so, individual strands can slip until they are tightly packed, and then there is large friction between them; only then is the modulus of the individual fibers evident. When SWNT ropes were pulled directly by two AFM tips [27], a realistic modulus for the individual tubes within the bundle was achieved only if the SWNT in contact with the tips were

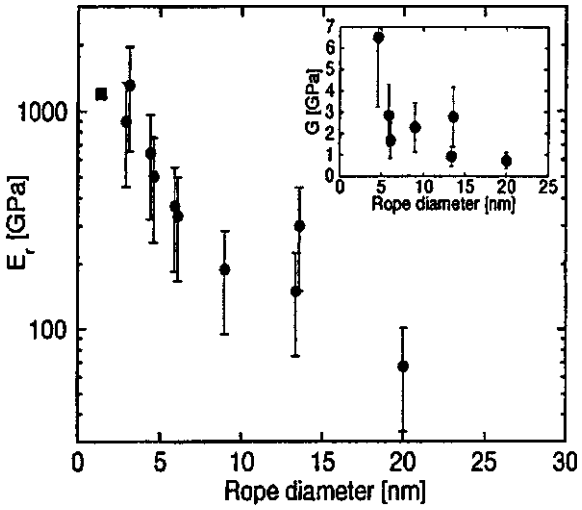

Fig. 2.4 A plot of modulus vs. SWNT rope diameter showing the decrease in the modulus of SWNT ropes as a function of rope diameter. This highlights the poor load transfer between the SWNT within the rope and the need for separating SWNT from the ropes for use in composites. Reprinted with permission from [23] copyright 1999, American Phyiscal Society

counted as the cross sectional area. If the whole rope was used to determine the cross sectional area, the modulus was much lower. The important implication of this finding is that the modulus of SWNT can be realized only when the SWNT are isolated from

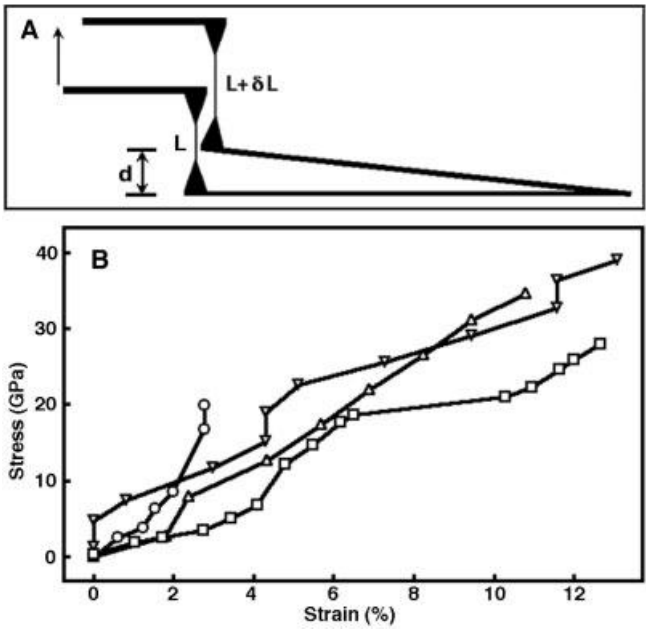

Fig. 2.5 Stress vs. strain curves for MWNT. The variation in the curves is partially a function of the difference in MWNT diameter. Reprinted with permission from [28]

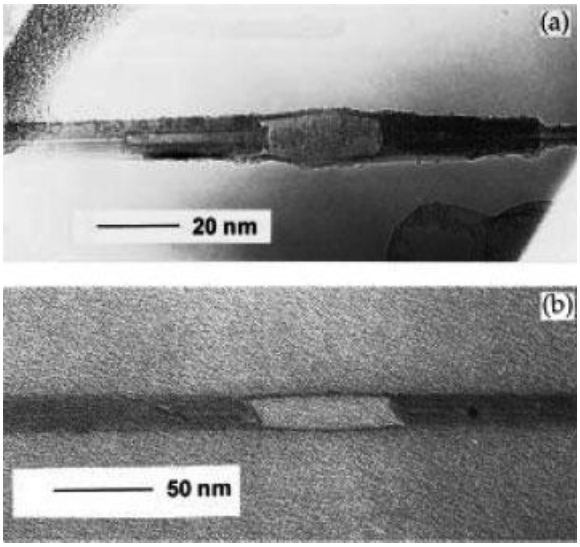

Fig. 2.6 Transmission electron micrographs showing the telescopic failure that can occur in MWNT. Reprinted with permission from [29] copyright 1998, American Institute of Physics

the bundles and/or the bundles are small enough that matrix is in contact with each one.

The most direct measurement of the mechanical properties of MWNT was conducted by Yu et al. [28] using two AFM tips (Figure 2.5). They found a range of modulus and strength. The range in modulus may again be due to difficulty in determining the cross sectional area. Failure occurred via a sword-and-sheath mechanism (telescoping) first observed by Wagner et al. [29] (Figure 2.6), implying that only the outermost nanotube is carrying the load and the rest are slipping inside. Therefore, a smaller cross sectional area may be required for appropriate calculations of the modulus. Thus, the variability in the number of layers in an MWNT probably accounts for the broad scatter in the modulus (Table 2.1). The important implication of this in composites, however, is that MWNT do not have the high modulus that is achievable with isolated SWNT. MWNT do have reversible deformation in compression, which may prove useful. Bower et al. [30] showed that MWNTs buckle under a compressive strain of about 4.7 % and that this buckling is reversible under very large strains, probably due to the ability of the nanotubes to slide within each other.

The fracture and deformation behavior of nanotubes is intriguing. Simulations have shown that highly deformed nanotubes switch reversibly into different morphological patterns with an abrupt release of energy. Nanotubes become flattened, twisted, and buckled as they deform [31]. They sustain large strains (40 %) in tension without showing signs of fracture. These changes in deformation modes, such as buckling, have been recorded by TEM. The flexibility is related to the in-plane flexibility of the planar graphene sheet and the ability of the carbon atoms to rehybridize, with the degree of $sp^2 - sp^3$ rehybridization depending on the strain. Such nanotube flexibility under mechanical loading is important for their potential application as nanoprobes and in na-

nocomposites. This behavior also offers an advantage against breakdown that could occur during composite processing.

In addition to the deformation mechanics described, new modes of plastic behavior have been predicted in nanotubes at higher temperatures (relevant to nanotube/ceramic composites, for example). Pairs of a 5 – 7 pair defect, called a Stone – Wales defect in sp^2 carbon systems, are created at high strains in the nanotube lattice and become mobile. Such mobility leads to a step-wise size reduction (localized necking) of the nanotube. It also introduces changes in helicity in the region where the defects have moved (similar to a change in lattice orientation where a dislocation passes through a crystal) [32].

High-temperature fracture of individual nanotubes under tensile loading has been studied by molecular dynamics simulation. Elastic stretching elongates the hexagons until, at high strain, some bonds are broken. The local defect is then redistributed over the entire surface by bond saturation and surface reconstructions. The final result of this process is that instead of fracturing, the nanotube lattice unravels into a linear chain of carbenes (carbon atoms linked by double bonds into a chain) [31]. Such behavior is unusual in crystals. It could play a role in increasing the toughness of nanotube-filled ceramic composites during high-temperature loading by increasing the energy absorbed during deformation.

The electrical properties of nanotubes are also unique. Calculations have predicted that all the armchair tubes (Figure 2.3c) are metallic, whereas zigzag and helical tubes are either metallic or semiconducting [33]. The electronic conduction process in nanotubes is unique because the electrons are confined in the radial direction in the singular plane of the graphene sheet. Conduction in the armchair (metallic) tubes occurs through gapless modes, because the valence and conduction bands always cross each other at the Fermi energy [34]. In most helical tubes that contain a large number of atoms in the unit cell, the 1D band structure shows an opening of the gap at the Fermi energy, lending it semiconducting properties. This unique electronic behavior occurs only in small nanotubes. As the diameter of the tubes increases, the band gap (which varies inversely as the tube diameter) tends toward zero, yielding a zero-gap semiconductor that is equivalent to the planar graphene sheet [35]. In an MWNT, the electronic structure of the smallest inner tubes is overshadowed by the outer, larger, planar, graphene-like tubes. Experiments in which the band structure obtained from individual MWNT resembles that of graphite substantiate this phenomenon. In a later section, discussion of the electrical conduction and optical properties of nanotube-filled polymer composites demonstrates the electronic importance of nanotube properties.

2.2.1.2 **Nanotube Processing**

The best methods to date for producing ideal nanotubes are based on the electric-arc and laser-ablation processes [36]. The material prepared by these techniques has to be purified by tedious chemical separation methods. Not one of these techniques is suitable for producing the quantities needed for industrial applications (e.g., in composites). In addition, this barrier has hindered research and development. In recent years, work has focused on developing chemical vapor deposition techniques using

catalyst particles and hydrocarbon precursors to grow nanotubes [37]. In the past, such techniques were used to produce large quantities of hollow nanofibers of carbon. The drawback of catalytic CVD-based nanotube production is the inferior quality of the structures, which contain gross defects (twists, tilt boundaries, etc.), particularly because the structures are created at much lower temperatures (600 – 1000 °C) compared to the arc or laser process (~2000 °C).

However, recently a major breakthrough has resulted in the efficient production of single-walled nanotubes by what is called a HiPCO process [38]. The technique, developed at Rice University, has become the main source for commercially available high-purity SWNT in gram quantities. The technique uses the high-pressure (several atmospheres) disproportionation of CO gas in the presence of iron carbonyl catalyst vapor [39]. The plan proposed by the Rice group is to produce nanotubes in pound quantities by the year 2005 at a reasonable price (a few dollars per gram). Nanotubes obtained by this method are greater than 80% pure by weight, and the 20% impurity consists principally of iron particles from the catalyst. These particles should not have much effect on the mechanical properties of nanotubes when used as filler but could certainly have effects on their electrical, magnetic, and optical properties.

In his first experimental report, Iijima [9] showed MWNT sticking to the ends of graphite electrodes that were used in the production of fullerenes. Fullerenes are formed in the vapor phase from the evaporation of graphite electrodes. MWNT are formed on the cathode surfaces used in such soot generation. A year after the discovery of MWNT, it was found that, if conditions are right, the evaporated carbon can be made to condense continuously on the cathode surface as a cigar-shaped deposit. This builds up into a boule a few centimeters long, made of a graphite shell packed with nanotubes and other forms of closed graphite nanoparticles [40]. The technique is similar to what Roger Bacon used almost 30 years ago to generate large (micrometer size) arc-grown carbon whiskers, although he used very different conditions in his experiment. The method is similar to the Kratschmer – Huffman method of generating fullerenes [41]. To generate MWNT, a dc arc is normally used (with a modest voltage of 20 V and currents of $<$100 amp) in an inert atmosphere of 500 torr helium. Surprisingly, such perfect structures as nanotubes self-assemble in the plasma created in the interelectrode region, where the temperature is close to 3500 °C. The time scale for formation of these nanostructures is extremely short; a MWNT 5 nm in diameter and 1000 μm long grows in about 10^{-4} s [42].

The inside of the deposit formed in the electric arc-discharge contains a highly porous network of randomly oriented MWNT structures that are organized on a macroscopic scale into pencil-like columns aligned in the axial direction of the deposit. Although MWNT grown by the electric-arc method has so far been the most perfect in terms of structure and properties, the technique suffers from drawbacks. Being a batch process limits the amount of material that can be produced, and the material in the deposit contains substantial amounts of nanoparticles that have polyhedral shapes and are low in aspect ratio. Several parallel attempts to make nanotubes through catalytic vapor deposition have overcome some of the problems of the arc process. In general, catalytic metal particles are exposed to a medium containing gaseous hydrocarbon species. Nanofibrils (twisted hollow fibers) are formed [43]. One good example

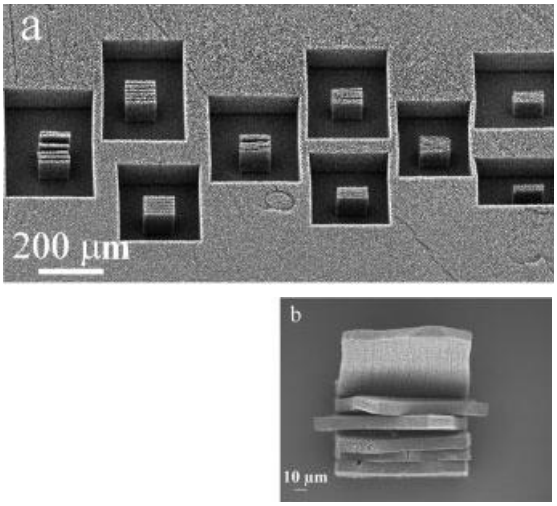

Fig. 2.7 Scanning electron micrographs showing MWNT grown by catalytic vapor deposition onto catalysts prefabricated into patterned arrays resulting in well aligned nanotube assemblies

is the Hyperion fibers that have been in commercial use for some time [44]. Controlling the size of the catalyst seed has enabled achieving uniformity in the size of the fibers. The process can be scaled to produce large amounts of material. In some cases, when the catalysts are prefabricated into patterned arrays, well-aligned nanotube assemblies are produced (Figure 2.7) [45]. Similarly, template-based approaches are also in use: the aligned pores of a nanoporous membrane (such as electrodeposited porous alumina) are filled with carbon species through vapor deposition and later graphitized to produce nanotubes. The template membrane is removed to obtain aligned nanotube arrays [46, 47].

Single-walled nanotubes are made with a combination of catalyst and dense carbon vapor. Both are simultaneously introduced into an inert atmosphere by an electric arc [48] or through laser ablation [49]. In the former, the setup is similar to that used for MWNT synthesis, but a hole is drilled in the anode and packed with a mixture of the metal catalyst and graphite powder. Several metals and combinations of metals have been used to obtain good yield of nanotubes. The best so far consists of a mixture of Ni and Y with graphite in a 15:5:80 weight ratio. When the electric arc is struck with such a modified electrode, spectacular growth occurs in the reaction vessel, which becomes decorated with a network of webs that contain SWNT. Upon closer look, the webs contain ropes of nanotubes that consist of tens of SWNT (Figure 2.8). The maximum density of nanotubes is seen in the product that grows around the cathode like a collar, which consists of $>50\,\%$ wt. nanotubes. The rest of the carbon soot contains fullerenes, partially graphitized carbon (glassy carbon), amorphous carbon, and finely distributed catalyst particles. In the laser-ablation technique, a metal (Ni-Co) containing a small percentage ($<1\,\%$ wt.) of graphite target placed in an oven is ablated with a strong laser pulse under an inert atmosphere. A felt of nanotube material is generated and is collected onto a water-cooled target by forced gas flow. Using two coordinated laser pulses breaks down the carbon formation better, producing a very high yield of nanotubes, with $>90\,\%$ of the collected material being SWNT.

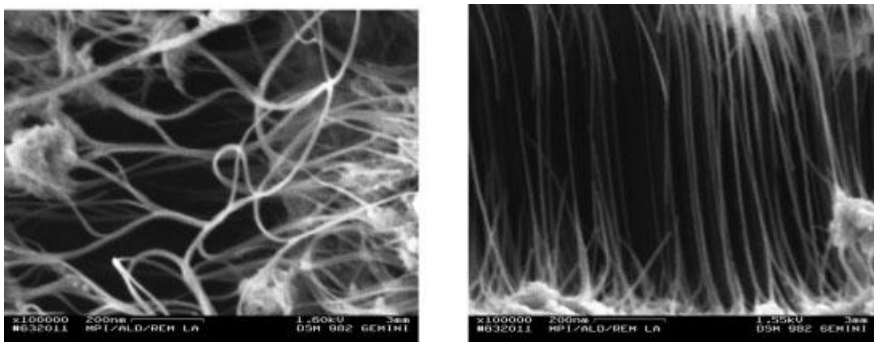

Fig. 2.8 Scanning electron micrograph showing SWNT grown by a catalyzed arc-discharge method

2.2.1.3 **Purity**

Nanotubes consisting of large impurity fractions are not useful for either laboratory studies or composite manufacture. For example, MWNT processed by the arc-discharge method have a significant volume fraction of other carbonaceous materials. In addition, they may contain a high content of scrolled layers instead of nanotubes. Figure 2.9a shows typical material as produced. Because the extra carbonaceous material and catalyst can play a significant role in determining the composite's properties, they must be removed. In addition, we still need better control in manipulating (slicing, joining, and making larger structures from nanotube building units) nanotubes, especially through generalized approaches such as chemistry.

Nanotubes are insoluble, and hence all the purification procedures must use filtration-based techniques. As a result, the nanotube products can never be as pure as, for example, fullerenes. All purification procedures follow certain essential steps: preliminary filtration to get rid of large graphite particles, dissolution to remove fullerenes (in organic solvents) and catalyst particles (in concentrated acids), microfiltration, settling, and chromatography to separate MWNT and nanoparticles or SWNT from the amorphous carbon impurities [50]. Nanotubes must be kept separated when in suspension and are typically dispersed with a surfactant (e.g., sodium dodecyl sulfate) prior to the last stage of separation. Some reports claim that SWNT samples with

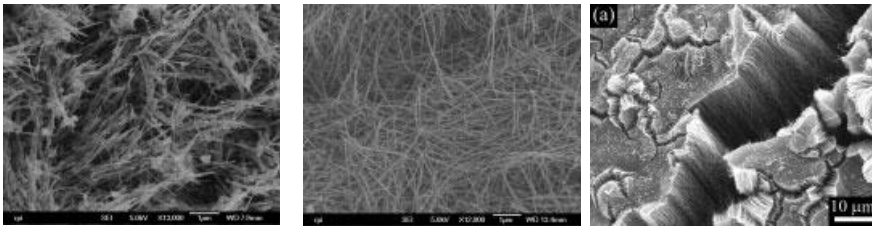

(a) (b) (c)

Fig. 2.9 Scanning electron Micrographs showing the purity of MWNT (a) as received MWNT produced by arc-discharge, (b) purified MWNT, (c) MWNT grown by CVD

>99% purity can be made by repeating some of these steps [51]. Recent efforts [52] to use size-exclusion chromatography have yielded good separation between nanotubes and nanoparticles. Curran et al. [53] achieved a 20% yield by using toluene. Oxidation of any remaining carbonaceous material in a 600 °C oven [54] can follow. Figure 2.9b shows the purity that can be obtained with this method, but the yield is very low [55]. Other oxidation methods, such as plasma or acid oxidation, work but damage the nanotubes [56]. Processing MWNT by chemical vapor deposition or pyrolysis [57] is an alternative, which yields MWNT contaminated with catalyst but with little else in the way of impurities. A higher concentration of defects may result (Figure 2.9c). MWNT processed by laser-deposition techniques, including the nanofibers produced by Hyperion [58], have a significant number of defects relative to pure MWNT but are produced purely. The effect of such defects on the mechanical properties is unclear, but they lead to early oxidation and probably reduce both the strength and the conductivity.

It is now possible to cut nanotubes (SWNT) into smaller segments by extended sonication in concentrated acid mixtures [59]. The resulting pieces of broken nanotubes (open pipes that are typically a few hundred nanometers long) form a colloidal suspension in solvents and can be deposited onto substrates or further manipulated in solution and functionalized at the ends. Such segments can perhaps be joined with appropriate chemical bridges to construct long nanotube chains resembling polymers. A whole gamut of possible chemistry based on nanotubes is just beginning to unfold. In the future, it may be possible to dissolve such functionalized nanotubes in organic solvents and later separate them to produce high-purity samples.

Because size and helicity are two important parameters that affect nanotube properties, selection on the basis of both these factors is important. This is mostly relevant to SWNT, because the MWNT shows average properties that tend to be semi-metallic only. Fortunately, the size distribution produced during the high-yield synthesis of SWNT is quite narrow, with an overwhelming majority of the nanotubes having diameters close to 1.4 nm. The nanotube diameter can be tuned in the range between 1.2 and 5 nm by altering the temperature (from 700 °C to 1200 °C) under which they are formed. It is fortuitous that, when SWNT are formed in high yield, a majority of the tubes have armchair (or close to armchair) arrangement, and this arrangement is independent of the conditions used in synthesis. This size and helicity have a strong bearing on the possible usability of nanotubes, especially in electronics.

2.2.1.4 **Other Nanotubes**

Other types of nanotubes require mention, and these could have some role in the fabrication of novel nanocomposite materials. The closest in structure and mechanical properties to carbon nanotubes are hexagonal boron/nitrogen nanotubes, which can be produced by arc-discharge, laser ablation, and CVD processes and can be fabricated into multiwalled and single-walled structures. The modulus and strength of BN nanotubes are very similar to those of their carbon counterparts [60]. The advantages of using them would be better oxidation resistance and their electrically insulating nature (for certain dielectric applications). The lattice of carbon nanotubes can be doped (to

certain levels) with boron and nitrogen, providing a broad range of possible BCN nanotube structures [61]. Boron has an exceptionally interesting effect: insertion of boron into carbon nanotubes during growth allows selection of their helicity (zigzag nanotubes are stabilized) [62]. The average length of nanotubes is also much higher if boron is added during growth, because boron acts as a surfactant near the growing ends, making it difficult for the structure to close. Nitrogen also can be inserted into the carbon nanotube lattice, but this insertion produces corrugated nanotube structures [63]. The presence of unsaturated nitrogen atoms in the lattice of nanotubes makes them more easily dispersed in solutions, and such nanotubes make good interfaces with certain polymers. Thus, doping nanotubes improves their surface reactivity. This could ultimately aid in the design of strong nanotube matrix (particularly polymer) interfaces, which is necessary in high-strength composites. These modified nanotube lattices also lead to modified electrical and optical properties and hence novel properties for composites in which they are embedded.

Most layered materials can be fabricated into nanotubes. Examples other than those noted above are nanotubes made of dichalcogenides (MoS_2, WS_2, etc.) [64], nanotubes of several oxides (V_2O_5, MoO_3, etc.) [65], and organic nanotubes [66]. These materials (including the BCN types) are not currently available in bulk quantities, and hence very little data is available on the mechanical and electrical properties of composites that contain these nanostructures. However, research is moving quickly in synthesizing several such nanotubular structures, which could ultimately find novel applications in multifunctional nanocomposites.

2.2.2 Plate-like Nanofillers

The most common 2D fillers are layered silicates. The most well known layered silicate is mica. Mica is made up of large sheets of silicate (on the order of centimeters or more) with relatively strong bonds between the layers. Smectic clays or phyllosilicates, on the other hand, have relatively weak bonding between the layers, and the layers are small flakes. Each layer consists of two sheets of silica tetrahedra (corner shared) with an edge-shared octahedral sheet of either alumina (aluminosilicates) or magnesia (magnesium silicates) [67]. Due to isomorphic substitution of alumina into the silicate layers (Al^{3+} for Si^{4+}) or magnesium for aluminum (Mg^{2+} for Al^{3+}), each unit cell has a negative charge between 0.5 and 1.3. The layers are held together with a layer of charge-compensating cations such as Li^+, Na^+, K^+, and Ca^+. These charge-compensating cations provide a route to the rich intercalation chemistry and surface modification required to disperse clays at the nanoscale into polymers. The cation-exchange capacity (CEC) defines the number of exchangeable interlayer cations and is usually described as mEq/100 g. Values range from 60–120 for smectic clays. A typical structure is shown in Figure 2.10 [68]. As they occur in nature or synthetically, the layers are 20–200 nm in diameter laterally and come in aggregates known as tactoids, which can be ~1 nm or more thick. Examples of smectic clays include montmorillonite (CEC ~76.4–119 mEq/100 g), which is an aluminosilicate; sapo-

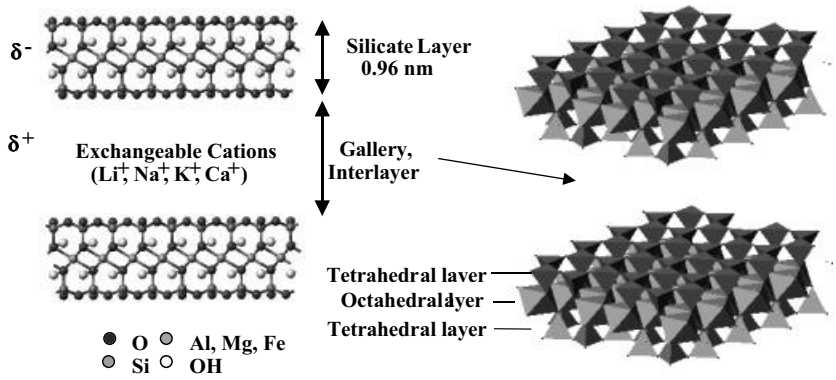

Fig. 2.10 Schematic of the crystal structure of 2:1 layered silicates (smectites). Van der Waals interlayer or gallery containing charge-compensating cations (M^+) separates covalently bonded oxide layers, 0.96 nm thick, formed by fusing two silica tetrahedral sheets with an edge-shared octahedral sheet of alumina or magnesia. Reprinted with permission from [68]

nite, a synthetic material that closely resembles montmorillonite; hectrite, which is a magnesium silicate (CEC ~55 mEq/100 g), and its synthetic equivalent Laponite. Montmorillonite tends to have sheets that are up to 200 nm wide, and Laponite sheets are 25 – 30 nm wide.

For these layered silicates to be useful as nanocomposites, the layers must be separated. Silicate clays are inherently hydrophilic, but polymers tend to be hydrophobic. This presents an interesting challenge in terms of being able to disperse the silicate layers in a polymer. Fukushima and Inagaki [69] demonstrated that an exchange reaction could be used to replace the inorganic exchange ions in the galleries between the layers with alkylammonium surfactants (dioctadecyldimethylammonium). This opens the galleries enough and makes them hydrophobic enough that a Nylon monomer could be intercalated between the layers, resulting in a clay/Nylon nanocomposite. Figure 2.11 [70] shows the increase in interlayer spacing, measured by x-ray diffraction, as a decrease in the peak position for montmorillonite swelled with alkylammonium surfactants of various lengths. The intercalation also modifies the polarity of the layers by lowering the interfacial free energy of the silicate [67]. The number of onium ions that can pack into the galleries depends on the charge density of the clay and the cation-exchange capacity. This, as well as the length of the surfactant chain, determines the distance between the layers. At lower charge densities, the surfactant packs in monolayers and, as the charge density increases, bilayers and trilayers can form (Figure 2.12) [4]. At very high CECs ($\geq$120 mEq/100 g) and long surfactants (>15 carbons), the packing can be ordered in a paraffin-type structure. The positively charged heads of the onium ions prefer to pack close to the clay layer, and the organic ends tend to fill the middle. Further processing of the layered silicates to form polymer composites is discussed in the processing section below.

In general, the properties of the clay layers are unknown, and estimates are made based on composite properties of similar materials in bulk. The properties are not unusual. For these fillers, it is the aspect ratio that is the most significant. Their

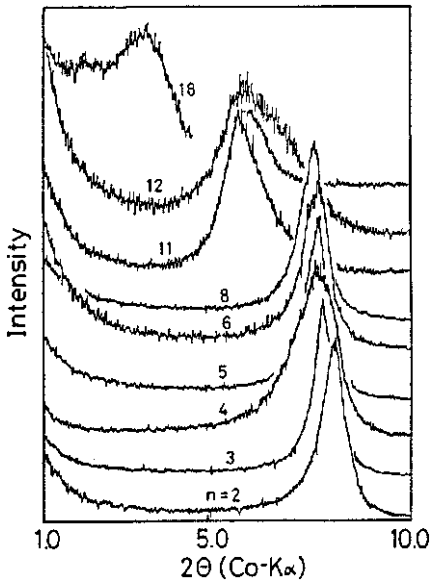

Fig. 2.11 X-ray diffraction patterns of n-montmorillonite as the length of the alkylammonium chain length increases. Reprinted with permission from [70]

high aspect ratio theoretically makes them efficient for carrying loads. Such clay layers are almost impermeable to gases and water through the layer thickness and thus provide an excellent barrier to gas and water in composites.

Layered silicic acids provide an alternative to smectic clays. The intercalation chemistry is similar to that of smectic clays, and they can be obtained with high purity and with structural properties that compliment those of clays [71]. Examples of layered silicic acids include kanemite ($NaHSi_2O_5$), makatite ($Na_2Si_4)_9 \cdot nH_2O$), octosilicate ($Na_2Si_8O_{17} \cdot nH_2O$), magadiite ($Na_2Si_{13}O_{29} \cdot nH_20$), and kenyaite ($Na_2Si_20O_{41} \cdot nH_2O$). The thickness of the layers varies from 0.5 nm for makatite to 1.77 nm for kenyaite [72]. The general structure of layered silicic acids involves layers of SiO_4 tetrahedra with an abundant hydroxyl siloxane surface. Interlayer alkali ions can be ex-

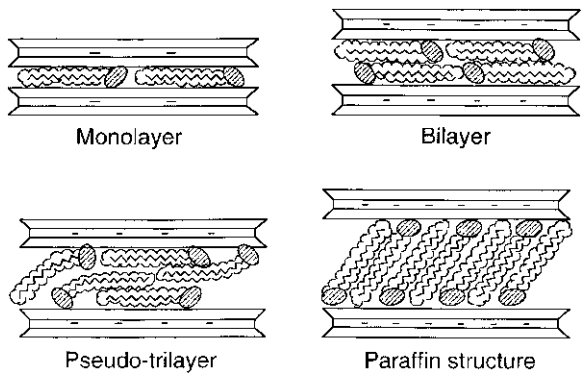

Fig. 2.12 Schematic of the orientation of alkylammonium ions in the galleries of layered silicates with different layer charge densities. Reprinted with permission from [4]

changed with the resulting active hydroxyl sites, leading to enhanced bonding with the intercalates.

Layered double hydroxides (LDH), for example, $Mg_6Al_2(OH)_{16}CO_3 \cdot 4H_2O$, have a positive (instead of negative) charge on the $Mg(OH)_2$ layers. They are produced synthetically [73] and provide an opportunity for intercalation with organic anions. They have been used successfully to make nanocomposites [74, 75].

Transition-metal dichalcogenides are layered materials that can be intercalated with lithium. After intercalation, MoS_2 and WS_2 can be placed in distilled water and exfoliation occurs [76, 77]. Titanium and tantalum dichalcogenides have also been used to make nanocomposites [78, 79]. Essentially any layered material, including graphite [80], with appropriate chemistry can be expanded, creating the potential for intercalation of a polymer.

2.2.3
Equi-axed Nanoparticle Fillers

Production of nanoparticles with controlled size and degree of aggregation is the goal of many research efforts. The primary driver for this interest is the effect of particle size on their properties. For example, the optical absorption spectrum of Au changes with the size of the Au particles. The electroluminescence of semiconducting nanoparticles is also size-dependent. One of the advantages of using nanoparticles in a composite structure is that the particle size and distribution can be stabilized. Materials that cannot be grown easily as single crystals can be used at the nanoscale and dispersed in a polymer to take advantage of the single-crystal properties. In addition, the particles can lend properties to the polymers that they cannot achieve alone or with traditional fillers. For example, nanoparticle-filled polymers can lead to an increase in modulus and strength, but also maintain the polymer's ductility. This is because the nanoparticles are such small defects relative to their micrometer-sized counterparts.

Nanoparticles have been available for more than a century. Carbon black made by pyrolysis is available in a range of surface areas and degrees of aggregation. Silica made by a variety of methods, including the wet chemical process developed by Stober [81], the commercial Ludox® process [82], as well as flame processes, have been available for years. Although recent developments have been made [83], these are well-established processes. These nanoparticles have found significant applications in the rubber industry, in catalysis, chemical mechanical polishing, water treatment, and other applications. In recent years, significant progress in the diversity of processes for making nanoparticles has led to a more diverse set of nanoparticles and better control of particle size, morphology, and surface properties. Recent developments in in-situ processing of nanoparticles within a polymer matrix are discussed in the composite processing section 2.4.3. In this section, we focus on the preparation of discrete particles that are subsequently incorporated into a polymer matrix.

Aerosol methods usually result in the formation of nanoparticles by condensation from a gas phase [references in 84–87]. One example of a highly successful commer-

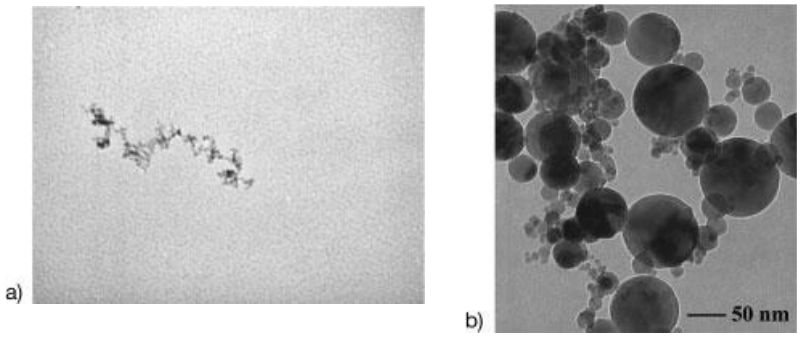

Fig. 2.13 Micrographs showing (a) typical silica nanoparticle agglomerates and (b) titania made via gas condensation. (Thanks to T. Li for these micrographs)

cial aerosol processes is flame hydrolysis. Here, a vapor precursor (such as silicon tetrachloride to make silica) is burned in a hydrogen/oxygen fuel mixture to produce the metal oxide. Titania, alumina, and zirconium oxide can all be produced this way. For silica, particle sizes range from 7 to 27 nm, and the surface areas range from 100 to 380 $m^2 g^{-1}$. The specific surface area and agglomerate structure can be controlled by adjusting the temperature and time of reaction. At higher temperatures, particle coalescence is fast, and low-surface-area materials result. At lower temperatures, coalescence is slow relative to the collision rate, and fractal agglomerates result [88]. Figure 2.13a shows a typical silica agglomerate.

Pyrolysis is another aerosol method and is commonly used to make carbon black, an amorphous form of carbon. The particles have a size range of 20 – 300 nm with surface areas of 20 – 500 $m^2 g^{-1}$.

In a third method, called gas condensation [89, 90], a metal vapor is formed in either an oxygen atmosphere or an inert gas. In an oxygen atmosphere, the metal reacts with the oxygen to form metal oxides, which are collected by cooling the gas and condensing the nanoparticles. A large range of metal oxides can be processed this way, including TiO_2, Al_2O_3, CuO, CeO_2, ZnO, ZrO_2, Fe_2O_3, and Y_2O_3 [91]. In an inert atmosphere, metal nanoparticles result. Advantages of this method are that the particle size distribution is narrow, the particles are crystalline, and the surfaces are clean. Figure 2.13b shows typical metal oxide particles that result from this process. They tend to be isolated, crystalline, and spherical. In the past dozen years or so, great progress has been made in understanding the processes by which such nanoparticles are made and the fundamental relationships between their sizes and structures and their special properties [92 – 95]. In the late 1990s these processes were improved and ton quantities of gas-condensed metal-oxide nanoparticles have been produced.

Laser ablation processes are another form of gas condensation. Here, targets (metal, metal oxide, or semiconductor) are ablated with a laser (often a pulsed laser). An inert or reactive gas is supplied to cool, condense, and sometimes react with the target material. By varying the pulse frequency, gas flow rate, and total pressure, the size of the particles and particle aggregates can be controlled. For example, increasing

the gas flow rate decreases the primary particle size, but increasing the laser fluence and total gas pressure produces larger primary particles. Significant quantities of nanoparticles can be produced this way. Many types of materials can be processed, including SiO_2, MgO, Fe_3O_4, Mg_2SiO_4, $CaTiO_3$, $MgAl_2O_4$ [96], Al_2O_3 [96–98], TiO_2 [97], Fe_2O_3 [97], and many others [99, 100].

Other methods for creating a vapor that condenses into nanoparticles include plasma and chemical vapor condensation, spray pyrolysis, electrospray, and plasma spray [101]. These processes can form a wide range of nanoparticles. One interesting variation on the aerosol process developed recently combines sol–gel processing with the aerosol process. Hydrolysis and condensation of TEOS is carried out in a laminar flow chamber at temperatures ranging from room temperature to 100 °C [102]. The advantage of this low-temperature process is that a large specific area ($400\,m^2\,g^{-1}$) can be produced because of the low coalescence rate relative to the collision rate. In addition, the agglomerates tend to be linear instead of highly branched.

A host of wet-chemistry methods exist in which one or two precursors are placed in an appropriate solution and nanoparticles form. These can be stabilized with an emulsion, surfactant, or a macromolecule that surrounds and protects the nanoparticles from agglomeration. Metal [103], metal-oxide [104], semiconducting [105–107], superconducting, and magnetic particles [108] have all been made this way. Using ZnO as an example, zinc acetate [$(CH_3COO)_2Zn \cdot 2H_2O$] can be reacted with NaOH [109] in the presence of poly(vinylpyrrolidone) to create very stable ZnO particles with an average diameter of 4 nm [110].

Metal nanoparticles can also be made by sonication chemistry [111]. This process takes advantage of the formation, growth, and implosive collapse of bubbles within a liquid to create localized spots with temperatures as high as 5000 K and pressures as high as 1800 atm. Under appropriate sonication conditions, precursors such as $Fe(CO)_5$ and $Co(CO)_3(NO)$ form nanoparticles. If sonication is done in the presence of an alkane, the particles can be separated, but sonication can also be done in the presence of a polymeric ligand to make stable colloids or in the presence of an inorganic support.

Metal oxides an also be formed by taking advantage of hydrodynamic cavitation [112]. Here, hydrodynamic cavitation is produced by using a high-pressure fluid system in the presence of a sol–gel solution. The local high temperatures and pressures due to collapse of bubbles result in the creation of nanoparticles. The pressure and the exposure time can be adjusted to control the particle size.

This section has clearly left out many details of nanoparticle processing, and many significant contributions have not been referenced. We introduce only the basics of nanoparticle processing here, because this topic is so broad and our focus is on nanocomposites.

2.3
Inorganic Filler–Polymer Interfaces

As mentioned in the Introduction, nanocomposites have at least an order of magnitude more interfacial area than traditional composites. This increase in interfacial area results in a 3D interfacial region within the polymer matrix that can have properties significantly different from those of the bulk polymer. The local chemistry, degree of cure, chain mobility, chain conformation, and degree of chain ordering or crystallinity can all vary continuously from the filler/matrix boundary to some point in the polymer bulk. To understand the significant effects nanoscale fillers have on polymer behavior, this interfacial region must be understood. The paragraphs below outline some of the literature describing the behavior of polymers near a surface.

Consider first a pure thermoplastic polymer film interacting with either air or a very flat inorganic surface. We know that surface/polymer interactions greatly influence the glass transition temperature (mobility, relaxation spectra) of thin polymer films. For example, the presence of a free surface, as observed in free-standing ultrathin films, reduces the glass transition temperature [113–116] (Figure 2.14), but an attractive surface increases the glass transition temperature [117, 118]. The mechanism causing these changes in Tg is currently under discussion in the literature. Molecular dynamics simulations [119] show that the decrease in Tg for free-standing thin films is caused by a decrease in the density, which in turn increases the mobility of the polymer chains. Monte Carlo simulations show that the presence of a neutral surface can increase the density and decrease the mobility of the polymer chains [120], although experimental data suggest that the surface must be attracting before Tg increases.

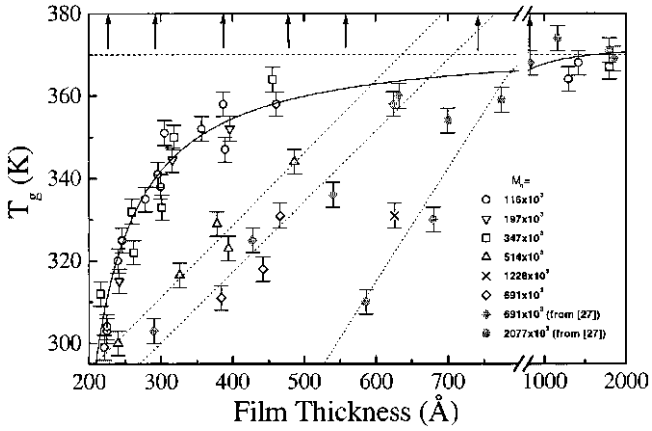

Fig. 2.14 The glass transition temperature as a function of film thickness for low and high molecular weight polystyrene free-standing films. Reprinted with permission from [113]

Composites, however, do not contain ideal 2D interfaces. In fact, the highly curved surfaces and the size scale close to that of a typical radius of gyration for a polymer chain make it difficult to apply 2D observations and measurement techniques directly to nanocomposites. Based on some early nanocomposite work on polymers filled with carbon black, one description of the interfacial region in nanofilled polymers is a bound polymer layer (where 'bound' implies a region of immobile polymer) with a distinct interface between the bound and unbound regions. The evidence for this is an insoluble fraction of polymer that results from the addition of nanoparticles [121]. In addition, the properties of the nanofilled polymers often scale with a parameter somewhat larger than the average particle diameter [122]. The argument has been that the stronger the polymer–particle interaction, the larger the bound polymer fraction, up to 2–9 nm thick [123].

The discrete bound polymer layer could result in a second glass transition temperature, according to some researchers [124]. Research on thin film, however, does not point to a discrete layer of affected material but to a far-field effect. Figure 2.14 [113, 118] shows the effect of film thickness on the glass transition temperature for free-standing polystyrene films of various molecular weights. The higher the molecular weight, the greater the film thickness at which the decrease in Tg begins. This suggests that some multiple of the radius of gyration may be a relevant parameter. Studies on diffusion using SIMS show that the effect can be up to 10 times the radius of gyration [125]. In addition, the thinner the film, the lower the Tg becomes. This indicates that the effect of the surface is a continuous function within the polymer. In addition, recent results [126] have shown that the nonlinear viscoelastic behavior of nanofilled polymer melts is strongly dependent on the surface treatment of the filler particles. The results suggest that the filler surface has a far-field influence on the chain motions. However, these effects are only apparent when finite shear–strain magnitudes are used to probe the behavior. Small-strain studies on the same composites in the vicinity of the glass transition temperature show that, although the glass transition temperature is increased by filler addition, the curves of normalized loss modulus vs. frequency superpose perfectly. These studies suggest that the distribution of relaxation times is shifted but otherwise unaltered. Taken together, these results indicate that the bound polymer layer is essentially a monolayer and that the far-field influence is due to entanglement trapping.

Further clarification reassures us that a discrete bound layer and a more diffuse region are not contradictory. First, a *bound polymer layer*, as originally defined, is simply the amount of polymer that is 'stuck' to a particle surface; the term was not intended to completely describe the mobility within that region or the effect of that region on the surrounding polymer. Thus, let us define a bound polymer layer as any polymer that is bonded to the particle surface. This sometimes occurs in nanocomposites, but not always. Let us define the interfacial region as the region of polymer surrounding the nanoparticle and having altered chain conformation and/or mobility due to the presence of the filler. Clearly, polymer chains strongly bound to the surface result in a different interfacial region than chains either repelled by the surface or weakly interacting. The magnitude of the effect this interfacial region has on the properties of a composite depends on the property being measured. For example, the effect

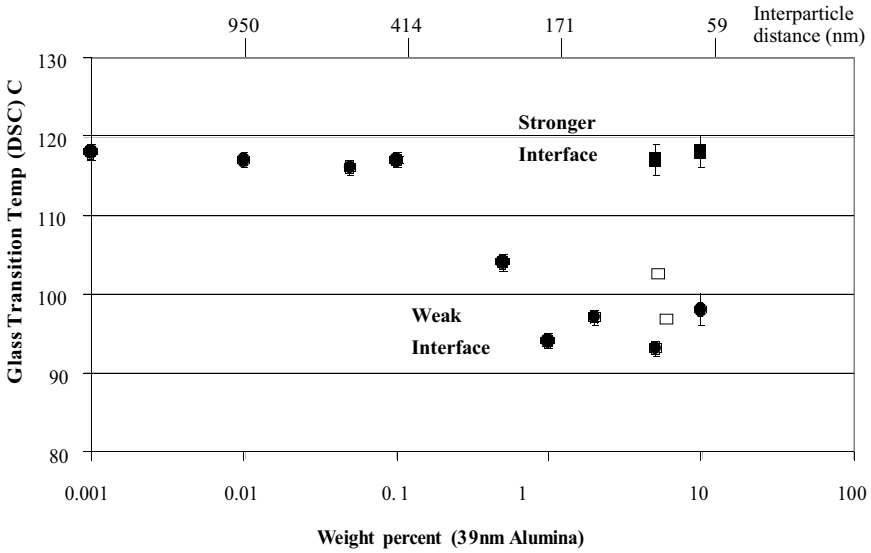

Fig. 2.15 Glass transition temperature vs. volume fraction of alumina particles for a PMMA matrix composite. The glass transition temperature does not decrease until a critical volume fraction is reached. In addition, when the nanoparticles interact strongly with the polymer, the glass transition temperature does not decrease. Reprinted with permission from [127]

of the interfacial region on the glass transition temperature, which is the result of cooperative segmental motions, may be different from its effect on diffusion, which depends on larger-scale mobility.

Consider for a moment, ignoring the specifics of their morphology and properties, the implications of both the bound polymer layer and the interfacial region on the behavior of nanofilled polymer composites. The film thickness at which a significant change in glass transition temperature occurs depends on the molecular weight, but can be as high as 80 nm. For a 30-nm particle dispersed in a polymer matrix, the average interparticle spacing is 80 nm at filler loadings as low as 1.5 vol. % (Figure 2.2). Thus large effects on bulk properties can be expected at low filler loading.

The glass transition temperature of a bulk part can be raised and lowered by the addition of nanoparticles [126–128]. Ash et al. [127] have shown that, for a non-wetting nanoparticle/polymer composite (alumina/PMMA), the glass transition temperature starts to decrease at a specific filler volume fraction corresponding to an interparticle distance of about 200 nm (Figure 2.15). On the other hand, if the PMMA is adsorbed on the particle surface, the glass transition temperature is stabilized. More commonly, an increase in Tg is observed [129, 130], which can be as large as 30° [80].

The situation becomes even more complicated for composites in which the polymers are confined between two flat layers (as in clay composites) [131]. For example, NMR studies on PEO-intercalated nanoclay showed that confinement of the chains increases segmental mobility at low temperatures, but at higher temperatures

a less mobile fraction is revealed. This suggests a broadening in the relaxation spectra. In addition, the glass transition temperature is suppressed. In thin films this is attributed to a highly immobilized polymer layer. Krishnamoorti [131], armed with the knowledge that the rate of polymer intercalation into the clay layers can be as fast as the diffusion rate in the bulk, suggested that this phenomenon is due only to noncooperative motion. This is clearly an area in need of further study and is discussed more below.

In addition to changes in the mobility of a polymer chain, the average chain conformation can be altered and/or the type and degree of crystallinity can change. Dhinojwala and coworkers recently reported measurements on a polystyrene (PS)/sapphire interface [132, 133], which revealed a nearly perpendicular orientation of the phenyl rings to the PS/sapphire interface. It is unclear how these conformations change in the presence of a nanostructured surface, particularly one with a high radius of curvature. Recent modeling, however, suggests that studies on flat surfaces may be relevant [134]; however, it is unclear how the many techniques used to study behavior on flat surfaces could be modified to measure this. Studies have focused on the effect of structural details of surfaces on protein structure and have found that the density of alkane chains on an alkylated surface directly affects the amount of protein adsorbed [135]. Other studies [136–138] showed that vitronectin (a mediator of osteoblast adhesion) remained folded on monolithic alumina with micrometer-sized grains, but showed enhanced adsorption as well as conformational changes when it was adsorbed on nanograined alumina. Vitronectin interactions with nanoceramics were correlated with significantly enhanced osteoblast adhesion. The change in polymer chain conformation, in contrast to that of proteins, is likely to be much more local, but could still affect bulk properties.

Crystallinity is also sensitive to surface interactions. This is seen dramatically in graphite fiber/polypropylene composites in which a transcrystalline layer develops perpendicular to the fiber [139]. Nanofillers can also change the degree of crystallinity, change the rate of crystallization, and/or suppress the formation of the thermodynamic crystal phase and stabilize the metastable phase [140, 141]. In silica-filled Nylon 11 that was thermally sprayed, the crystallinity increased due to the presence of the nanoparticles [142]. In montmorillonite/HDPE nanocomposites, the polymer crystals decreased in size and the crystallization rate decreased [143], whereas in polyamide (Nylon 6) composites the metastable hexagonal phase formed instead of the typical monoclinic phase [144]. Another example in Nylon 6 occurs under high pressure: by annealing montmorillonite/ Nylon 6 at high pressures, a higher-temperature monoclinic phase forms (α), and the orthorhombic (γ) phase is suppressed [145].

Finally, changes in the chemistry can occur in the interfacial region. A dramatic example of this is the preferential adsorption of a curing agent onto the nanofiller. When this occurs, the region surrounding the nanoparticle consists of a 'layer' of stoichiometrically crosslinked thermoset with excess curing agent, surrounded by a 'layer' of depleted curing agent and thus less-than-stoichiometric crosslinking. This phenomenon has been observed in fiber-filled polymers [146] and is presumed to exist in nanoscale titania-filled epoxy [147]. More subtle changes could also occur, such as preferential adsorption of low-Mw material to the surface.

In summary, the interfacial region is complex, and when the interfacial area is very large, the whole polymer matrix may essentially be interfacial region. This presents one of the essential challenges in polymer nanocomposites: to develop technology to control the interface, to describe the interface mathematically, and to be able to predict properties taking into account the interfacial region. Traditional composite theory, although very far advanced in describing properties that are relatively independent of the interface, is still in its infancy in taking into account the role of the interfacial region. Significant progress has been made in understanding the interaction of polymers with flat surfaces, but the interaction of polymers with highly curved surfaces and at scales similar to that of the radius of gyration is not well understood. The nanocomposites community has their work cut out for them.

2.4 Processing of Polymer Nanocomposites

One of the key limitations in the commercialization of nanocomposites is processing. Early attempts at clay-filled polymers required processing that was not commercially feasible, but this situation has changed. Similarly, processing of other nanocomposites is becoming easier and more commercially viable as our understanding improves. A primary difficulty is proper dispersion of the fillers. Without proper dispersion and distribution of the fillers, the high surface area is compromised and the aggregates can act as defects, which limit properties. To facilitate discussion, we will define the state of aggregation in those nanocomposites. Distribution of a nanofiller describes the homogeneity throughout the sample, and the dispersion describes the level of agglomeration. Figure 2.16 schematically illustrates good distribution but poor dispersion (a), poor distribution and poor dispersion (b), poor distribution but good dispersion (c), and good distribution and good dispersion (d). The state of aggregation is further defined in layered silicate/polymer nanocomposites later in this chapter.

2.4.1 Nanotube/Polymer Composites

The processing of nanotube/polymer composites is still in its infancy. Although nanotubes have been incorporated into composites commercially, the literature describing the processes is limited. Significant issues remain to be solved about purification, dispersion, and bulk processing.

The ability to disperse SWNT and MWNT into a polymer may be the most critical processing parameter for controlling properties. Nanotubes that are in clumps or are agglomerated with other carbonaceous materials create defect sites that will initiate failure. In addition, they limit the efficiency with which the nanotubes carry load. This limitation has been illustrated explicitly in both polymer and ceramic matrix composites [148, 149]. CVD-grown MWNT, which are easily dispersed and less agglomerated, increased the modulus and strength of polystyrene without compromising the

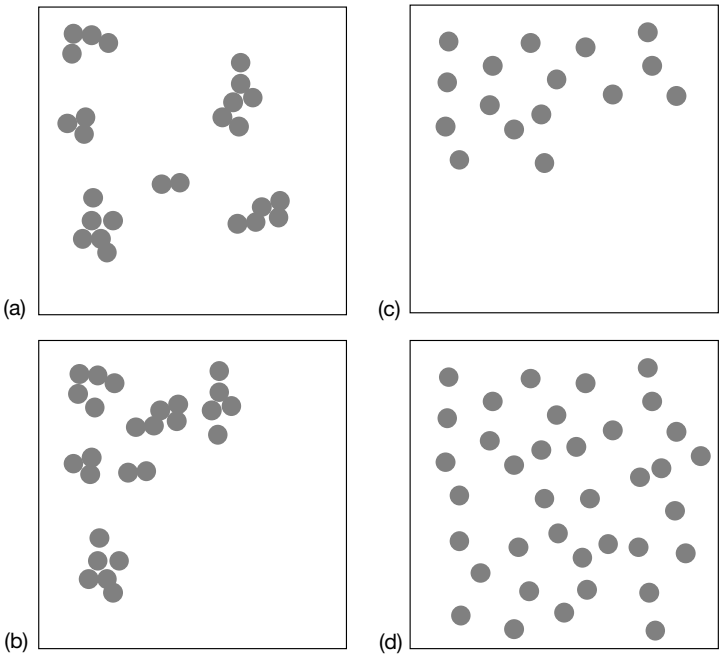

Fig. 2.16 A schematic illustrating the difference between dispersion and distribution and giving examples of good and poor for each

strain-to-failure factor significantly. Other work on arc-discharge-grown MWNT, which were not fully purified and not as well dispersed, did not show the increase in toughness observed for well-dispersed MWNT. Similarly, the toughness of MWNT/alumina composites with excellent dispersion increased significantly compared to composites with somewhat worse dispersion.

Dispersion has been achieved primarily by sonication of nanotubes in a solvent. The most focused efforts have been on the dispersion of SWNT. Chemical modification of the surface with the aid of surfactants [150], by functionalization of the end-caps with long aliphatic amines [151], or by functionalization of the sidewalls with fluorine [152] or alkanes [153] has resulted in stable suspensions of nanotubes. None of these methods is ideal for composite processing. The use of surfactant results in an impurity in the composite. Functionalizing the ends limits further chemical modifications for controlling bonding with the matrix, and modification of the sidewalls can affect the mechanical properties [154]. As an alternative, the best solvents for direct dispersion of SWNT were identified as NMP, DMF, hexamethylphosphoramide, cyclopentane, tetramethylene sulfoxide, and ε-caprolactone [154]. These solvents are all strong Lewis bases without hydrogen donors, although not all solvents with these characteristics were good solvents for SWNT.

After dispersion, drying the dispersion on a glass slide and placing resin directly onto a thin film of nanotubes [29, 155, 156] can produce small-scale composites. Mix-

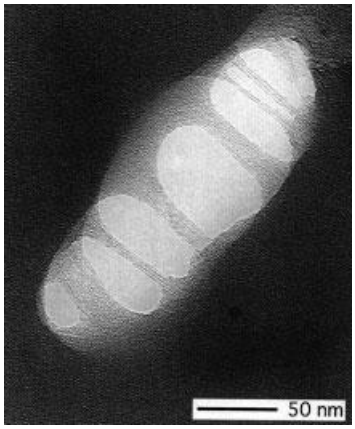

Fig. 2.17a Transmission electron micrograph of aligned singlewall carbon nanotube ropes bridging an elliptical hole in a polymer film. Reprinted with permission from [157]

ing both the nanotubes and the polymer in the presence of a solvent [25, 30, 157, 158], often with the help of a surfactant [159], can also produce composites. Figure 2.17a shows the wetting and the dispersion of SWNT dispersed in ethanol and then mixed with an epoxy resin [157]. Figure 2.17b [148] shows the dispersion achieved with CVD-grown MWNT, dispersed in toluene with dissolved polystyrene and casting films. Excellent dispersion was achieved. Nanotubes have also been dispersed directly into liquid urethane acrylate polymer [160], methylmethacrylate monomer [161], and epoxy resin [162], followed by curing or polymerization. Damage to the nanotubes is a tradeoff that must be considered.

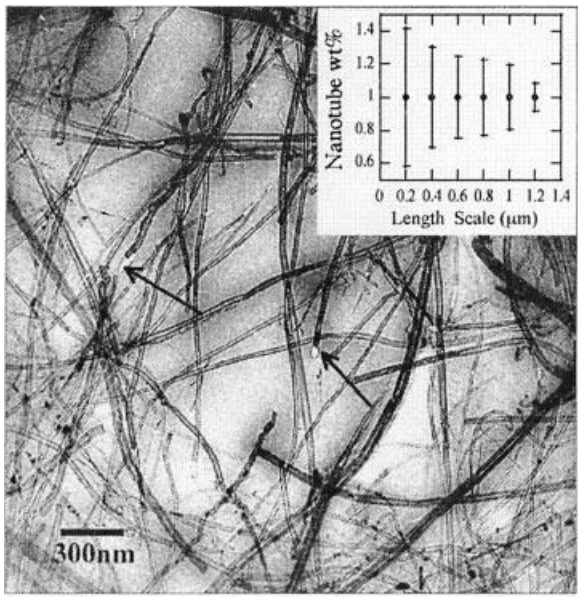

Fig. 2.17b Treansmission electron micrograph of MWNT-PS film in which the nanotubes are homogeneously distributed in the polystyrene matrix at a $\sim$1 μm length scale. The inset is the MWNT weight fraction as a function of length scale, which was determined by measuring the weight fraction of nanotubes at areas in the image. The error bars represent the standard deviation of the experimental data, which reflects the homogeneity of the distribution. Reprinted with permission from [148]

Nanofibers have been successfully melt-mixed with polyphenylene ether/polyamide matrices in a twin screw extruder. This process has led to a commercial product in conductive thermoplastics for electrostatic painting without the loss of mechanical properties [163].

An interesting composite processed from nanotubes is a macroscopic fiber that is a mixture of nanotubes and a traditional material used for carbon fibers, such as pitch or PAN. This was achieved with a pitch-based matrix and led to interesting improvements in properties, because the pitch fibers were not subjected to the typical high temperature processing [164].

2.4.2 Layered Filler–Polymer Composite Processing

Scientists have known for about 40 years that polymers interact strongly with montmorillonite and that the clay surface can act as an initiator for polymerization [165, 166]. Patents for clay/Nylon 6 composites were not issued until the 1980s, at which point the clay/polymer nanocomposites were commercialized [167]. The improvement that led to commercialization was the appropriate dispersion of the clays at the nanometer scale.

The first step in achieving nanoscale dispersion of clays in polymers is to open the galleries and to match the polarity of the polymer or monomer so that it will intercalate between the layers. This is done by exchanging an organic cation for an inorganic cation (Figure 2.18). The larger organic cations swell the layers and increase the hydrophobic properties of the clay [168] (Figure 2.18), resulting in an organically modified clay. The organically modified clay can then be intercalated with polymer by several routes. Solution processing involves dispersion of both the organically modified clay and the polymer in a common solution. Variations on this process include emulsion or suspension polymerization [169, 170]. Highly polar polymers such as Nylon [171] and polyimides [8] are more easily intercalated than nonpolar polymers such as polypropylene, because polar polymers have a higher affinity for the polar clay galleries. In situ polymerization intercalates monomer directly into the organically modified clay galleries, and the monomer can either adsorb onto the layer surface [172] or be anchored by free radical techniques [173]. Melt intercalation involves mixing the clay and a polymer melt, with or without shear. The success of melt intercalation is surprising, given that the gallery spacing is only about 2 nm and the radius of gyration of the polymer is significantly larger than this. Even more surprising is that the speed of melt intercalation is faster than that of self diffusion of polymers and scales with the inverse of the molecular weight [174]. Coarse-grained molecular dynamics studies predict a rate twice that of self-diffusion, with the rate scaling inversely with the molecular weight. The results of molecular dynamics and experimental studies agree that the stronger the clay/polymer interaction, the slower the intercalation rate [175]. In addition, layer flexibility seems to control the mechanism of intercalation [176], perhaps due to a recently proposed mechanism called the 'kink' model of melt intercalation [177], in which sufficient shear force causes a kink to form in the clay sheet (a form

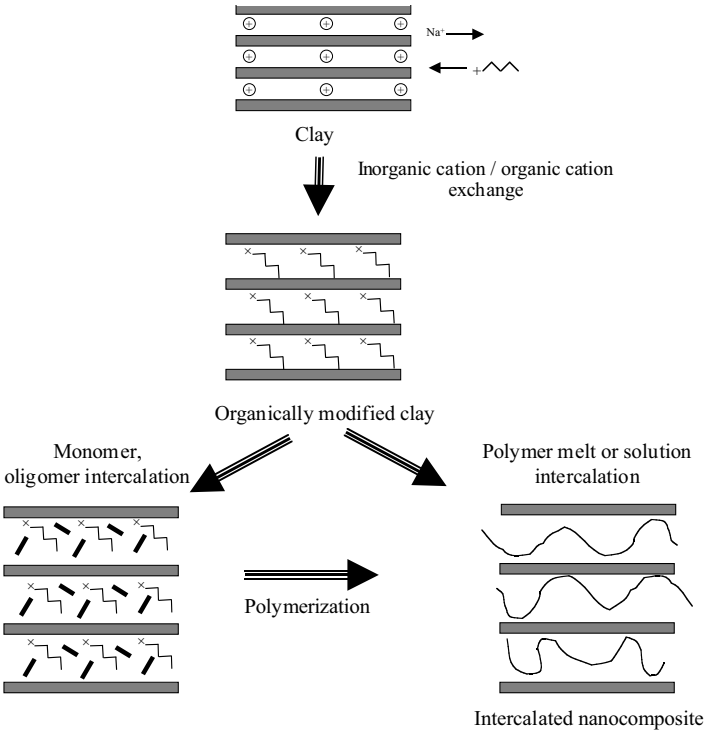

Fig. 2.18 Schematic of the basic steps in processing clay-filled polymers

of compression failure) (Figure 2.19). Polymer can then penetrate the new space between the layers. This kink can propagate along the layer, and more polymer can intercalate. This mechanism can explain both the fast intercalation rate (which is enhanced by the space created by kinking) and the dependence on layer flexibility. Layers with a lower modulus should kink more easily. A rigorous test of this model is still required. Models have also been developed to test the tendency for chains to melt-intercalate in the absence of shear [178, 179]. These studies showed that there is an optimal interlayer separation (slightly larger than the pseudobilayer for intercalation of polystyrene) and an optimal chemical interaction (the greater the hydrophilicity of the polymer, the shorter the organic modifier should be). This minimizes unfavorable interactions between the polymer and the aliphatic chain. Polar polymers are also more likely to intercalate.

As the layer spacing increases, the process can be monitored by x-ray diffraction (XRD). Intense peaks between 3° and 9° indicate an intercalated composite, but if the peaks are extremely broad or disappear completely, this indicates complete exfoliation. Figure 2.20 [180] shows the XRD pattern of organically modified montmorillonite (d), an intercalated montmorillonite (c), and two exfoliated montmorillonite nanocomposites (a, b).

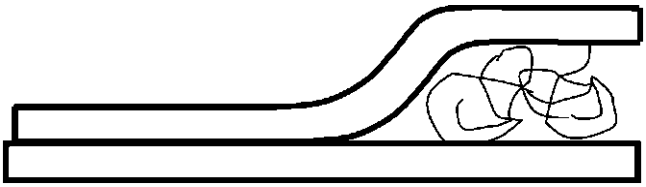

Fig. 2.19 Schematic of the kink model of melt intercalation. Ag denotes the agglomerated (immiscible) portion of the clay, and Int. denotes the intercalate state. Redrawn from Fig. 1(a) of [177]

Once the clays have been intercalated with polymer, the nanocomposites can be processed by traditional melt-processing methods. This final processing of the composite is important in determining the final properties. Mixing facilitates nanoscale dispersion and can lead to clay and/or polymer chain alignment. The degree of shear during molding determines, not only the degree of clay layer alignment, but also the degree of crystallite alignment. For example, extruded Nylon sheet with a draw ratio of 4:1 had a higher modulus than a sheet processed by injection molding [181]. This may be due to a higher degree of platelet and crystallite alignment and is a common phenomenon in the drawing of Nylon. In some cases, the crystallinity increases

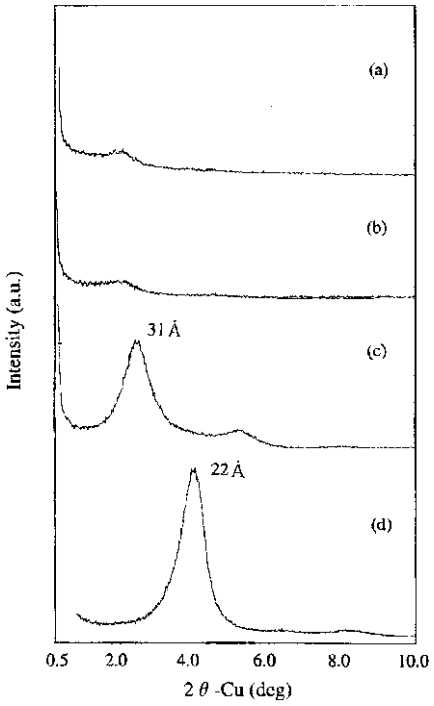

Fig. 2.20 X-ray diffraction data showing the diffraction patterns that result from (a), (b) exfoliated clays, (c) intercalated clays, (d) organically modified clays. Reprinted with permission from [180]

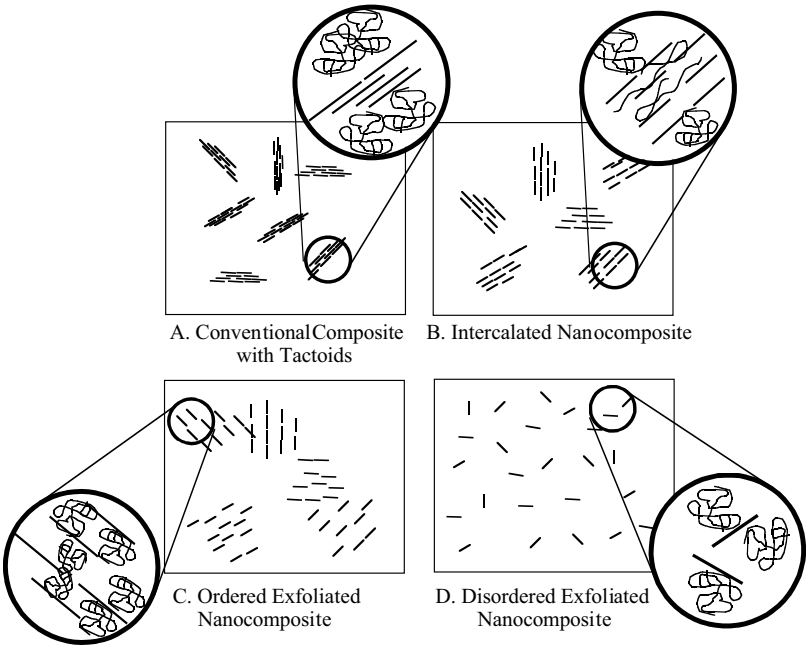

Fig. 2.21 Schematic of the microstructures that can develop in clay-filled polymer composites: (a) a conventional composite with tactoids, (b) an intercalated nanocomposite, (c) an ordered exfoliated nanocomposites, (d) a disordered exfoliated nanocomposite

(36 % – 38 %, compared to 31 % for unfilled Nylon) and remains constant with filler content [140]. Other studies, however, have shown decreases in crystallinity [182]. Increasing the pressure during processing to 0.1 – 0.6 GPa favors the α phase [145]. The clay platelets also enhance alignment of the Nylon 6 chains and the crystallites [140], though the extent is governed by the degree of shear and can vary across the thickness of an injection-molded part [183]. Understanding and optimizing the mixing and taking advantage of interesting rheology and other phenomenon such as strain hardening and rheopexy is in its infancy, and significant fundamental work still needs to be done [184].

The resulting nanocomposites can have several structures (Figure 2.21). The structure of an intercalated nanocomposite is a tactoid with expanded interlayer spacing, but the clay galleries have a fixed interlayer spacing. Exfoliated nanocomposites are formed when the individual clay layers break off the tactoid and are either randomly dispersed in the polymer (a disordered nanocomposite) or left in an ordered array.

The following sections give some details on processing clay/polymer nanocomposites. The discussion is organized by matrix type.

2.4.2.1 Polyamide Matrices

Nylon-6/Nylon-12/clay hybrid composites were the first exfoliated smectic clay composites made [187]. Montmorillonite, with a CEC of 119 mEq/100 g, was intercalated with 12-aminolauric acid, which increased the intergallery spacing from 1.0 to 1.7 nm. This '12-montmorillonite' was then mixed with ε-caprolactam, which increased the intergallery spacing even further, to 4.0 nm, indicating that the ε-caprolactam had intercalated into the galleries. Heating to 250 °C led to polymerization, forming a clay/Nylon-6 nanocomposite. Further research [185] determined that ε-caprolactam could intercalate directly into the galleries of montmorillonite in a hydrochloric acid solution and, upon intercalation, becomes oriented vertically in the galleries. The modified montmorillonite then mixed easily with additional molten ε-caprolactam and 6-aminocaproic acid, yielding a Nylon-6 homopolymer/clay nanocomposite. The montmorillonite was completely exfoliated. Recently [186], montmorillonite/Nylon 6 nanocomposites were processed by melt intercalation. Although the degree of exfoliation was not as high as in nanocomposites produced by the above methods, at weight fractions less than 0.1 the composites were primarily exfoliated.

2.4.2.2 Polyimide Matrices

The preparation of polyimide matrix clay nanocomposites involves several steps [8, 187] (Figure 2.22). By intercalating montmorillonite with the ammonium salt of dodecylamine, it becomes soluble in dimethylacetamide (DMAC). DMAC is also a solvent for 4,4'-diaminodiphenylether and pyrometllitic dianhydride, the precursors for polyamic acid and, as such, polyimides. After intercalation of the ammonium salt of

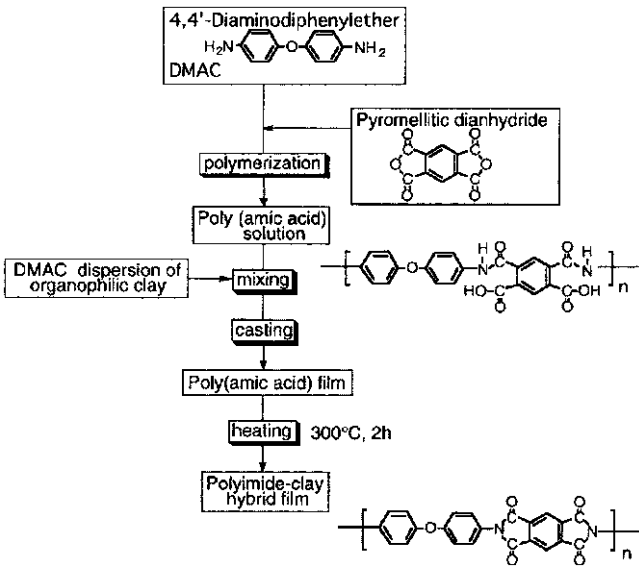

Fig. 2.22 Schematic of the synthesis of polyimide-clay hybrid film. Reprinted with permission from [187]

dodecylamine, x-ray studies [188] showed that hectrite (CEC = 55 mEq/100 g) has one monolayer of organic material between the layers, whereas saponite, montmorillonite, and synthetic mica (all with CEC > 100 mEq/100 g) have two. After composite formation, however, only the montmorillonite and the synthetic mica have exfoliated completely, but the hectrite and saponite remain in a somewhat aggregated state. Lan et al. [189] found aggregates of montmorillonite after using a similar procedure. More recently, P-phylenediamine in an HCl solution was also found to form organic-modified montmorillonite that dissolves in DMAC [190]. This same study showed that the presence of a small amount of nanoscale organoclay can decrease the imidization temperature by 50 °C (from 300 °C to 250 °C), and at 250 °C the imidization time decreased by 15 min. The activation energy decreased by 20%. Clearly, the organoclay surface is acting as a catalyst.

2.4.2.3 Polypropylene and Polyethylene Matrices

Nonpolar polymers are very difficult to intercalate into smectic clays, because the clays are strongly polar. This challenge has been met [191, 192] by first intercalating stearylamine into montmorillonite and synthetic mica. Melt-mixing the organoclays with maleic anhydride-modified polypropylene oligomers results in PP-MA intercalation. The modified organoclay is then melt-mixed with a polypropylene matrix. There is a balance between creating a polar oligomer with enough maleic anhydride to intercalate well, but nonpolar enough to mix with the polypropylene. Unfortunately, the oligomer limits the extent of property improvement achieved to date. Polyethylene has also been successfully melt-mixed with modified montmorillonite and saponite after ion exchange with dioctadecyldimethylammonium bromide. The degree of dispersion is not excellent, and the layers are certainly not exfoliated; yet, significant modification of both the crystal structure and properties has been observed [143].

2.4.2.4 Liquid-Crystal Matrices

Smectic clay/liquid crystalline nanocomposites exhibit interesting optical properties [193, 194]. Upon initial formation, the composites are opaque, but when an electric field is applied they became transparent. To process these composites, montmorillonite was intercalated with lauryl ammonium or 4-(4'-cyanobiphenyl-4-oxy) butyl ammonium (CBAM), or 4-cyano-(4'-biphenyloxy) undecyl ammonium cation and solution-mixed with a nematic crystal matrix such as 4-pentyl-4'-cyanobiphenyl (5CB) and nematic TFALC (a mixture of low-molar-mass liquid crystals).

2.4.2.5 Polymethylmethacrylate/Polystyrene Matrices

The processing of clay/PMMA or clay/PS composites was first done by directly intercalating the monomer into the clay, followed by polymerization [195]. This method was not successful in exfoliating the clays. At issue again is the compatibility between the clay and the monomer. One solution for PMMA has been to use appropriate ammonium salts [196, 197], which may be reactive [198]. Another solution is to use a comonomer as a compatibilizer [199]. A similar solution was found for polystyrene by using

the reactive cationic surfactant vinylbenzyldimethyldodecylammonium as the intercalant [200]. Exfoliated graphite/polystyrene composites have been made by similar processing methods [80]. Recently, a commercially viable process was developed [180] for polystyrene in which montmorillonite intercalated with octadecyl trimethyl ammonium chloride was melt-mixed with a styrene methylvinyloxazoline copolymer. This process resulted in complete exfoliation, which could not be achieved with pure polystyrene [201]. The hypothesis is that the hybridization is due to strong hydrogen bonding between the oxazoline groups and oxygen groups in the silicate clays.

2.4.2.6 **Epoxy and Polyurethane Matrices**

Epoxy is a widely used thermoset, with applications ranging from household glues to high-performance composites. To improve performance, increasing the Tg of epoxy and improving its properties above the Tg are desirable. Adding clays and layered silicic acids to epoxy [6, 71, 202–204] can greatly improve its mechanical performance, particularly at temperatures above Tg. The processing has been studied in detail [71, 205]. In the smectic clay/epoxy composites, the length of the intercalated organic amine determines the ease of exfoliation, and only clays with primary and secondary onium ions form exfoliated nanocomposites [71, 206]. After intercalation of the organic amines, the epoxy resin or a combination of resin and curing agent can be intercalated into the smectic clays or layered silicic acids. If enough resin and curing agent are intercalated and the curing process is controlled, exfoliated nanocomposites result. Figure 2.23 shows a diagram of the process [207]. The acidic onium ions catalyze the intragallery polymerization or curing of the resin. If this reaction occurs more rapidly than extragallery curing, then the clay exfoliates. Otherwise, an intercalated nanocomposite results. Therefore, careful control of temperature and time is required [71], or the ratio of resin to curing agent must be significantly less than the stoichiometric ratio [205] in order to achieve exfoliation. An approach similar to that used for epoxy composites was used to make intercalated montmorillonite/polyurethane composites [208].

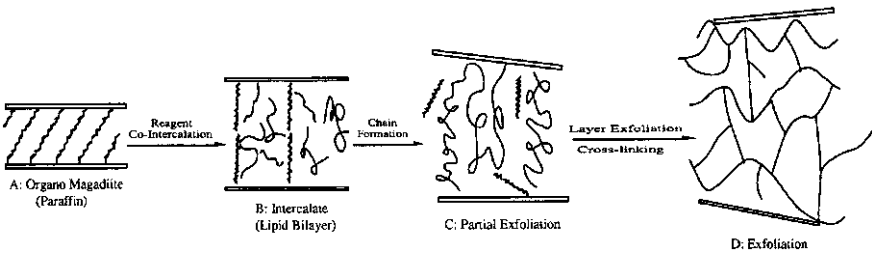

Fig. 2.23 Proposed pathway for formation of an epoxy-exfoliated magadiite nanocomposite: (A) Initial organomagadiite with a paraffin-like gallery structure of onium ions and neutral amine. (B) Reorientation of the alkylammonium ions into a lipid-like bilayer structure to accommodate the cointercalation of epoxide and curing agent. (C) Rapid intragallery formation of a polymer gel and expansion of the gallery height beyond a lipid-like layer. (D) Silicate nanolayers are completely exfoliated in a fully crosslinked epoxy polymer network. Reprinted with permission from [207]

2.4.2.7 Polyelectrolyte Matrices

Polyelectrolytes can be used in electrochemical devices such as solid-state batteries, electrochromic devices, and sensors [209]. The addition of layered silicates to polyelectrolytes increases the conductivity, improves the mechanical stability, and improves the interfacial stability with electrode materials. Polyelectrolytes are characterized by a large number of ionizable groups and thus are highly polar. This makes them excellent candidates for intercalation into smectic clays. Polyvinylpyridines are of particular interest because of the variety of processing methods available [210]. Intercalated nanocomposites can be formed easily from the water-soluble hydrobromide salt of the 1,2 or 1,6 polyelectrolyte (1,2 or 2,6 polyvinylpyridinium cations). However, only a single layer of polymer intercalates, and exfoliation does not occur. A slower, but ultimately more effective process, uses neutral poly-4-vinylpyridine and results in an exfoliated composite. A second method involves intercalation of 4-vinylpyridinium salts, followed by polymerization.

Poly(ethylene oxide) (PEO) matrix composites have also been processed both by intercalating PEO in solution into organically modified smectic clays [209] and by melt- mixing clay with PEO and PEO/PMMA mixtures [211,212]. In neither case does an exfoliated composite result. Aranda and Ruiz-Hitzky [209] dissolved PEO in acrylonitrile and found that the structure of the PEO changed when the interlayer cation was changed. Use of Na^+ montmorillonite or NH_4^+ montmorillonite resulted in either a helical PEO or a bilayer zigzag PEO structure in the galleries. The PEO arrangement was reversible with exchange of the interlayer cations.

2.4.2.8 Rubber Matrices

Several applications of rubbers might benefit from inclusion of exfoliated clays. Their greatly reduced permeability [213] would be useful for the inner liners of tires and inner tubes [214]. In addition, modification of the glass transition temperature and/or the loss modulus might be useful in a variety of damping applications. Montmorillonite has been ion-exchanged with a protonated form of butadiene and acrylonitrile copolymer. This was subsequently mixed with nitrile butadiene rubber in the presence of crosslinking agents and resulted in highly dispersed nanocomposites. Nanocomposites have also been prepared from dioctadecyldimethyl ammonium-exchanged montmorillonite in poly(styrene-*b*-butadiene) matrices [215].

Silicone rubbers have also been successfully intercalated into smectic clays. Burnside and Giannelis [216] intercalated Na^+ montmorillonite with dimethylditallow ammonium bromide and then sonicated in a silanol-terminated poly(dimethylsiloxane) (Mw = 18,000) with a tetraethyl orthosilicate and tin 2-ethylhexanoate crosslinking agent. Hexadecyltrimethylammonium bromide has also been used successfully as the intercalating agent [217]. Recently, a latex method was developed in which unmodified clays were mixed with a rubber latex, leading to improved properties over solution intercalation [218].

2.4.2.9 Others

Clay/polymer nanocomposites that include poly(ε-caprolactone) have been made via in-situ polymerization [7]. Composites that include poly(p-pheylenevinylene) have been made via intercalation of poly(xylylenedimethylsulfonium bromide) and subsequent elimination of the dimethylsulfide and HBR [219]. Those including cyclic polycarbonate [220] or polyethyleneterephthalate have been made via monomer intercalation and subsequent polymerization [221]; and those including polyaniline via in-situ polymerization of aniline monomer [222].

2.4.3 Nanoparticle/Polymer Composite Processing

There are three general ways of dispersing nanofillers in polymers. The first is direct mixing of the polymer and the nanoparticles either as discrete phases or in solution. The second is in-situ polymerization in the presence of the nanoparticles, and the third is both in-situ formation of the nanoparticles and in-situ polymerization. The latter can result in composites called hybrid nanocomposites because of the intimate mixing of the two phases.

2.4.3.1 Direct Mixing

Direct mixing takes advantage of well established polymer processing techniques. For example, polypropylene and nanoscale silica have been mixed successfully in a two-roll mill [5], but samples with more than 20 wt. % filler could not be drawn. This is typical and is a limitation of this kind of processing method. Nanoscale silica/PP composites have been processed in a twin-screw extruder, but the dispersion was successful only after modification of the silica interface to make it compatible with the matrix [223]. A Brabender high-shear mixer has been successfully used to mix nanoscale alumina with PET, LDPE [224]. Thermal spraying has also been successful in processing nanoparticle-filled Nylon [142]. When these traditional melt-mixing or elastomeric mixing methods are feasible, they are the fastest method for introducing new products to market, because the composites can be produced by traditional methods. This has been successful in many cases, but for some polymers, the viscosity increases rapidly with the addition of significant volume fractions of nanofiller, which in turn can limit the viability of this processing method.

In addition to viscosity effects, nanoparticles can either enhance or inhibit polymer degradation. One method for measuring degradation is to place the polymer in a high-shear mixer and measure the torque as a function of time and temperature. As the material crosslinks, the torque begins to increase (at a constant speed), and when chain scission begins, the torque decreases. This leads to a peak in the torque, whose position is often used as a measure of the degradation time. A recent study on ZnO/LDPE composites showed that, for nanoparticle/matrix mixtures, the time at the peak increased by a factor of almost 2 [224]; however, micrometer-size particles decreased the degradation time. In other instances, the catalytic nature of the nanoparticles greatly decreases the degradation time [225]. Whether degradation is inhibited or en-

hanced depends on the particle surface activity and the increased interfacial area (particle size).

2.4.3.2 Solution Mixing

Some of the limitations of melt-mixing can be overcome if both the polymer and the nanoparticles are dissolved or dispersed in solution. This allows modification of the particle surface without drying, which reduces particle agglomeration [226]. The nanoparticle/polymer solution can then be cast into a solid, or the nanoparticle/polymer can be isolated from solution by solvent evaporation or precipitation. Further processing can be done by conventional techniques.

2.4.3.3 In-Situ Polymerization

Another method is in-situ polymerization. Here, nanoscale particles are dispersed in the monomer or monomer solution, and the resulting mixture is polymerized by standard polymerization methods. One fortunate aspect of this method is the potential to graft the polymer onto the particle surface. Many different types of nanocomposites have been processed by in-situ polymerization. A few examples are silica/Nylon6 [227, 228], silica/poly 2-hydroxyethylmethacrylate [229], alumina/polymethylmethacrylate [230], titania/PMMA [231], and $CaCO_3$/PMMA [232]. The key to in-situ polymerization is appropriate dispersion of the filler in the monomer. This often requires modification of the particle surface because, although dispersion is easier in a liquid than in a viscous melt, the settling process is also more rapid.

2.4.3.4 In-Situ Particle Processing – Ceramic/Polymer Composites

An interesting method for producing nanoparticle-filled polymers is in-situ sol–gel processing of the particles inside the polymer. The process has been used successfully to produce polymer nanocomposites with silica [233] and titania [234] in a range of matrices [235]. The overall reaction for silica from tetrethylorthosilicate (TEOS) is shown below.

$$Si(OC_2H_5)_4 + \text{excess } H_2O \rightarrow SiO_2 + 4C_2H_5OH$$

The composites can be formed in one of several ways. In the first method, a copolymer of the matrix polymer and silica precursor are mixed, and the sol–gel reaction is allowed to progress. Figure 2.24 shows an example of the process for silica/polystyrene composites [233]. During drying, the polymer blocks phase-separate and the silica regions coalesce. A second approach mixes a silica precursor such as TEOS [236] with a polymer such as polyvinylacetate [237], polyetherimide [238], or polymethylmethacrylate [239]. For example, a recent paper on the processing of TiO2/poly(styrene maleic anhydride) resulted in excellent dispersion of TiO_2 in PSMA [234]. Direct addition of TiO_2 to a PSMA solution resulted in serious aggregation. Therefore, PSMA was dissolved in THF, and then tetrabutyl titanate was added under the appropriate conditions. Because the uncondensed TiOH and maleic anhydride could react, the polymer

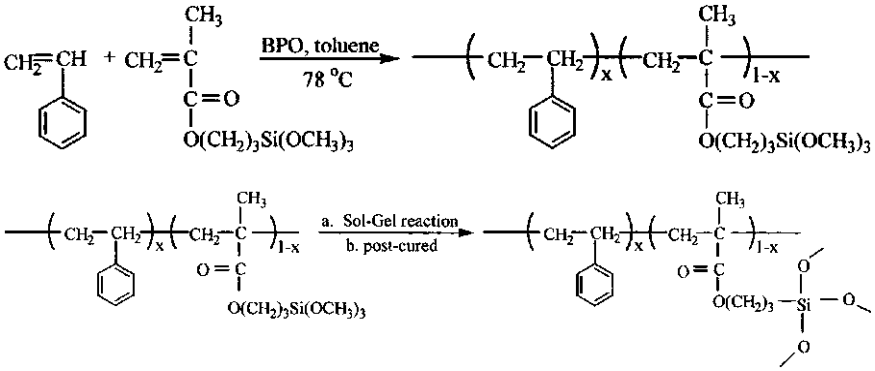

Fig. 2.24 Example of in-situ synthesis of silica particles in polystyrene. Reprinted with permission from [233]

coated the titania particles as they formed and prevented agglomeration. A combination of these first two methods has been used for silica/polydimethylsiloxane (PDMS) composites in a two step process. First, an unfilled PDMS network was formed, with TEOS as the end-linking agent. The network was then swelled with TEOS and the sol–gel reaction was catalyzed [240]. Significant work on determining the parameters affecting particle size has been accomplished with this method [241].

Finally, the polymer and ceramic can be polymerized simultaneously, and composite materials ranging from a few percent to 100% inorganic phase can be formed [242]. For example, silica/polyacrylate nanocomposites were formed with the simultaneous polymerization of HEMA (2-hydroxyethyl methacrylate) and tetraethoxysilane (TEOS) [229]. This resulted in a continuous interpenetrating network of silica and polyacrylate. There is a rich chemistry here that has been reviewed elsewhere on the processing of materials that range from glasses to polymers [243, 244] in which there is little if any phase separation between the organic and inorganic. We focus here on systems with discrete, isolated phases.

An interesting variation on in-situ formation of nanoparticles and polymerization is CVD deposition of nanocomposite films [245]. Here, the chemical precursors are modified separately and are mixed only just before deposition. Dichloro-*p*-xylylene was used as a precursor for poly(dichloro-*p*-xylyene), and diacetoxydi-tert-butoxysilane was used a precursor for silica. The resulting microstructure has discrete polymer and silica phases. This method is promising for the creation of interlayers with a low dielectric constant.

Barium titanate/polymer nanocomposites have also been prepared in situ by mixing a titanium alkoxide with a polymer and then casting and drying films. The films are then reacted with an aqueous solution containing barium, resulting in nanoscale barium titanate particles within a polymer matrix [246, 247]. Making the precursor and the polymer compatible improves the degree of dispersion, and using compounds that tend to form micelles can introduce controlled heterogeneity [246].

Nanosized calcium phosphate particles have been processed by an in-situ deposition technique in the presence of polyethylene oxide (PEO) or PEO/PVAc mixtures [248].

In this method, a polymer-calcium chloride complex is blended with trisodium phosphate. As the phosphate and chloride ions diffuse through the polymer, a gel-like precipitate forms. This can be separated; the size and morphology can be varied by changing the polymer and/or the polymer concentration.

2.4.3.5 In-Situ Particle Processing – Metal/Polymer Nanocomposites

Metal/polymer nanocomposites have also been processed via in-situ formation of metal particles from suitable metal precursors. The reaction occurs in the presence of a protective polymer, which limits the size of the particles. Figure 2.25 [249] shows a reduction scheme that uses a gold precursor and polypyrrole. Once a stable suspension of metal particles is prepared in the presence of a polymer, the composite can be cast, or additional monomers, of the same or a different polymer type, can be added to form a nanocomposite.

Mayer [250] wrote an excellent review paper on the processing of metal/polymer nanocomposites via in-situ methods in 1998. She reviewed the parameters that affect particle size, stability, and morphology. Several primary parameters controlled the particle size, including the choice of metal precursor and the metal/polymer interaction. For example, if $PdCl_2$ is compared with $(NH_4)_2PdCl_4$, the former tends to form halogen-bridged complexes and thus tends to form agglomerates of nanoparticles, but the latter does not. The interaction of the metal precursor with the polymer is also important. If the polymer has a stronger interaction with the precursor, then the particle size tends to be reduced [251], because the metal precursors are prevented from phase separating. In general, because most polymers are hydrophobic, precursors with a more hydrophobic character result in stronger interactions and thus smaller particle size. Complicating this situation is the ability of the polymer to form a stable suspension in solution. The rate of reduction affects the particle size, with faster reduction methods resulting in smaller particles [252, 253].

Another method giving more specific control over particle size and morphology is the use of either micelles formed from amphiphilic block copolymers (ABC) [254] or crosslinked/gelled matrices. For example, through the use of crosslinking and gelation

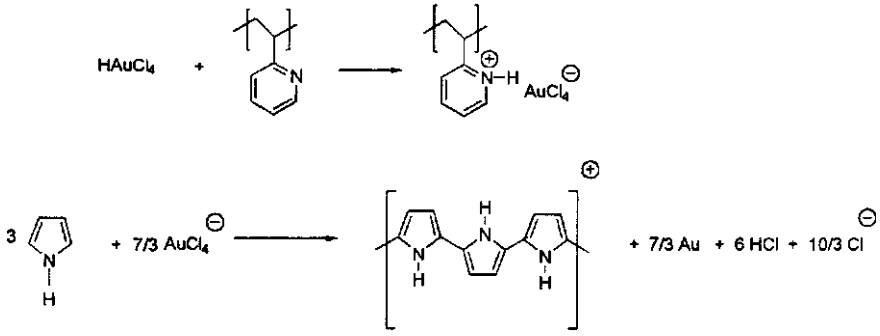

Fig. 2.25 Schematic of reaction leading to in-situ gold particles in a polymer. Reprinted with permission from [249]

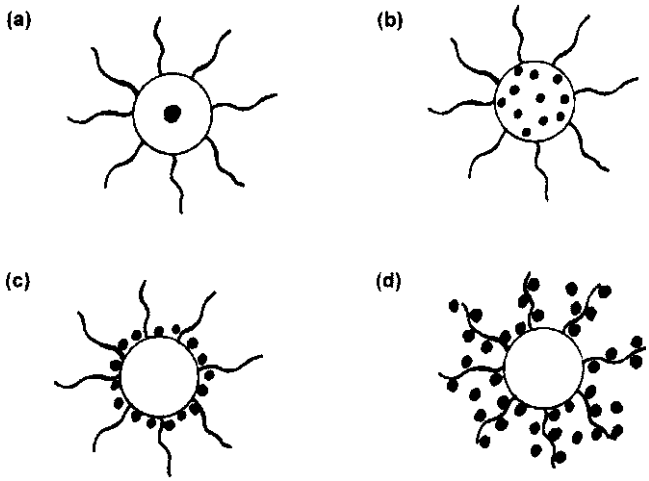

Fig. 2.26a Overall morphologies of block copolymer-metal systems involving spherical micelle formation of the amphiphilic block copolymers: (a) cherry morphology, (b) raspberry morphology, (c) strawberry morphology, (d) proposed red currant morphology. Reprinted with permission from [250]

reactions, dendritic gold particles can be formed [255]. Amphiphilic block copolymers provide another avenue of control. Here, block copolymers are used to form micelles. Metal salts then either penetrate into the micelles or are stable in the micelle corona. The reducing agent can be added, and metal particles form either within the micelles or in the corona, resulting in several morphologies shown schematically in Figure 2.26a [250]. Figure 2.26b [294] shows an example of the raspberry morphology for Pd colloids in a polystyrene-b-poly (4-vinylpyridine) block copolymer matrix that was reduced with hydrazine. Changing the block length can control the particle size.

This same principle is applicable to other block copolymer morphologies, such as rods and layers, and leads to interesting morphologies. One thing that is not clear, and needs to be addressed by theory, is which of these morphologies will lead to the best properties. Because of the range of metal particles that can be formed, including gold, silver, palladium [256], platinum, semiconductors [257], and metal oxides [234], tremendous opportunity exists to tune the properties of these systems.

Other methods are available for producing metal nanoparticle-filled polymers, such as deposition of a metal film onto the polymer [258, 259] and subsequent annealing to form particles, or electrochemical methods [260], both of which lead to highly controlled thin-film composite structures.

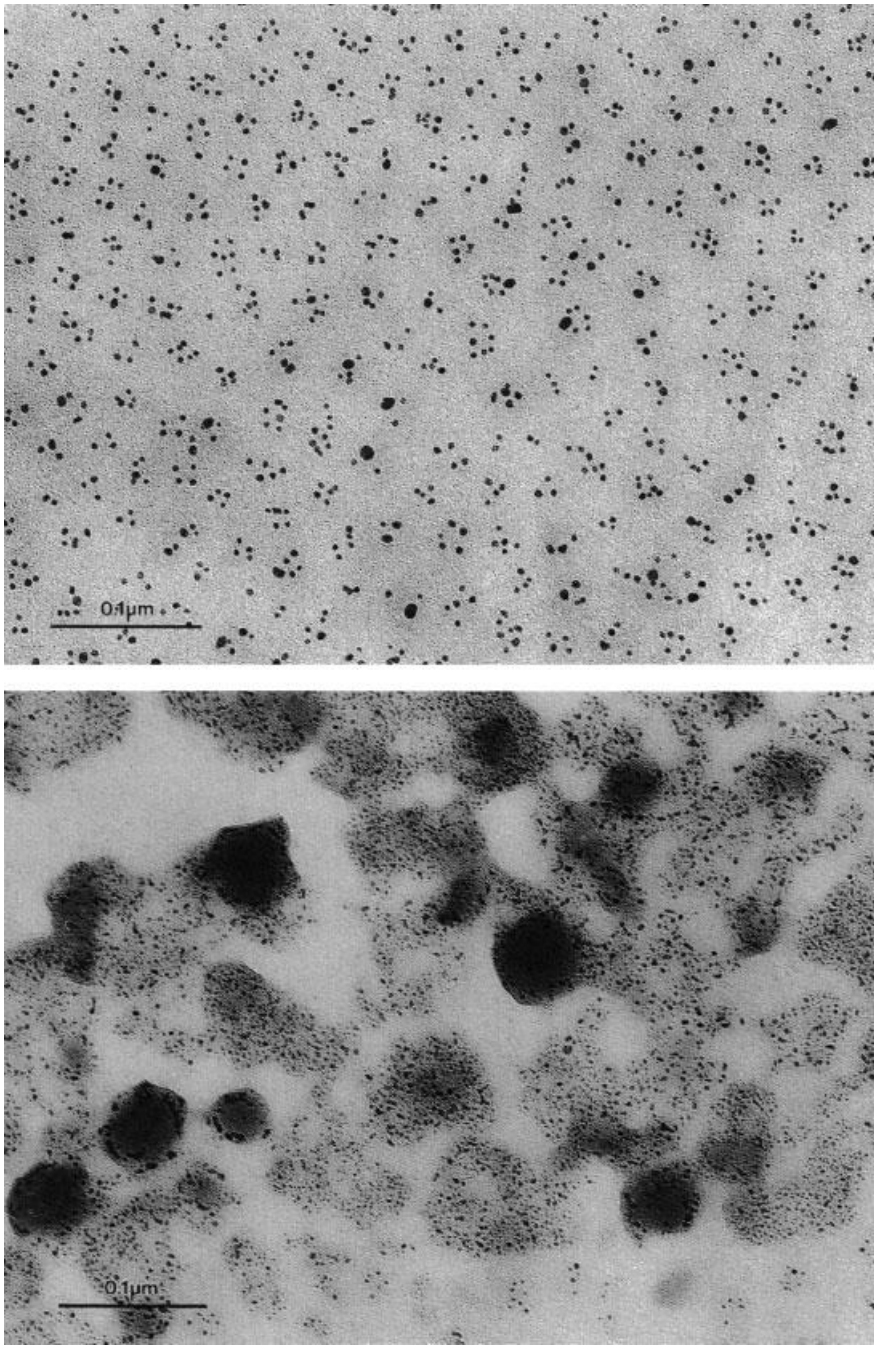

Fig. 2.26b Electron micrographs of Pd colloids synthesized in Ps-*b*P4VP block copolymers via reduction with hydrazine. Reprinted with permission from [253]

2.4.4 Modification of Interfaces

Literature on the modification of interfaces of traditional composite fillers is extensive. Many of the methods, however, are not directly applicable to nanocomposites for several reasons. Carbon and glass fibers are usually coated as long fibers on a spool, which is not practical for nanofibers. In addition, methods that require drying the particles are not appropriate for metal oxide and metal nanoparticles, because during drying (even at only 100 °C), they may agglomerate significantly. Freeze-drying methods are more appropriate. Although describing the relevant chemical processes is important for understanding nanofiller interface modification, this section focuses primarily on the results of modification, instead of on the detailed chemistry.

2.4.4.1 Modification of Nanotubes

Several reasons exist for modifying nanotubes. The first is to render them more dispersible in solution, thus providing a route toward further functionalization or use in applications. The second is to improve the interaction of the nanotubes with polymer matrices. Modifying the surface activity of MWNT has focused primarily on doping them with other elements. Doping MWNT with boron has resulted in changes in the electronic states [261, 262] and formation of a p-type semiconductor. In addition, boron substitution, as well as other electron-rich substitutions, may very well lead to out-of-plane bonding configurations that increase the reactivity of the surface with a polymer matrix. Nitrogen doping of MWNT creates an n-type semiconductor and leads to a bamboo-like structure having ordered regions connected via disordered regions [263]. The nitrogen creates nitrogen-rich cavities in the otherwise graphitic nanotube. Preliminary work has shown that nitrogen doping changes the interface enough to improve the dispersion of nanotubes and results in enough bonding with epoxy matrices to increase the glass transition temperature by 20° as well as in increased modulus and strength [264]. In addition, acid treatments and subsequent chemical reactions can lead to attachment of epoxy groups or even particles to MWNT [265, 266].

SWNT are assembled as ropes or bundles. To maximize their interaction in a polymer matrix, they need to be chemically modified and separated from the bundles. One way to increase the chemical activity is to use an SWNT with a smaller radius of curvature [267]. A second method is to add functional groups to the ends of SWNT. Carboxylic groups have been linked to SWNT ends, and then the SWNT have been tethered to nanoparticles via thiol linkages [268–270]. SWNT have been placed in solvent through the addition of octadecylamine groups on the ends and a small amount of dichlorocarbenes on the sidewalls [271]. The first successful method for adding functional groups to the sidewalls involved fluorination at elevated temperatures. The tubes could then be solvated in alcohols and reacted with other species, particularly strong nucleophiles such as alkylithium reagents [272]. A simpler route based on a process used on other carbon species [273, 274] was developed, in which an aryl diazonium salt was reduced electrochemically, resulting in a free radical that can attach to the carbon surface of small diameter tubes [271] (Figure 2.27).

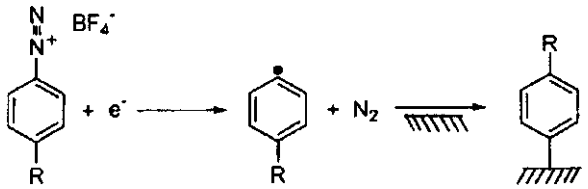

Fig. 2.27 Electrochemical reduction of an aryl diazonium salt to yield, giving a reactive radical that covalently attaches to a carbon surface. Reprinted with permission from [271]

The most exciting development in terms of composites, however, is the dissolution of full-length SWNT that have been separated from the bundles [275]. Given the issues of slipping of nanotubes within a bundle discussed earlier, their use in composites requires separation from the bundles. The process involves, first, partially breaking up the SWNT bundles in an acidic solution. Carboxylic acid groups are then added to the ends of the tubes. Finally, the SWNT are placed in an octadecylammonium (ODA) melt for several days. This results in exfoliated nanotubes. This important result should eventually lead to SWNT/polymer composites with the SWNT separated in the polymer, which will provide an avenue for taking advantage of the extraordinary properties of SWNT.

The development of methods to attach polymers to nanotubes has progressed significantly. First, separation of the nanotubes from their aggregates is required. This separation can be achieved by dispersion in the appropriate solvents with or without the aid of a surfactant [276] and/or by choosing an appropriate synthesis method. A polymer chain can then be attached to a bonding site by sonication [277], plasma activation [278], chemical etching of the tube ends [279], or chemical adsorption [280]. These advances should lead in the near future to some very interesting copolymers with SWNT as one block in the polymer and a rich interfacial chemistry. Some evidence suggests that polymers can be patterned by the nanotube surface, providing a method for templating polymer structures near the surface [281]. It is not clear yet what role this interface control will have in terms of properties of composites, but to develop technology that fully exploits the properties of nanotubes in composites, control over the interface is required.

2.4.4.2 **Modification of Equi-axed Nanoparticles**

A recent review by Frank Caruso [282] provides extensive background on the modification of nanoparticle surfaces. He cites two primary methods for modifying an inorganic nanoparticle surface with organic molecules. The first requires connecting a short-chain molecule such as a siloxane onto the surface through grafting or strong hydrogen bonding. The second involves application of a coating by polymerizing a polymer onto the nanoparticle. In addition, inorganic coatings can be applied.

2.4.4.3 **Small-Molecule Attachment**

Both metal and metal-oxide nanoparticles are readily modified with small molecules. They tend to have hydroxyl groups on the surface, although the number of hydroxyl groups and the strength of the metal-OH bond varies. The most common method

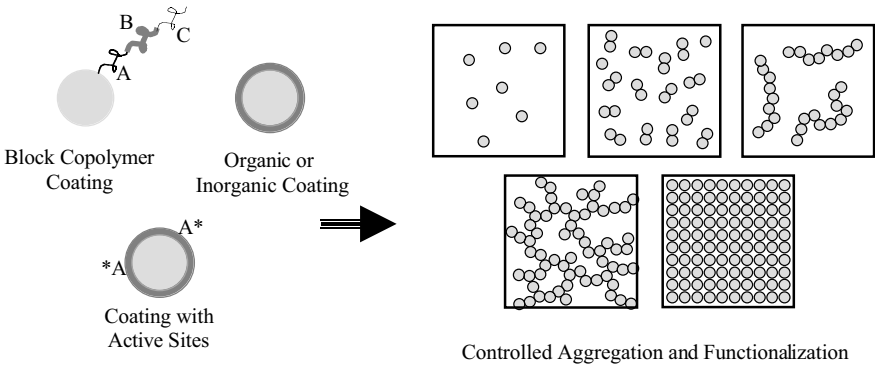

Fig. 2.28 Schematic summarizing many of the possibilities for modifying equi-axed nanoparticles

takes advantage of a long history of modifying metal-oxide glass fiber or filler surfaces. The hydroxyl group on the nanoparticle surface reacts with a silane coupling agent. The relative ease of the reaction depends on the nature of the nanoparticle surface (basicity vs. acidity). The silane coupling agent can have a large variety of functionalities attached to the silanol to modify the surface. The chains can be long or short, hydrophilic or hydrophobic, and linear or bulky. This provides tremendous flexibility in choosing a coupling agent. Changing the coupling agent can lead to control over the strength of the interaction between the filler and the matrix, from covalent bonding to repulsion. The change in bonding leads to increases or decreases in both glass transition temperature and the modulus, but large effects occur only for particles much less than 100 nm [128].

Of course, reacting with molecules other than silanes is also common. Nanoscale titania has been coupled with chelating agents such as lauryl sulfate [283] and with carotenoids (natural pigments) containing a terminal carboxylate group that reacts with OH groups on the surface [284].

One creative study underway provides a method for placing one, two, or several active functional groups on the surface of nanoparticles, followed by passivation of the rest of the particle. This will result in controlled aggregation of the particles into dimers, chains, or branched chains [285] (Figure 2.28).

2.4.4.4 **Polymer Coatings**

Historically, polymer coatings have provided control over the compatibility of the polymer with the matrix and the strength of the interaction. The coating can be grafted onto the surface of the particle or just highly adsorbed. After the particles are coated they can be dispersed easily in a matrix of similar chemistry to make low-volume-fraction composites. The exciting news is that controlling interfacial interactions has moved well beyond single-component coatings. The possibility for assembling coated nanoparticles directly into useful structures, the core-shell approach, has driven significant development in multicomponent organic and inorganic coatings. The possibilities of this approach seem almost endless. We currently know how to graft or strongly adsorb

several types of polymers onto a surface. In addition, we know how to polymerize polymers with very monodisperse molecular weight and we know how to make block (di and tri) copolymers [286]. Progress has also been made in placing inorganic coatings onto particles. This provides flexibility in our ability to engineer the surface of the particles being placed in composites. No longer will the coating be only for controlling the extent of the interaction, for it may contain several layers. The role of the first layer may be to bond with the surface. The second layer may provide electrical, mechanical, or optical functionality, and the third layer may make the particle compatible with the matrix and help in controlling the properties. The final layer may have some reactive sites that could be used to bond particles together and lead to controlled aggregation of the nanoparticles (Figure 2.28).

In principle, polymer coatings can be produced on organic and inorganic particles by a variety of polymerization methods. Monomer adsorption and subsequent polymerization, heterocoagulation – polymerization [287], and emulsion polymerization [288] have been demonstrated on micrometer-scale filler surfaces [287], although not all have been applied to nanoparticles. Monomer adsorption has been used successfully in several studies, and initiation has occurred both chemically [289] and via irradiation [290]. One recently reported method can be used to place nanoparticles (in this case fumed silica) into a monomer such as styrene or methylmethacrylate. The mixture is

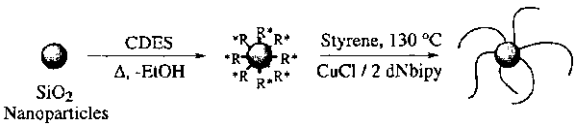

Fig. 2.29a Synthetic scheme for structurally well defined polymer-nanoparticle hybrids. Reprinted with permission from [292]

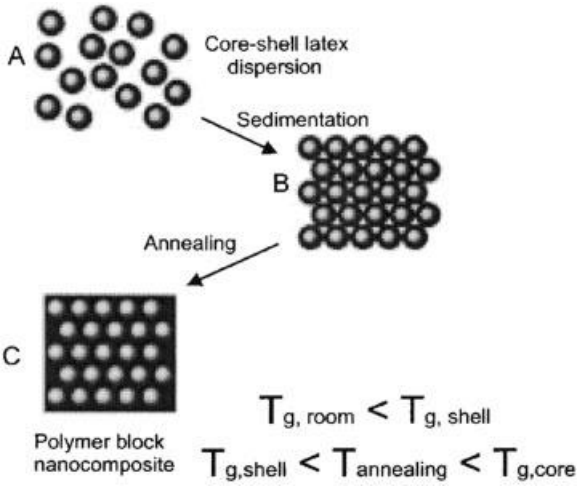

Fig. 2.29b Proposed approach to formation of 3-D polymer nanocomposite material. Stage A: synthesis of the core-shell latex particles with hard functionalized cores and soft inert shells. Stage B: assembly of latex particles in a 3-D close-packed structure. Stage C: heat treatment of the 3-D compact structure, which leads to flow of soft shells and formation of a nanocomposite polymers. Reprinted with permission from [294]

then irradiated [290]. The monomer penetrates the silica aggregates, and after grafting, the surfaces are more hydrophobic and blend more easily with polymers such as polypropylene. This treatment leads to more uniform distribution of the particles and greatly enhanced composite ductility. In some cases, the polymer is not directly grafted onto but interacts strongly with the surface via hydrogen bonding. For example, carboxylic acids are strongly adsorbed to alumina. If the acid contains a polymerizable group, then after adsorption, a polymer can be grown from the molecule attached to the surface. This has been shown for maleic acid adsorbed onto a surface and was used to attach AIBN-initiated 1-octadecene polymers to the surface [291].

Another method that leads eventually to a composite with an ordered array of nanoparticles involves grafting an initiator onto the surface of the nanoparticles and then polymerizing a grafted polymer onto the surface [292]. If living radical polymerization is used, then the particles can be processed into a composite without additional matrix, to make high-volume-fraction composites with particles in an ordered array. Figure 2.29a shows this for silica particles with grafted polystyrene packed into an ordered matrix [292]. This process lends itself nicely to block copolymer coatings and even triblock copolymers. Another method that can lead to multilayer structures is the use of self-assembled polymer layers in a 'layer-by-layer colloid templating strategy' [293]. Here, charged polymers are adsorbed onto charged particles, resulting in a coated particle with surface charge. A second charged polymer can then be exposed to the previously charged particles. When this polymer is adsorbed, the surface charge of the particle is reversed, and the particles have a bilayer coating. This method can be repeated and enables careful control of the coating thickness and functionality.

A similar core–shell approach has been used to coat a low-Tg polymer onto a high-Tg latex particle. The coated polymer particles were then taken out of solution and annealed to create an ordered array of polymer in polymer [294] (Figure 2.29b). The concept applies to coated nanoparticles other than latex as well.

2.4.4.5 **Inorganic Coatings**

Inorganic coatings have also been applied to submicrometer particles via either precipitation of the inorganic coating onto the particles or deposition via a sol–gel type process. With these methods, silica [295], yttria [296], titania [297], titanium nitride [298], and zirconia [299] have all been applied to support particles, usually other metal oxides. The advantage of such coatings is that the nanoparticles (both organic and inorganic) can be coated with inorganics for further functionalization. For example, conducting coatings can be applied, and the optical properties can be tuned.

Sonochemistry can also be used to apply inorganic coatings in much the same way as described above for the processing of nanoparticles. For example, ZnS coatings (1–5 nm) on colloidal silica have been prepared in this way [300].

2.5 Properties of Composites

2.5.1 Mechanical Properties

One of the primary reasons for adding fillers to polymers is to improve their mechanical performance. For example, the addition of high-modulus fillers increases the modulus and the strength of a polymer. In traditional composites, unfortunately, this often comes at the cost of a substantial reduction in ductility, and sometimes in impact strength, because of stress concentrations caused by the fillers. Well-dispersed nanofillers, on the other hand, can improve the modulus and strength and maintain or even improve ductility because their small size does not create large stress concentrations. In addition, the large interfacial area of nanocomposites provides an opportunity for altering the matrix properties in unique ways. This section highlights the potential effect of nanofillers on the modulus, failure stress/strain, toughness, glass transition, and wear behavior of polymers.

2.5.1.1 Modulus and the Load-Carrying Capability of Nanofillers

In traditional composites, the modulus can be predicted, within bounds, and the mechanism that leads to a change in modulus is load transfer. For example, if a high-modulus filler is added to a lower-modulus polymer, then load transfers from the matrix to the filler, leading to an increase in modulus. One important question for nanocomposites is how load is transferred from the matrix to the filler. This is a complicated question, because in some nanocomposites the polymer chain and filler are almost the same size, and in others, the fillers are atomically smooth, with few functional groups to which the polymer can bond. The importance of load transfer is easily illustrated with the shear lag discussion commonly applied to graphite fiber/polymer composites. Figure 2.30a shows a stress – strain curve for a typical high-modulus fiber, a thermoplastic matrix, and the resulting composite. At a given applied composite strain, the fiber carries more load than the matrix; therefore stress must be transferred from the matrix to the fiber. Figure 2.30b shows the stress-transfer behavior on the micromechanical level. At the fiber end (or at a fiber break) the fiber does not carry stress. Stress is transferred via a shear stress at the filler/matrix interface, and the rate of load transfer depends on the shear stress. This highlights the role of the interface in controlling the modulus of filled polymers. For example, the higher the interfacial shear stress and the shorter the load transfer length, the more efficient the filler is in carrying load and the higher the composite modulus. In addition, the higher the aspect ratio of the filler, the longer the length that carries the maximum load, and the higher the composite modulus.

To fully understand the modulus of nanocomposites, a second mechanism in addition to load transfer must be considered. For example, the filler can constrain the mobility of the polymer chains as well as their relaxation spectra [120], which can change the glass transition temperature [120, 121] and modulus of the matrix. Nano-

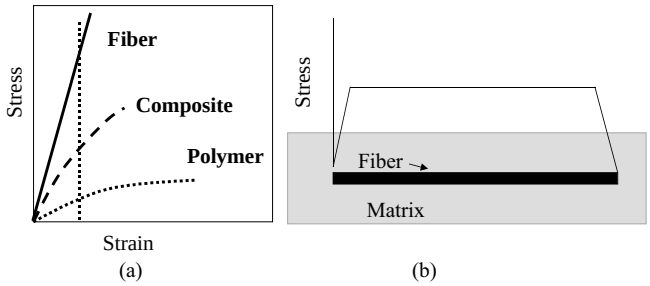

Fig. 2.30 Schematics of (a) stress vs. strain curve for a typical high modulus fiber, a thermosetting polymer, and the resulting composite, (b) transfer of strain from the matrix to the fiber near the fiber end

fillers can also change the degree or type of crystallinity in a polymer, which also changes the modulus [140, 141]. These two mechanisms of reinforcement are addressed for each geometry of nanofiller below.

Nanotubes

Consider nanotube-filled polymer composites. The modulus of nanotubes may be significantly higher than that of any graphite fiber, and therefore, they have the potential to yield higher composite moduli at the same filler volume fraction than a graphite fiber composite. In addition, because of their small size, if properly dispersed, nanotubes may not decrease the strain-to-failure. But, how is load transferred to a nanotube? Qian et al. [148] and Yu et al. [28] have shown, as first described by Wagner [29], that MWNTs fail via a sword-and-sheath mechanism (see section 2.2.1). This implies that, even if load is transferred to the outermost nanotube in a MWNT, the inner tubes slide within the concentric cylinder and do not carry much load. This situation limits the efficiency of MWNT/polymer composites, because only a small portion of the volume fraction of the MWNT carries load. Evidence for this was shown for MWNT/polystyrene composites, in which the effective modulus of the MWNT in the composite was only 500 GPa [148] but the measured modulus of the MWNT is close to 1TPa. Therefore, to minimize the number of layers not carrying load, 2–3 layers are preferable.

For SWNT composites, the SWNT are in a bundle and, as was suggested earlier, individual SWNTs may slip within the bundle. Work by Yu et al. [27] showed that, if only the nanotubes on the outer edge of a SWNT in a bundle are used to calculate the modulus, it is close to the predicted 1 TPa. However, if the whole area of the bundle is used, the calculated modulus is considerably lower. This suggests that, until the SWNT are isolated from the bundles or the bundles are crosslinked, the modulus of composites made from these materials will be limited. Fortunately, progress is being made in obtaining significant volume fractions of exfoliated nanotubes [279].

A final issue of relevance is the waviness of the nanotubes. If they are not straight when placed in the composite, then, as recently reported [301], the modulus of the composite is significantly decreased.

Clays

Plate-like fillers can also increase the modulus of a polymer significantly. A comparison of the upper bound modulus prediction (assuming incompressibility) shows that the modulus for well-aligned platelets can be three times that for well-aligned fibers [302]. In addition, there is direct evidence that nanoclay carries load; for example, as the aspect ratio of the clay layers increases, the modulus increases. Some indirect evidence [303] also shows that the stiffness of the clay layers affects the modulus (e.g., a stiffer filler leads to a higher composite modulus). Neither of these observations is surprising if the clay platelets are carrying load. Other studies, however, suggest that the modulus increase is not entirely due to the load-carrying ability of the platelets, but is caused by the volume of polymer constrained by the platelets [174]. This suggests that, to optimize the increase in modulus, the degree of dispersion must be optimized to maximize the degree of matrix/filler interaction. Work on PP nanocomposites [304], in which adding maleic anhydride (MA) to the matrix changed the degree of filler dispersion, supports this suggestion. Despite the plasticizing effect of MA, the modulus improved, due to enhanced dispersion of the clay. Additional evidence [305] (Figure 2.31) relates the interlayer spacing to the modulus. Lan and Pinnavaia [202] found that, as the degree of exfoliation increased by changing the length of the alkylammonium intercalating chain, the modulus and strength improved. As the polymer intercalates and swells, the layers and the area of interaction between the polymer and the filler increase, and the modulus increases significantly.

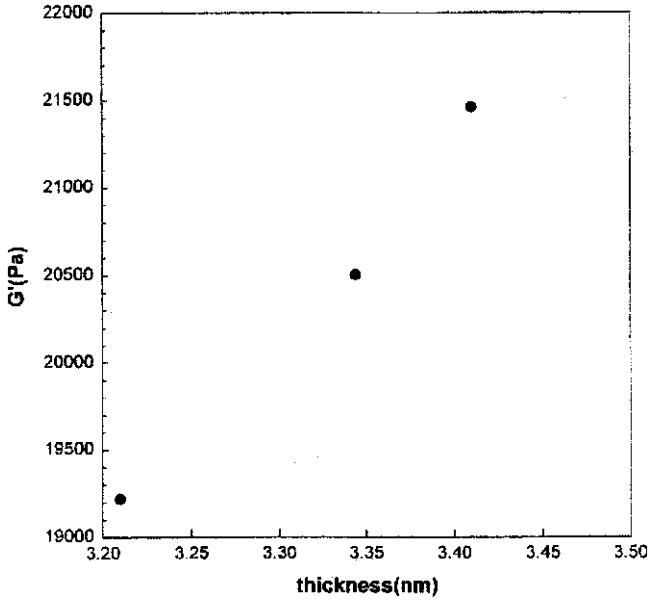

Fig. 2.31 Relationship between storage modulus and interlayer spacing during the melt intercalation process. Reprinted with permission from [305]

The specific role of the clay/polymer interface in controlling the modulus is also becoming clearer. An interesting study on the modulus of clay/Nylon 6 composites examined the modulus as a function of the ionic strength (as measured via ^{15}N-NMR chemical shifts) of the clay [182] (Figure 2.32). Another study determined the types of matrix/filler interactions responsible for modulus changes [306] (Figure 2.33). Using short-chain alkylammonium ions minimized the type-B interactions, allowing more of the polymer (epoxy) to interact directly with the clay surface (type-A interactions). Direct interaction of the matrix with the clay basal planes led to a larger increase in the modulus. It is not clear if the modulus increase caused by the type of interaction and/or the ionic strength is due to an increase in the interfacial shear stress (the load-bearing efficiency of the clays), the ability of the clay to constrain the polymer, or increases in the degree of crystallinity. These effects are all related, and the exact mechanism is still an open question.

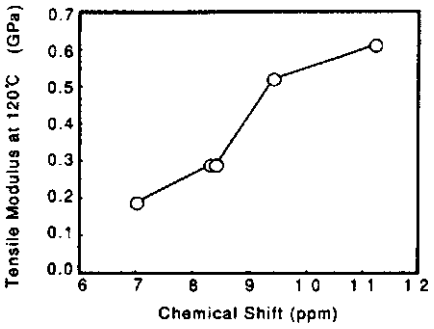

Fig. 2.32 Relationship between strength of polymer/filler interaction as measured by ^{15}N-NMR shift and the tensile modulus at 120 °C of clay/nylon hybrids. Reprinted with permission from [182]

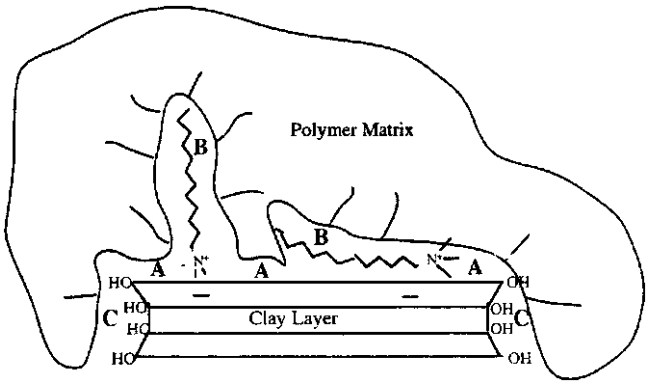

Fig. 2.33 Schematic of the types of interfacial interactions occurring in polymer-organoclay nanocomposites including direct binding (adsorption) of the polymer to the basal siloxane oxygens (type A), "dissolving" of the onium ion chains in the polymer matrix (type B), and polymer binding to hydroxylated edge sites (type C). Reprinted with permission from [206]

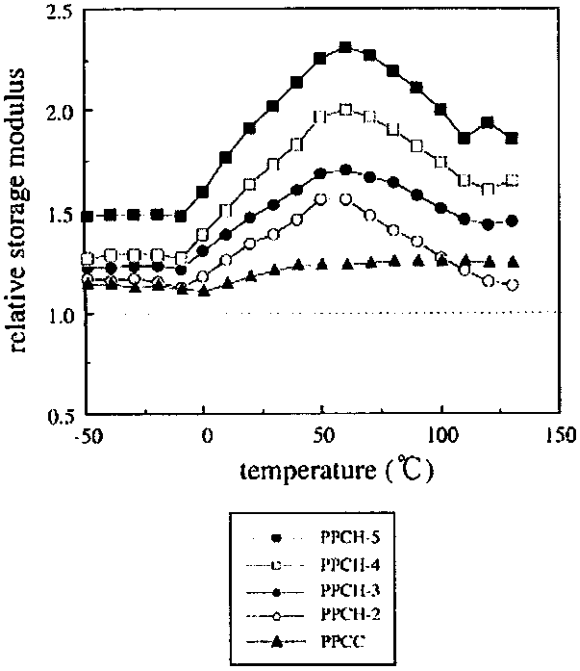

Fig. 2.34 Relative dynamic storage modulus of polypropylene clay hybrids as a function of temperature at filler loadings of 2–5 wt. percent. Reprinted with permission from [304]

Further evidence that the polymer/clay interaction plays a significant role in controlling mechanical behavior is that the improvement in properties tends to be higher above the glass transition temperature than below it [307]. Figure 2.34 shows this explicitly for montmorillonite/modified PP matrix composites. Below Tg, the modulus increases by a factor of 2, and above Tg it increases by a factor of 2.5. This behavior is also seen for epoxy matrices. When a brittle epoxy with a Tg well above room temperature was reinforced with organically modified montmorillonite (OMMT), the increase in modulus at room temperature was modest. In contrast, when an epoxy with a Tg below room temperature was used as the matrix, the modulus (and strength) improved by a factor of 10 at 15wt. % of filler [202]. A strong clay/polymer interaction affords more opportunity for immobilization above Tg than below Tg. In addition, if the surface area for interaction decreases, the modulus decreases. This result was also observed in OMMT/polyimide composites. The modulus increased by 1.4 over that of unfilled polyimide, but at higher volume fractions it started to decrease, presumably due to aggregation of the filler [308].

Equi-axed nanoparticles

The size scale for equi-axed nanoparticle/polymer composites ranges from hybrid nanocomposites, in which the matrix and filler are so intimately mixed that they are no longer truly distinct, to discrete particles in a continuous matrix. We focus here on discrete fillers more than approximately 5 nm in diameter. The matrix significantly influences changes that occur in modulus and strength. For example, in

alumina/PMMA composites, the modulus decreased for very weak particle/polymer interactions [127]. In silica/polystyrene composites in which the particle was grafted to a polymer chain, however, the modulus increased [129]. In addition to the reinforcing effect that the particles can contribute, the increase or decrease in modulus is also related to the effect of the particles on the polymer's mobility. Changes in the Tg are strong evidence that polymer mobility is significantly altered. Tg increases for strong polymer/filler interactions and decreases for weak interactions [129]. Given the sensitivity of the polymer modulus to the temperature relative to Tg, changes in Tg can lead directly to changes in modulus. A third mechanism, namely localized yielding near the particles, may also decrease the modulus at very low and seemingly macroscopic elastic strains.

2.5.1.2 **Failure Stress and Strain – Toughness**

The addition of rigid micrometer-scale fillers to a polymer often increases its strength, but decreases the toughness. This tradeoff is a significant technical problem for commercial applications of filled polymers. The reason for the decrease in ductility is straightforward: the fillers or agglomerates act as stress concentrators, and the defects initiated at the filler quickly become larger than the critical crack size that causes failure.

Well-dispersed nanoparticles are much smaller than the critical crack size for polymers and need not initiate failure. Thus, they provide an avenue for simultaneously toughening and strengthening polymers. Proper dispersion is critical for achieving this. For example, Hasegawa et al. [307] studied the dispersion of clays in polypropylene. When they achieved exfoliation, the strain-to-failure ratio remained high (>200%) at loadings as high as 3%, but even a small amount of aggregation decreased the strain-to-failure ratio to 5%–8%. Another example is polyimide matrices, in which the exfoliation is not complete and the strain-to-failure ratio decreases by 72% with just 1% of OMMT [308]. Further addition of OMMT causes further aggregation and a precipitous drop in the strain-to-failure ratio. Many authors report an optimum volume percent of filler and claim that the decrease in strain-to-failure ratio above the optimum is due to agglomeration [147].

Although the small size of nanoparticles, based on the explanation above, should not decrease the strain-to-failure, it also should not cause the observed increases in the strain-to-failure [127]. Clearly, there is a second mechanism operating. The lack of discussion on toughening polymers with rigid particles means we must turn to the literature on rubber toughening of polymers to obtain hints about the second mechanism. An excellent review on rubber toughening [309] provides the background required for this discussion. First, the toughness of a material can be defined as the energy to cause failure. This is related to the deformation in the material, but also to the volume of material undergoing deformation. Even brittle amorphous polymers such as polystyrene and polymethylmethacrylate have the potential for large deformation, but the volume of material undergoing deformation is small. Material must first strain-soften after yielding and eventually strain-harden. If the material does not strain-soften, then defects in the material lead to stress concentrations that cause

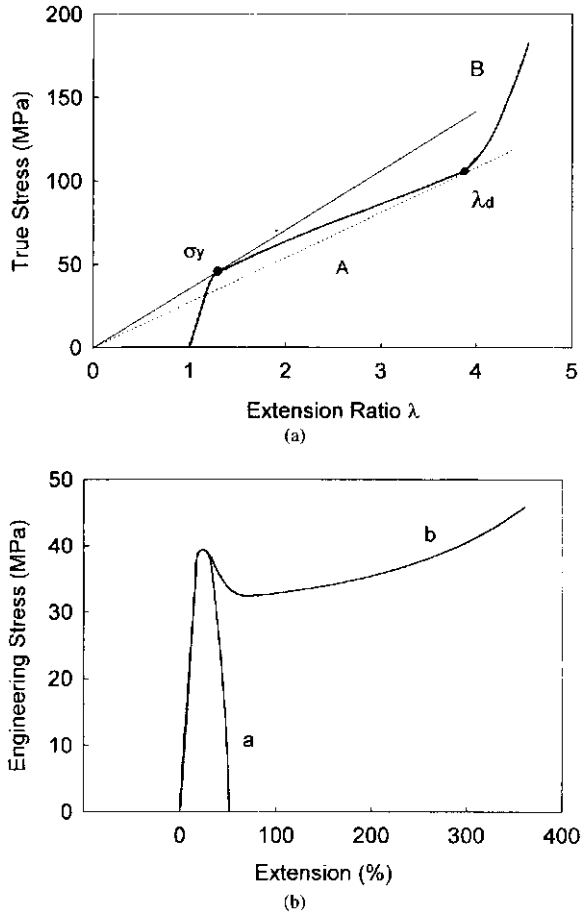

Fig. 2.35 Schematic of Considere's construction. True stress is plotted against extension ratio, and tangents are drawn through the origin. The first tangent defines the strain at which the tensile load reaches a maximum (the engineering yield stress, σ_y). The second tangent marks the point at which strain hardenening stabilizes the neck (the natural draw ratio λ_d). Failure at point A between the two tangents gives a low extension to break (curve a). Failure beyond the second tangent gives curve b. Reprinted with permission from [309]

catastrophic brittle failure. If strain softening occurs prior to strain hardening, then the strain-hardened region draws a larger volume of material into the deformation zone and a large strain-to-failure results. If strain softening occurs, but not strain hardening, the initially strain-softened material propagates the crack. Figure 2.35 [309] illustrates all three scenarios with Considere's construction.

Plastic deformation and strain hardening can occur via two different mechanisms: crazing and shear yielding. Crazing is the result of dilatational strains that cause an increase in volume and subsequent drawing of the material between the voids (fibrils). Thus, strain softening occurs due to dilatational strains in front of a craze tip and at the craze/matrix boundary, and strain hardening occurs, which allows drawing and strain hardening of the material in the craze. In principle, this allows the crazes to thicken and the volume of deformed material to increase significantly. Unfortunately, in many brittle amorphous polymers, failure initiates at the craze/bulk polymer interface and the volume of deformed material is small.

Shear yielding also results in strain softening and strain hardening and can result in stable neck formation and significant toughness. Due to the large change in shape that shear stress causes, a triaxial stress state forms in the center of the sample, which can lead to void formation and crack growth.

In rubber particles having a shear modulus <0.1 that of the matrix, the yield stress decreases due to the stress concentration caused by the soft rubber (which is essentially a void in terms of stiffness). If the particle does not cavitate, then the only effect of the addition is to delocalize the stress and allow a significant volume of material to yield and to limit craze formation. This effect leads to modest improvements in strain-to-failure and toughness and may occur at a critical interparticle spacing [310]. If, on the other hand, the rubber particle cavitates, then the stress state in the matrix between particles is biaxial or uniaxial and can lead to significant drawing (strain hardening) of the matrix. By this mechanism, large volumes of matrix are drawn into the deforma-

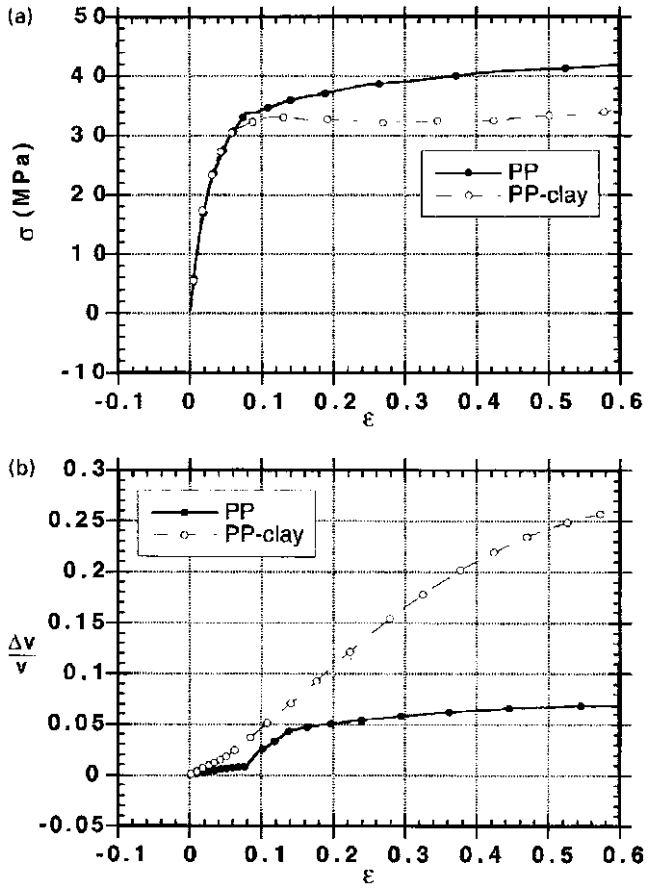

Fig. 2.36 (a) True stress–true strain curves at room temperature for PP-based materials. (b) Corresponding volume strain versus elongation for the PP-based materials. Reprinted with permission from [311]

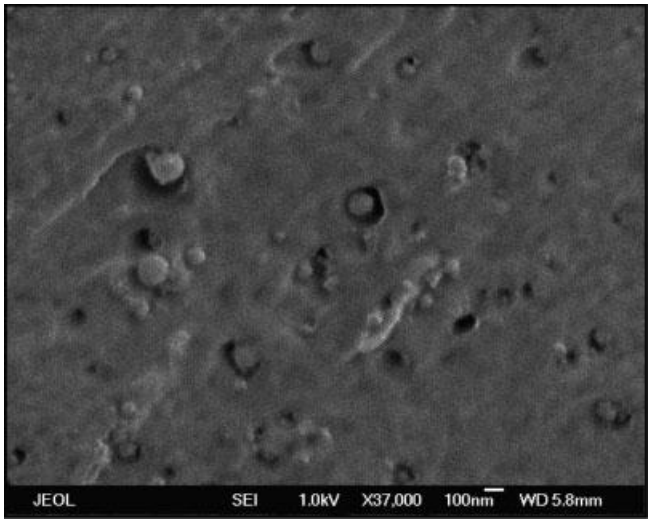

Fig. 2.37 Field-emission electron micrograph showing cavitation surrounding weakly bound 39 nm alumina particles in PMMA. (Thanks to B. Ash for this micrograph)

tion zone and toughening occurs. In addition, the rubber particles strain-harden and thereby strengthen the most highly deformed regions, allowing a large volume of material to participate in the deformation process.

How does this apply to nanoparticle-filled polymers? First of all, if the particle/polymer interaction is weak, then the nanoparticles can essentially act as voids, which initiate yield and allow for shear bands to form and then thicken. Evidence of this mechanism is provided by several studies. Video extensometry was used to monitor the volume strain as well as the true stress-vs.-strain behavior of clay-filled PP and nylon 6 [311]. The results are fascinating. The typical failure mechanism for nylon is shear banding, but the addition of well-dispersed montmorillonite encouraged cavitation. This added another mechanism of deformation and increased the volume of material involved in deformation. Figure 2.36 shows a graph of the volumetric strain, as well as a scanning electronmicrograph of the fibrillation. Interestingly, this result occurred only for weak polymer/clay interactions or for strong interfacial interactions at temperatures above Tg. In addition, crystalline alumina-filled PMMA [127] with weak particle/polymer interactions exhibited an order of magnitude increase in the strain-to-failure. Evidence for cavitation was seen via fractography (Figure 2.37).

Another example in which nanoparticle inclusions lead to significant improvements in strain-to-failure and/or toughness is rubber matrices. Here, even if the interaction between the particle and polymer is strong, the soft material around the particle can easily lead to interface failure. In rubbery epoxy, the strain-to-failure is maintained for exfoliated nanocomposites [202] and can be improved by using magadiite to reinforce relatively ductile epoxy [207]. The addition of OMMT to polyurethane improved the strain-to-failure by a factor of two [208]. This may be due to a plasticizing effect of

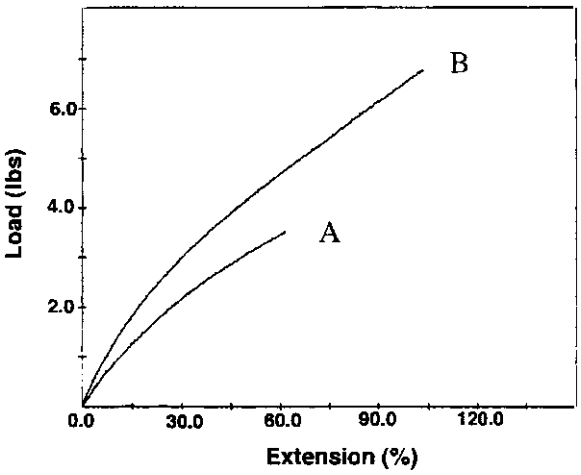

Fig. 2.38 Stress–strain curves for (a) a pristine polyurethane elastomer, and (b) a polyurethane-clay nanocomposite at a strain rate of 1.0 in/min. Reprinted with permission from [208]

the alkylammonium ions, but did not result in a decrease in strength or modulus. Figure 2.38 shows the stress – strain curve for a representative sample. Other investigators have found similar results [312], which can be maximized when the intercalating agent acts as a crosslinking agent.

2.5.1.3 Glass Transition and Relaxation Behavior

As discussed in section 2.1, the interfacial region is extremely large in nanocomposites. The interaction of the polymer with the nanoparticles gives significant opportunity for changing the polymer mobility and relaxation dynamics. For example, polystyrene chains intercalated between the layers of a smectic clay have more mobility locally than in the bulk polymer [313]. This greater mobility may be due to an ordering that occurs between the layers, which creates low- and high-density regions, thus providing the opportunity for mobility in the low-density regions [314]. If, however, the polymer is tethered to the clay, the relaxation spectra broaden to include slower relaxation times, suggesting that the clay can reduce the mobility locally. Recent work on silica/polyvinylacetate nanocomposites indicates that, for equi-axed particles, the overall effect of the filler is to create a weak network structure that contains both physical entanglements in the matrix phase and 'trapped' entanglements arising from temporary bonds to the filler particles. This suggests a greater far-field effect of altering chain dynamics than simply a local immobilization of the polymer chain [318]. Another example of altered mobility was found for gold particles dispersed in poly(*tert*-butylacrylate). For particle sizes <10 nm, the viscosity of the low molecular weight polymer at 30 vol. % filler increased by a factor of 4 [315]. The authors claim this result is due to bridging of the polymer chains between the particles. The bridges have relatively long lifetimes and decrease segmental motion at the interface compared to the bulk.

Although the specific mechanics of chain dynamics discussed above are not yet completely understood, it is very clear that the rheology/glass transition temperature of a polymer can be controlled by changing the polymer mobility with nanocomposite

interfaces. For example, the glass transition temperature can be eliminated for clay nanocomposites with intercalated polymer chains. This indicates a limited ability for cooperative chain motion when the polymers are confined between the layers [131]. If the clays are exfoliated, and thus the polymer is not confined between layers, the Tg does not change significantly.

Without the help of confinement, the Tg can be increased if the polymer is tightly bound to the nanofiller. Increases of 10° have been observed for clay-filled Nylon, PMMA, and PS [196], as well as for polyimide composites [308]. The behavior is not limited to clays. A Tg increase of almost 30° was observed for exfoliated graphite/polystyrene composites [80], as was a 20° increase for nitrogen-doped carbon nanotube/epoxy composites [264]. The Tg also changes in nanoscale equi-axed particle-filled composites. The addition of $CaCO_3$ to PMMA resulted in a 35° increase Tg at 6 wt. % filler when the composites were prepared via an in-situ process [232]. Smaller increases were observed for silica/PMMA [128] nanocomposites.

The Tg can decrease if the interaction between the filler and the matrix is weak, as has been observed with silica [128] and alumina-filled PMMA [316]. This decrease in Tg was recently given more attention in nanoalumina/PMMA composites, where it was found that the Tg did not decrease until a critical volume fraction was reached. Furthermore, changing the particle surface and making it compatible with the matrix eliminated the Tg depression.

The explanation for the increase or decrease in Tg in the thermoplastics may be related to the thin film results discussed in section 2.3.

Of course, chain dynamics affect much more than the glass transition temperature. Recent studies have attempted to understand the role of filler/polymer interaction, to begin to understand the role of nanofillers in controlling damping, melt rheology, and other dynamic processes [131, 317, 318].

2.5.1.4 **Abrasion and Wear Resistance**

Although it is well known that the abrasion resistance of filled polymers depends on particle size, the incorporation of nanoscale fillers has led to unexpected results. For filler particles that are larger than the abrasive particles, most of the filler particles are stable and increase the abrasion resistance of the composite. As the filler size is decreased to a size similar to that of the abrading particles, filler particles are removed, and the abrasion resistance is compromised. This does not happen on the nanoscale, however. For example, the addition of nanoscale $CaCO_3$ to PMMA resulted in a significant decrease (factor of 2) in material loss due to abrasion at only 3 wt. % of filler [232]. In addition, nanoparticles can simultaneously improve wear resistance and decrease the coefficient of friction. With larger-scale fillers, increased wear resistance is accompanied by an increased coefficient of friction, which has been observed for silica/Nylon [319] as well as for polyetheretherketone matrix composites filled with ZrO_2, SiC, SiO_2, and Si_3N_4 [320–323] and for sheet silicates in polyimide [324]. The coefficient of friction measured as dry sliding against steel decreased monotonically with increasing weight percent of fillers. The authors attributed this finding to an improved and tenacious transfer film that was generated on the counterface, an area that needs further exploration.

2.5.2 Permeability

The reduced gas and liquid permeability of nanofilled polymers makes them attractive membrane materials. The large change in permeability of liquid or gas through a composite material can be explained from simple predictions [325, 326]. Given a plate-like material with an aspect ratio of L/W dispersed parallel in a matrix, Nielson calculated the tortuosity factor τ as

$$\tau = 1 + (L/2W)V_f \tag{1}$$

where V_f is the volume fraction of plate-like filler. The relative permeability coefficient Pc/Pp, where Pc and Pp are the permeability coefficients of the composite and polymer matrix, respectively, is given by

$$Pc/Pp = 1 \;/\; (1 + (L/2W)V_f) \tag{2}$$

A slightly more rigorous analysis for a random in-plane arrangement of plates yields

$$Pc/Pp = 1 \;/\; (1 + \mu(L/W)^2(V_f^2/(1 - V_f) \tag{3}$$

where μ depends on the distribution of the plate-like material. In either case, the higher the aspect ratio of the filler, the larger is the decrease in permeability. Yano et al. [188] compared Eq. 2 to data on clay-filled polyimide (Figure 2.39) and found a good fit. The large reductions in permeability (Figure 2.39) occur at only 2 wt. % for exfoliated composites (Figure 2.40) [8]. The barrier, however, is sensitive to the degree of dispersion and the alignment of the plates. Significant reductions in permeability were also reported for exfoliated clay/PET [327], Nylon [328], and polycaprolactone [7] composites. The reduction is linear with the wt. % of filler for polycaprolactone [7], but for polyimide [8] (Figure 2.40), the decrease in permeability with wt. % of filler is nonlinear.

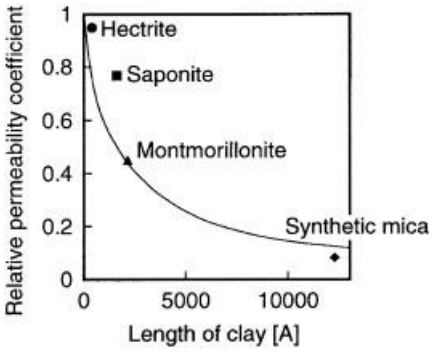

Fig. 2.39 Effect of clay layer size on relative permeability compared with the prediction from Eq. 4.2.2. for clay/polyimide nanocomposites. Reprinted with permission from [188]

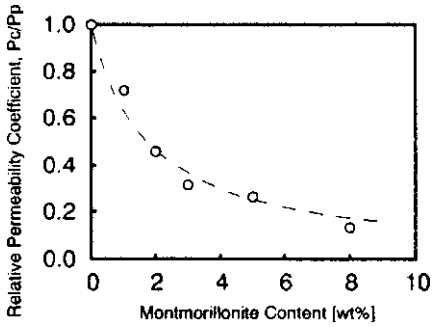

Fig. 2.40 Effect of montmorillonite content on relative permeability coefficient of water vapor in polyimide nanocomposites. Reprinted with permission from [8]

Several nanocomposites are being produced commercially for barrier applications [327]. They include a vermiculite clay/PET composite with oxygen permeation values of $\leq$1 cc m^{-2} d^{-2}, produced by ICI Corporation, which is significantly less than that of pure PET. Ube Industries produces a Nylon/clay hybrid whose permeability is less than that of Nylon by a factor of 2 at 2 wt. % filler.

Apparently, significant improvements in barrier properties are also achievable with nonplate-like nanoparticles [329]. Nano Material Inc. reports that a PVA/EVOH matrix composite with 7 nm silica and titania nanoparticles exhibits a gas permeability of 1 cc m^{-2} d^{-1} atm^{-1} and moisture permeability of less than 1 g m^{-2} d^{-1}. Although this is achieved at very high loadings, the material is melt processable.

The absorption of water into composites is significant. For example, one of the limitations of Nylon is the reduction in mechanical properties that accompanies the absorption of water. The addition of exfoliated montmorillonite increases the resistance to water permeation after 30 min from 2% to 1% at 5 wt. % of filler [330]. The mechanism of the reduction is attributed to the constrained region of the Nylon. If the constrained region is taken into account, the diffusion coefficient follows a rule of mixtures. Figure 2.41 shows the change in diffusion coefficient of water in Nylon in response to clay content.

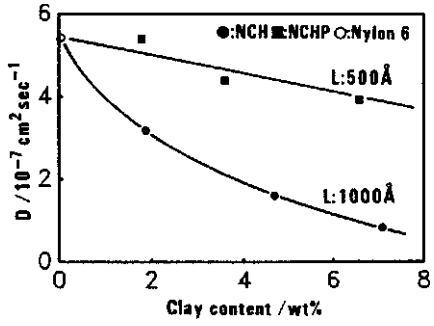

Fig. 2.41 Dependence of diffusion coefficient of water on clay content for montmorillonite with a layer width of 100 nm, and saponite with a layer width of 50 nm. Reprinted with permission from [330]

2.5.3 Dimensional Stability

Dimensional stability is critical in many applications. For example, if the layers of a microelectronic chip have different thermal or environmental dimensional stabilities, then residual stresses can develop that cause premature failure. Poor dimensional stability can also cause warping or other changes in shape that affect the function of a material.

Nanocomposites provide methods for improving both thermal and environmental dimensional stability. The first mechanism by which nanofillers can affect the coefficient of thermal expansion (CTE) of a polymer is also observed in traditional fillers. The composite CTE changes according to the volume average of the two CTEs. For traditional fillers, at low volume fractions of filler, this change in CTE is almost linear. Figure 2.42 shows the CTE for polyimide filled with exfoliated montmorillonite [8]. In contrast to traditional fillers, the dependence is nonlinear. This leads to the second mechanism effecting CTE – the interfacial region. It may be that the nonlinear effect is due to the increase in volume of polymer that is behaving similar to a thin film and has a lower CTE than the bulk matrix. Observations that, in thin films that interact with a substrate, the CTE decreases as the film thickness decreases below 10 nm [118] support this possibility.

Nonlinear dimensional changes are also observed for nanofilled rubbers that swell in the presence of a liquid. This is a well-known phenomenon [331] and is again due to the interfacial region around the particles, as discussed in section 2.3. The effect of this layer increases as the strength of the particle/polymer interaction increases [332]. The behavior is also observed in recently developed nanofilled rubbers. In comparisons of the behavior of montmorillonite/PDMS composites with other conventional aluminosilicates or carbon black [216], the relative swelling of the montmorillonite/PDMS composites was about half that of both unfilled PDMS and carbon black/PDMS. Meanwhile, kaolinite increased the swelling. The authors argued that the decrease in swelling is due to a bound polymer layer and that the large surface area and very strong polymer/filler interaction enhance swelling resistance. Reduced swelling was observed recently in nanoparticle titania/epoxy composites [147].

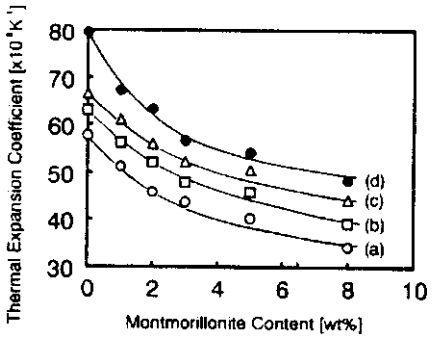

Fig. 2.42 Effect of montmorillonite content on thermal expansion coefficient of polyimide clay hybrids at (a) 150 °C, (b) 200 °C, (c) 250 °C, (d) 295 °C. Reprinted with permission from [8]

A recent paper described the addition of OMMT to the type of PMMA used in dental work [333]. Here, PMMA is added to MMA monomer, and the resulting mixture is polymerized under ultraviolet light. The shrinkage occurs largely during polymerization, which causes internal stresses and reduces the lifetime of the filling. The addition of OMMT to the PMMA/MMA mixture, however, reduces shrinkage considerably and thus lowers the stresses that form. This may provide an excellent method for increasing longevity.

2.5.4 Thermal Stability and Flammability

The first indications that nanoclays could increase the thermal stability of polymers was demonstrated in 1965 for montmorillonite/PMMA composites. The degradation temperature (defined as 50% mass loss) increased about 50 °C for a composite with only 10 wt. % PMMA (90 wt. % filler) [334]. More recently, the degradation temperature of PDMS was found to increase about 140 °C with 10 wt. % montmorillonite for a delaminated nanocomposite [216]. A 50 °C increase was found for intercalated clay/PE composites [143]. The dispersion of the clays is critical to increasing the degradation temperature. Delaminated composites have significantly higher degradation temperatures than intercalated nanocomposites or traditional clay composites [335]. Some speculate that this increase in stability is due to the improved barrier properties of the composites. If oxygen cannot penetrate, then it cannot cause oxidation of the resin [216]. In addition, the inorganic phase can act as a radical sink to prevent polymer

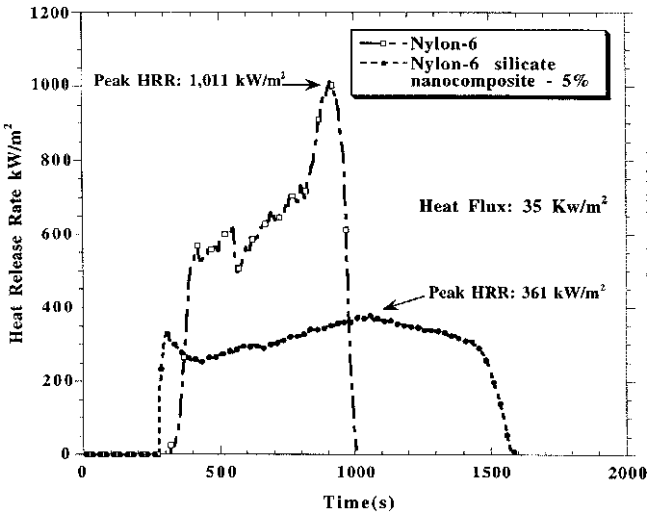

Fig. 2.43 Comparison of the heat release rate (HRR) plot for Nylon-6, Nylon-6 silicate-nanocomposite (mass fraction 5 percent) at 35 kW/m^2 heat flux, showing a 63 percent reduction in HRR for the nanocomposite. Reprinted with permission from [338]

chains from decomposing. The improved thermal stability of some composites may be limited by the lower thermal stability of alkylammonium ions. For example, in intercalated clay/polystyrene composites, the intercalating agent decomposes at about 250 °C. Bonding the intercalating ion to the polystyrene matrix noticeably improved the thermal stability. Polyimide [308] and polymethylmethacrylate [333] also become more thermally stable with the addition of OMMT.

In addition to thermal stability, the flammability properties of many clay/polymer nanocomposites are also improved [336, 337, 338]. Figure 2.43 shows typical plot of the heat release rate (HRR) vs. time for Nylon-6 and a clay/Nylon-6 nanocomposite with only a few wt. % of filler. The HRR increases at a lower temperature for the nanocomposite, but levels off quickly. Clay nanocomposites commonly show a 60 % reduction in peak HRR relative to unfilled polymer (Table 2.2). In addition, the mass loss rate is the same for the two materials until a char forms, and then the nanocomposite exhibits a significantly lower mass loss rate. Observation of the char suggests that the layered silicate collapses during combustion and forms a uniform layered structure (interlayer spacing about 1.3 nm). The layers act to reinforce the char and reduce the permeability of the char, reducing the rate of volatile product release. The structure of the char was fairly uniform for several different matrices and independent of the initial microstructure of the composite (intercalated or delaminated).

Combining traditional flame retardants with intercalated or exfoliated clays can result in further improvements in flame retardance [339, 340]. An additional advantage

Tab 2.2 Cone calorimeter data. Heat flux: 35 kW/m^2, Hc: heat of combustion, peak heat release rate, mass loss rate, and specific extinction area (SEA) data are reproducible to within ±10 %. The carbon monoxide and heat of combustion data are reproducible to within ±15 %. Reprinted with permission from [338].

Sample ***(structure)***	**Residue yield (%) ± 0.5**	**Peak HRR (Δ %) (kW/m^2)**	**Mean HRR (Δ %) (kW/m^2)**	**Mean H_c (MJ/kg)**	**Mean SEA (m^2/kg)**	**Mean CO yield (kg/kg)**
Nylon-6	1	1010	603	27	197	0.01
Nylon-6 silicate-nanocomposite 2 % *delaminated*	3	686 (32 %)	390 (35 %)	27	271	0.01
Nylon-6 silicate-nanocomposite 5 % *delaminated*	6	378 (63 %)	304 (50 %)	27	296	0.02
Nylon-12	0	1710	846	40	387	0.02
Nylon-12 silicate-nanocomposite 2 % *delaminated*	2	1060 (38 %)	719 (15 %)	40	435	0.02
PS	0	1120	703	29	1460	0.09
PS silicate-mix 3 % *immiscible*	3	1080	715	29	1840	0.09
PS silicate-nanocomposite 3 % *intercalated*	4	567 (48 %)	444 (38 %)	27	1730	0.08
PS w/DBDPO/Sb_2O_3 30 %	3	491 (56 %)	318 (54 %)	11	2580	0.14
PP	0	1525	536	39	704	0.02
PP silicate-nanocomposite 2 % *intercalated*	5	450 (70 %)	322 (40 %)	44	1028	0.02

of nanoclay composites relative to traditional flame retardants is the improvement in other properties, such as the heat distortion temperature and the bending modulus.

The flammability resistance of clay-filled polymers indicates that their ablation resistance might also be excellent. As a material is heated during ablation, the surface of the material reacts and forms a tough char. If the char is not reinforced, it fails and is removed from the surface, exposing more material [341]. Traditional composites require a significant weight fraction of filler (more than 30 wt. %) to achieve significant ablation resistance. On the other hand, 2 – 5 wt. % nanoclay-filled Nylon 6 exposed to a mock solid rocket motor firing rig formed a layer of char on the surface that was tough and significantly retarded further erosion [341]. In addition, oxygen plasma forms a passivation layer on Nylon 6/layered silicate nanocomposites, which significantly retards further erosion of the composite surface [342]. This behavior is not a strong function of the organic molecules used to modify the clay or the strength of the clay/polymer interaction [342], but is a function of the degree of exfoliation [341].

2.5.5 Electrical and Optical Properties

The electrical and optical properties of nanofilled polymers are exciting areas of research. This is particularly true because of the possibility of creating composites with unique combinations of functionalities, such as electrically conducting composites with good wear properties that are optically clear. Such properties can result because nanoparticles, with diameters distinctly below the Rayleigh scattering limit, still display their solid-state physical properties when embedded in transparent matrices.

Optical composites have been defined as composites consisting of optically active nanoparticles embedded in a transparent host material, often a polymer [343]. Optical composites take advantage of the optical properties of materials that are hard to grow in single-crystal form or that require protection from the environment and give them the ease of processing afforded many polymers. In addition, sometimes the material must be used at the nanoscale to achieve specific optical properties, and the matrix is used just to hold the particles together and provide processability. For example, high-grade optical composites, with properties otherwise obtainable only in optical glasses, become accessible through the use of polymer molding techniques.

The following sections briefly review some of the literature in this area.

2.5.5.1 Resistivity, Permittivity, and Breakdown Strength

Electrical properties are expected to be different when the fillers get to the nanoscale for several reasons. First, quantum effects begin to become important, because the electrical properties of nanoparticles can change compared to the bulk. Second, as the particle size decreases, the interparticle spacing decreases for the same volume fraction. Therefore, percolation can occur at lower volume fractions. For example, the high aspect ratio of carbon nanotubes or exfoliated graphite leads to percolation at a lower volume fraction and thus increases in electrical conductivity of polymers at a

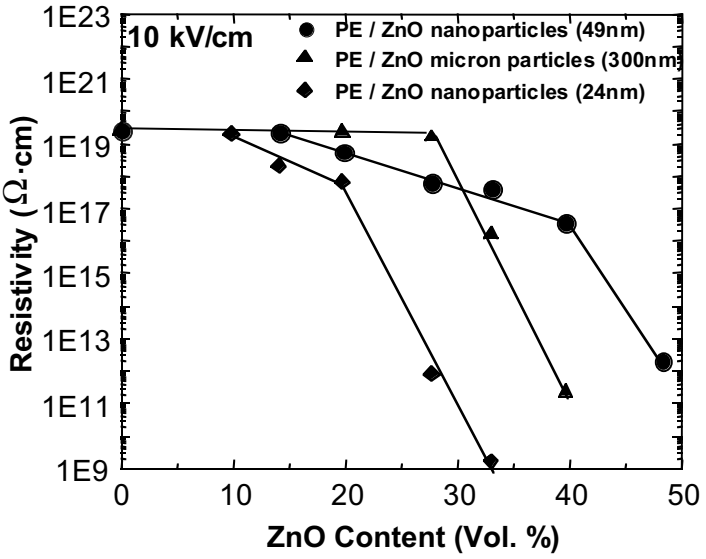

Fig. 2.44 Resistivity vs. volume fraction for nanoscale and micrometer scale ZnO filler in low density polyethylene. (Thanks to J. Hong for this figure)

lower volume fraction than in nonexfoliated graphite [80]. This can be understood from geometric considerations. Figure 2.44 [344] shows an example of this behavior for ZnO-filled low-density polyethylene. In addition, the rate of resistivity decrease is lower than in micrometer-scale fillers. This is probably due to the large interfacial area and high interfacial resistance.

The permittivity of polymers can also be increased with the addition of many metal oxide fillers, on both the micro- and nanoscale. The use of micrometer-scale fillers for this application, however, results in a significant decrease in breakdown strength due the field concentration created by the particles. One of the significant advantages of using nanoscale fillers instead of micrometer-scale fillers may be a reduction in the loss in breakdown strength. The breakdown strength decreases for micrometer-scale fillers because of the field concentration the particles create. Nanoscale fillers do not lead to as large a reduction in breakdown strength. Preliminary results using ZnO/low-density polyethylene composites show that at 50 wt. % of filler, the breakdown strength of the nanofilled LDPE is about 10% higher than that of LDPE filled with submicrometer ZnO [344]. In addition, fundamental to controlling the breakdown strength of insulating polymers is the cohesive energy density [345] and the free volume or mobility of the polymer [346].

Nanotubes can also be used to change the resistivity. Recently, such a behavior was demonstrated in a conjugated luminescent polymer, poly(*m*-phenylenevinylene-co-2,5-dioctoxy-*p*-phenylenevinylene) (PPV), filled with MWNT and SWNT. Nanotube/PPV composites have shown large increases in electrical conductivity compared to the pristine polymer, of nearly 8 orders of magnitude, with little loss in photolumi-

nescence/electroluminescence yield. In addition, the composite is far more robust than the pure polymer with respect to mechanical strength and photo-bleaching properties (breakdown of polymer structure due to thermal buildup). Preliminary studies indicate that the host polymer interacts weakly with the embedded nanotubes but that the nanotubes act as nanometric heat sinks. Recent experimentation with composites of conjugated polymers such as PPV and nanotubes, show a promising new phenomenon. Apparently, the polymer chains wrap around nanotubes suspended in dilute solutions of the polymer. Microscopy suggests that coiled polymer chains can interact strongly with nanotubes and assemble on the nanotubes, leading to the creation of unique interfaces affecting the electronic and optical properties of the polymer [347].

An interesting example of how nanocomposites may affect electronics is the development of photo-patternable hybrid inorganic–organic polymers with negative resist behavior. They are composed of inorganic oxidic structures that are cross-linked or substituted by organic groups. They are synthesized from organosilane precursors reacted by sol–gel processing in combination with organic cross-linking of monomers. The processing is often integrated with micro-patterning technologies to fabricate dielectric and passivation layers in microelectronic systems and devices as well as cladding for optical applications [348].

2.5.5.2 Optical Clarity

A limitation in the development of optical composites or transparent nanocomposites with improved mechanical or electrical performance is minimizing light scattering due to the presence of the particles. The scattering power for light propagation through a collection of scattering particles can be predicted by Rayleigh scattering:

$$P_{scat} - 24\,\pi^4\,P_o\,\rho\,(\,(n' - n)/n^2)\,(V^2/\lambda^4)$$

Where P_o is the incident power, ρ is the concentration of particles, n' is the refractive index of the particles, n is the refractive index of the matrix, V is the volume of a single particle, and λ is the wavelength of light. Therefore, to minimize scattering, the particles must be as small as possible with an index of refraction as close as possible to that of the matrix material. This equation assumes, however, that the particles are much smaller than the wavelength of light, and if this is not true, Rayleigh–Debye calculations are required [349].

Relatively good optical clarity has been obtained in many nanocomposites, particularly at low volume fractions. Studies on PMMA modified with n-dodecylmethacrylate during polymerization were shown to maintain optical clarity up to 10 wt. % of bentonite [199]. In addition, when exfoliation was achieved in polyimide matrix composites, the 2 wt. % hybrid was relatively transparent [8] compared to nonexfoliated clay. A comparison between smectic clays and magadiite (a layered silicic acid) shows that magadiite results in much better optical clarity than smectic clay, probably due to index of refraction matching [203]. Optically clear nanofilled polyurethanes have also been prepared [208]. The addition of UV-absorbing nanoparticles have been used to create a clear coating on polymers to prevent degradation Figure 2.45 shows a quantitative

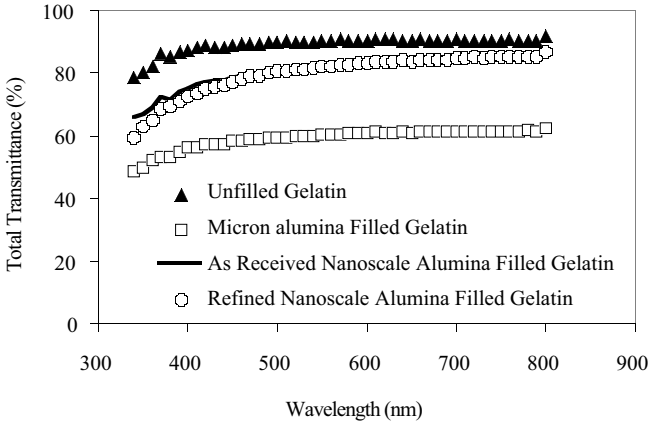

Fig. 2.45 Optical transmittance vs. wavelength for a nanoscale alumina-filled gelatin at 17 wt. percent filler. (Thanks to G. Irvin, Q. Chen for this figure [350])

example of the transmission achieved in nanoscale alumina/gelatin nanocomposites as a function of wavelength [350].

2.5.5.3 **Refractive Index Control**

Preparation of clear nanocomposites with refractive indices over the entire range of <1 to >3.9 is possible, and these values are by far the lowest and highest ever achieved for any polymer system. An excellent example of the use of nanoparticles to obtain a specific index of refraction was presented by Zimmerman et al. [351]. They found that the index of refraction scaled closely with the volume fraction of lead sulfide nanoparticles in a gelatin matrix. Indices of refraction as high as 3.9 were obtained [352]. The addition of nanoscale iron sulfide to polyethylene increased the index of refraction to between 2.5 and 2.8 [353].

2.5.5.4 **Light-Emitting Devices**

After the discovery of electroluminescence from conjugated polymer materials (such as PPV), polymer-based light emitting diodes (LEDs) have attracted much attention. The practical advantages for polymer-based LEDs are low cost, low operating voltage, ease of fabrication, and flexibility. Organic light emitting diodes (OLEDs), however, suffer from low quantum efficiency and low environmental stability (against oxidation, etc.).

Functionalization of nanotubes and doping of chemically modified nanotubes in low concentration into photoactive polymers such as PPV can affect the hole-transport mechanism and hence the optical emission of the polymer. Small loadings of nanotubes are used in these polymer systems to tune the color of emitted light from organic LEDs. Although there have been some initial attempts at quantification of nanotube/conducting polymer interactions, little has been done to understand how excitonic

transport in a polymer might be modified by the presence of a high-aspect 1D metal such as a carbon nanotube. Recently, Ago et al. [354] proposed 'hole collecting' properties of multi-wall carbon nanotubes from a conjugated polymer at the composite interfacial region. Such hole collecting properties seem to be common in some conjugated polymers. Specifically, SWNTs in a polymer matrix trap holes injected from the anode in OLEDs [355].

The addition of layered silicates may combat the low quantum efficiency and poor stability to oxygen and moisture of OLEDs [356]. Devices made from organically modified clay and (poly[2-methoxy-5-(2'-ethyl-hexyloxy)-1,4-pheneylenevinylene]) (MEH-PEV) posses an external quantum efficiency 100 times that of the pure polymer (~0.38 % photons/electron) [357]. The composite also shows increased photoluminescence efficiency, due to increased excitation within the two-phase composite.

The addition of equi-axed nanoparticles to electroluminescent polymers also increases current densities, radiances, and power efficiencies. When nanoscale titania and silica were added to MEH-PPV, the current density and light output increased by an order of magnitude at low driving voltages [358]. Lifetime was sacrificed slightly. The explanation for the improvement at low voltages was that the nanoparticles created a high surface area contact with the cathode and thus improved charge injection into the polymer. The improvement at high voltages may be due to the thin regions of MEH-PPV that exist between the nanoparticles. This creates regions of higher current density and thus higher light output. Nanoparticles can also lead to changes in the color of emitters. For example, CdSe/polymer nanocomposites emit blue light [359].

2.5.5.5 Other Optical Activity

The dispersion of metal particles into liquids or polymers leads to interesting absorption spectra that can be controlled by changing the metal used, the particle size, degree of dispersion, and the polydispersity of the particle size [360]. This has provided an impetus to look for new applications of nanocomposites in areas such as optoelectronic devices, nonlinear optical devices, and color filters. In these applications, the metal particle and/or the polymer matrix can be active optical components.

If the particle is the optically functioning component, then the optical properties of the composite material can be tuned by adjusting the particle size and the average separation between particles. The polymer in these situations plays the role of stabilizing the nanoparticles. It is often possible to create ordered arrays (2D or 3D) of nanoparticles in the polymer matrix. This involves size-selective deposition of nanoparticles, as well as surface modification of the particles to prevent agglomeration during processing. An example of a transparent, mechanically stable nanocomposite film is a continuous periodic array of self-assembled thiol-passivated Ag nanocrystals in a polystyrene matrix. The film is formed at an air – water interface by the Langmuir – Blodgett technique. The spatial distribution of particles in the film is altered by changing the thickness of the film. The films so produced have applications in optical filters [361].

The addition of relatively monodisperse silver particles to polyethylene, followed by drawing them into films has led to anisotropic absorption of light and a color that depends on the polarization of incident light [362]. In addition, annealing the com-

posite led to further changes in color, giving and added dimension of control. The silver particles formed pearl-necklace type strings upon drawing, which gave rise to anisotropy. The films were easy to process, strong, and flexible.

Interesting nonlinear optical activity has also been obtained with nanoparticle-filled polymers. For example, by using Cr:forsterite (Cr:Mg_2SiO) in a polymer with a matched index of refraction, relative optical amplification was achieved [343]. Unfortunately, large particles, cracks in the films, and poor coupling to the electronics limited the gain obtained. The authors suggested that cubic materials with isotropic optical properties might be most appropriate for such applications.

The optical limiting behavior of polymer nanocomposites has been investigated, a good example being nanotube filled polymer composites [363]. Polymerization of

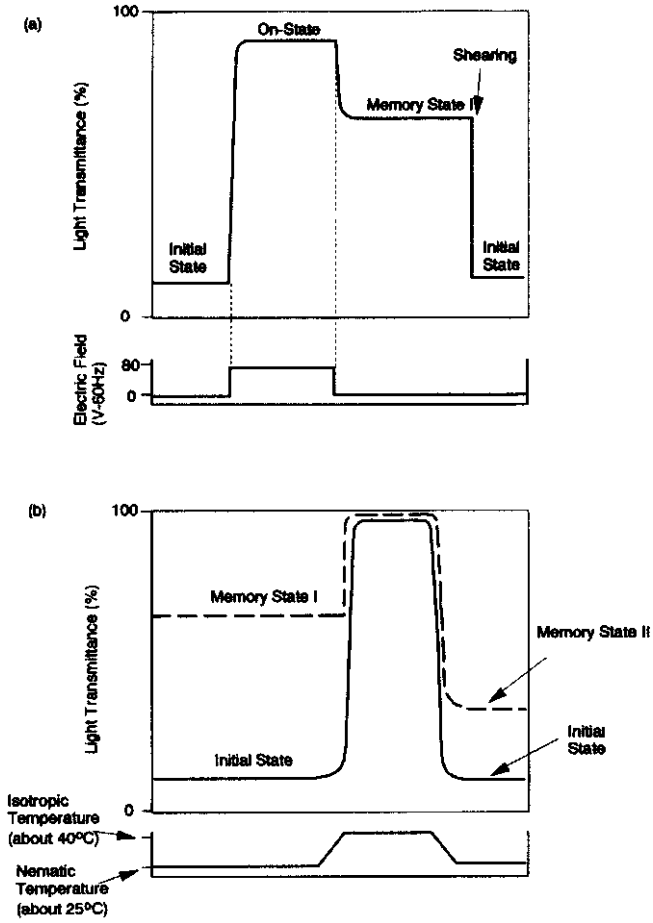

Fig. 2.46 Typical change in transmittance of clay-filled nematic liquid crystals (cell gap 12 μm) due to various fields: (a) electric field and shearing liquid at liquid crystalline temperature (about 25 °C), (b) thermal change. Reprinted with permission from [193]

phenylacetylene in the presence of short nanotubes yields a solvated product of tubules wrapped with poly(phenylacetylene). The optical limiting properties of this composite are excellent and far better than those of the pristine polymer and of polymer filled with other carbon structures. These composites also fare well in photovoltaic applications, suggesting that such nanocomposites could find an array of potential applications in optics-related and laser-based technologies [363].

Liquid crystalline materials have an interesting optical behavior that changes with electric field and with temperature. The addition of intercalated smectic clay to nematic liquid crystals added a memory effect to their behavior [193, 194]. Upon imposition of an electric field, the initially opaque composite became transparent. When the electric field was removed, the composite remained transparent (with a slight decrease in transparency). When heated so as to return to the initial state, the composite instead went into a new state (Memory State II) with light transmittance between that of the initial state and the first memory state (Figure 2.46).

2.6 Summary

The primary purpose of this chapter was to introduce common types of fillers used in nanocomposites, to emphasize the role of the interfacial region, to provide a basic level of understanding of how nanocomposites are currently processed, and to excite the reader about the multifunctional and as yet incompletely explored properties of nanofilled polymers.

Today, our ability to control the structures and properties of nanocomposites is limited only by our current understanding of how to manipulate these nanoscale structures. This area of research will clearly lead to fruitful commercial applications, with significant economic effect, driven by materials with new combinations of properties.

Acknowledgements

Sincere thanks go to the funding agencies that gave me the opportunity to enter this field, including the National Science Foundation, the Office of Naval Research, the Army Natick facility, Eastman Kodak Inc., General Electric, ABB, and Albany International. In addition, sincere thanks to several people for helpful discussions and reviews as well as for contribution of figures: Benjamin J. Ash, Elena Petrovicova, Sanford S. Sternstein, Brian C. Benicewicz, Richard W. Siegel, Keith Nelson, Jung Il Hong, Tao Li, and Quan Chen. In addition, I would like to thank several editors, including Kathy Westbrook, Thomas Feist, Margaret Schadler, and Harvey Schadler.

References

1 A. M. Bueche, J. Polym. Sci., 25, 139 (1957).
2 B. Kuriakose, S. K. De, S. S. Bhagawan, R. Sivaramkrishnan, S. K. Athithan, J. Appl. Polym. Sci., 32, 5509 (1986).
3 M. Sumita, T. Shizuma, K. Miyasaka, K. J. Shikawa, Macromol. Sci., Phys., B22, 601 (1983).
4 P. C. LeBaron, A. Wang, T. J. Pinnavaia, Appl. Clay Sci., 15, 11 (1999).
5 M. Sumita, Y. Tsukumo, K. Miyasaka, K. Ishikawa, J. Mater. Sci., 18, 1758 (1983).
6 P. B. Messersmith, E. P. Giannelis, Chem. Mater., 6, 1719 (1994).
7 P. B. Messersmith, E. P. Giannelis, J. Polym. Sci., Part A: Polym. Chem., 33, 1047 (1995).
8 K. Yano, A. Usuki, A. Okada, T. Kuraychi, O. Kamigaito, J. Polym. Sci., Part A: Polym Chem., 31, 2493 (1993).
9 S. Iijima, Nature, 354, 56 (1991).
10 D. T. Colbert, R. E. Smalley, *Past, Present, and Future of Fullerene Nanotubes: Buckytubes*, Proc. Int. Fullerenes Workshop, Tokyo Japan, February 20–21, 2001, Kluwer, Dordrecht, Netherlands.
11 L. T. Drzal, M. J. Rich, M. F. Koenig, J. Adhes., 16, 133 (1983).
12 R. Bacon, J. Appl. Phys., 31, 283 (1960).
13 T. W. Ebbesen, *Carbon Nanotubes: Preparation and Properties*, CRC Press: Boca Raton, FL, USA, 1997; M. S. Dresselhaus, G. Dresselhaus, P. C. Eklund, *Science of Fullerenes and Carbon Nanotubes*; Academic Press: New York, NY, USA, 1996.
14 P. M. Ajayan, T. W. Ebbesen, Rep. Prog. Phys., 60, 1025 (1997).
15 S. Iijima, T. Ichihashi, Nature, 363, 605 (1993).
16 D. S. Bethune, C. H. Kiang, M. S. de Vires, G. Gorman, R. Savoy, J. Vazquez, R. Beyers, Nature, 363, 605 (1993).
17 J. W. Mintmire, B. I. Dunlap, C. T. Carter, Phys. Rev. Lett., 68, 631 (1992).
18 N. Hamada, S. Sawada, A. Oshiyama, Phys. Rev. Lett., 68, 1579 (1992).
19 D. L. Carroll, P. Redlich, P. M. Ajayan, J.-C.Charlier, X. Blase, A. De Vita, R. Car, Phys. Rev. Lett., 78, 2811 (1997).
20 H. W. Kroto, J. R. Heath, S. C. O'Brien, S. C. Curl, R. E. Smalley, Nature, 318, 162 (1985).
21 M. S. Dresselhaus, G. Dresselhaus, K. Sugihara, I. L. Spain, H. A. Goldberg, *Graphite Fibers and Filaments*, Springer-Verlag, New York, NY, USA, 1988.
22 D. Qian, G. J. Wanger, W. K. Liu, Appl. Mech. Rev., 55, 495 (2002).
23 J.-P. Salvetat, G. A. D. Briggs, J.-M. Bonard, R. R. Bacsa, A. J. Kulik, T. Stockli, N. A. Burnham, L. Forro, Phys. Rev. Lett., 82, 944 (1999).
24 D. A. Walter, L. M. Ericson, M. J. Casavant, J. Liu, D. T. Colbert, K. A. Smith, R. E. Smalley, Appl. Phys. Lett., 74, 3803 (1999).
25 J. R. Wood, M. D. Frogley, E. R. Meurs, A. D. Prins, T. Peijs, D. J. Dunstant, H. D. Wagner, J. Phys. Chem., 103, 10388 (1999).
26 C. M. Leech, Int. J. Mechan. Sci., 44, 621 (2002).
27 M.-F. Yu, B. S. Files, A. Sivaram, R. S. Rodney, Phys. Rev. Lett., 84, 5552 (2000).
28 M.-F. Yu, O. Lourie, M. J. Dyer, K. Moloni, T. F. Kelly, R. S. Ruoff, Science, 287, 637 (2000).
29 H. D. Wagner, O. Lourie, Y. Feldman, R. Tenne, Appl. Phys. Lett., 72, 188 (1998).
30 C. Bower, R. Rosen, L. Jin, J. Han, O. Zhou, Appl. Phys. Lett., 74, 3317 (1999).
31 B. I. Yakabson, C. J. Brabec, J. Bernholc, J. Comput.-Aided Mater. Des., 3, 173 (1996).
32 B. I. Yakabson, Appl. Phys. Lett., 72, 918 (1998).
33 P. M. Ajayan, T. W. Ebbesen, Rep. Prog. Phys., 60, 1025 (1997).
34 J. W. G. Wildoer, L. C. Venema, A. G. Rinzler, R. E. Smalley, C. Dekker, Nature, 391, 59 (1998).
35 M. S. Dresselhaus, G. Dresselhaus, P. C. Eklund, *Science of Fullerenes and Carbon Nanotubes*; Academic Press, New York, NY, USA, 1996.
36 T. W. Ebbesen, *Carbon Nanotubes: Preparation and Properties*, CRC Press, Boca Raton, FL, USA, 1997.
37 R. Andrews, D. Jacques, A. M. Rao, F. Derbyshire, D. X. Qian, E. C. Dickey, J. Chen, Chem. Phys. Lett., 303, 467 (1999).
38 M. J. Bronikowski, P. A. Willis, D. T. Colbert, K. A. Smith, R. E. Smalley, J. Vac. Sci. Technol., 19, 1800 (2001).
39 P. Nikolaev, M. J. Bronikowski, R. K. Bradley, F. Rohmund, D. T. Colbert, A.

Smith, R. E. Smalley, Chem. Phys. Lett. 313, 91 (1999).
40 T. W. Ebbesen, P. M. Ajayan, Nature, 358, 220 (1992).
41 W. Krätschmer, L. D. Lamb, K. Fostiropoulos, D. R. Huffman, Nature, 347, 354 (1990).
42 E. G. Gamaly, T. W. Ebbesen, Phys. Rev. B, 52, 2083 (1995).
43 C. N. R. Rao, R. Sen, B. C. Satishkumar, A. Govindaraj, Chem. Commun., 15, 1525 (1998).
44 C. Niu, E. K. Sichel, R. Hoch, D. Moy, D. H. Tennet, Appl. Phys. Lett. 7, 1480 (1997).
45 Z. J. Zhang, B. Q. Wei, G. Ramanath, P. M. Ajayan, Appl. Phys. Lett., 77, 3764 (2000).
46 W. Z. Li, S. S. Xie, L. X. Qian, B. H. Chang, B. S. Zou, W. Y. Zhou, R. A. Zhao, G. Wang, Science, 274, 1701 (1996).
47 G. Che, B. B. Lakshmi, E. R. Fisher, C. R. Martin, Nature, 393, 346 (1998).
48 C. Journet, W. K. Maser, P. Bernier, A. Loiseau, M. Lamy de la Chappelle, S. Lefrant, P. Deniard, R. Lee, J. E. Fischer, Nature, 388, 756 (1997).
49 A. Thess, R. Lee, P. Nikolaev, H. Dai, P. Petit, J. Robert, C. Xu, Y. H. Lee, S. G. Kim, A. G. Rinzler, D. T. Colbert, G. E. Scuseria, D. Tomanek, J. E. Fischer, R. E. Smalley, Science, 273, 483 (1996).
50 H. Ago, T. Kugler, F. Cacialli, W. R. Salaneck, M. S. P. Shaffer, A. H. Windler, R. H. Friend, J. Phys. Chem. B, 103, 8116 (1999).
51 K. Tohji, H. Takahashi, Y. Shinoda, N. Shimizu, B. Jeyadevan, I. Matsuoka, Y. Saito, A. Kasuya, S. Ito, Y. Nishina, J. Phys. Chem. B, 101, 1974 (1997).
52 G. S. Duesberg, M. Burghard, J. Muster, G. Phillip, S. Roth, Chem. Commun. 3, 435 (1998).
53 S. Curran, A. P. Davey, J. Coleman, A. Dalton, B. McCarthy, S. Maier, A. Drury, D. Gray, M. Brennan, K. Ryder, M. Lamy de la Chapelle, C. Journet, P. Bernier, H. J. Byrne, D. Carrol, P. M. Ajayan, S. Lefrant, W. Blau, Synth. Met., 103, 2559 (1999).
54 A. Eitan, personal communication.
55 T. W. Ebbesen, P. M. Ajayan, H. Hiura, K. Tanigaki, K., Nature, 367, 519 (1993).
56 S. C. Tsang, P. J. F. Harris, M. L. H. Green, Nature, 362, 520 (1993).
57 M. Terrones, N. Grobert, J. Olivares, J. P. Zhang, H. Terrones, K. Kordatos, W. K. Hsu, J. P. Hare, P. D. Townshend, K. Prassides, A. K. Cheetham, H. W. Kroto, Nature, 388, 52 (1997).
58 C. Niu, E. K. Sichel, R. Hoch, D. Moy, H. Tennet, Appl. Phys. Lett. 7, 1480 (1997).
59 J. Liu, A. G. Rinzler, H. Dai, J. H. Hafner, R. K. Bradley, P. J. Boul, A. Lu, T. Iverson, K. Shelimov, C. B. Huffman, F. Rodriguez-Macias, Y. Shon, T. R. Lee, D. T. Colbert, R. E. Smalley, Science, 280, 1253 (1998).
60 R. Tenne, A. K. Zettl, pp. 81 – 109 in *Carbon Nanotubes: Synthesis, Structure, Properties and Applications*, ed M. S. Dresselhaus, G. Dresselhaus, P. Avouris, Springer, New York, NY, USA, 2000.
61 O. Stephan, P. M. Ajayan, C. Colliex, P. Redlich, J. M. Lambert, P. Bernier, P. Lefin, Science, 266, 1683 (1994).
62 X. Blase, J.-C. Charlier, A. de Vita, R. Car, P. Redlich, M. Terrones, W. K. Hsu, H. Terrones, D. L. Carroll, P. M. Ajayan, Phys. Rev.Lett., 83, 5078 (1999).
63 M. Terrones, H. Terrones, N. Grobert, W. K. Hsu, Y. Q. Zhu, H. W. Kroto, D. R. M. Walton, P. Kohler-Redlich, M. Rühle, J. P. Zhang, A. K. Cheetham, Appl. Phys. Lett., 75, 3932 (1999).
64 R. Tenne, Adv. Mater., 7, 965 (1995).
65 P. M. Ajayan, O. Stephan, P. Redlich, C. Colliex, Nature, 375, 564 (1995).
66 G. John, M. Masuda, T. Shimizu, Adv. Mater., 13 (10), 715 (2001).
67 R. A. Vaia, E. P. Giannelis, MRS Bull., 26, 394 (2001).
68 R. E. Grim, *Clay Mineralogy*, 2nd edit., p. 362, McGraw Hill, New York, NY, USA, 1968.
69 Y. Fukushima, S. Inagaki, J. Inclusion Phenom., 5, 473 (1987).
70 A.Okada, A. Usuki, T. Kurauchi, O. Kamigaito, Chapter 6 in *Hybrid Organic – Inorganic Composites*, ed. J. E. Marck, C. Y.-C. Lee, P. A. Bianconi, ACS Symp. series 585.
71 Z. Wang, T. J. Pinnavaia, Chem. Mater., 10, 1820 (1998).
72 W. Schwieger, D. Heidemann, K. H. Bergk, Rev. Chim. Miner., 12, 639 (1985).
73 W. T. Riechle, J. Catal., 94, 547 (1985).
74 P. B. Messersmith, S. I. Stupp, J. Mater. Res., 7, 2599 (1992).

75 C. O. Oriakhi, I. V. Farr, M. Lerner, J. Mater. Chem., 6, 103 (1996).
76 D. Yang, P. Westreich, R. F. Frindt, Nanostruct. Mater., 12, 467 (1999).
77 V. Sanchez, E. Benaventa, M. Angelica Santa Ana, G. Gonzalez, Chem Mater., 11, 2296 (1999).
78 F. R. Gamble, J. H. Osiecki, M. Cais, R. Pisharody, F. J. DiSalvo, T. H. Geballe, Science, 174, 4939 (1971).
79 L. Hernan, P. Lavela, J. Morales, L. Sanchez, J. L. Tirado, J. Mater. Chem. 6, 861 (1996).
80 P. Xiao, M. Xiao, K. Gong, Polymer, 42, 4813 (2001).
81 W. Stober, A. Fink, E. Bohn, J. Colloid Interface Sci., 26, 62 (1968).
82 Dupont Commercial Process, E.I. du Pont de Nemours, Wilmington, DE, USA.
83 P. A. Buining, L. M. Liz-Marzan, A. P. Philipse, J. Colloid and Interface Sci., 179, 318 (1996).
84 M. K. Wu, R. S. Winderler, C. K. R. Steiner, T. Bors, S. K. Friedlander, Aerosol Sci. Technol., 19, 527 (1993).
85 S. K. Friedlander, *Smoke, Dust and Haze: Fundamentals of Aerosol Behavior*, Wiley Interscience, New York, NY, USA. (1977).
86 J. C. M. Marinjnessen, S. Pratsinis, *Synthesis and Measurement of Ultrafine Particles: Proceedings of the International Workshop on the Synthesis and Measurement of Ultrafine Particles*, Delft University Press, Delft, Netherlands (1993).
87 Proc. Joint NSF–NIST Conf. Nanoparticles, May 12–13, 1997, Arlington, VA, USA.
88 S. K. Friedlander, "Synthesis of nanoparticles and their agglomerates," in *R&D Status and Trends*, ed. R. W. Siegel, E. Hu, M. C. Roco, Kluwer, Dordrecht, Netherlands (1998).
89 K. Kimoto, Y. Kamiya, M. Nonoyama, R. Uyeda, Jpn. J. Appl. Phys. 2, 702 (1963).
90 C. G. Granqvist, R. A. Buhrman, J. Appl. Phys., 47, 2200 (1976).
91 Nanophase Technologies Corp., http://www.nanophase.com/
92 H. Gleiter, Prog. Mater. Sci., 33, 223 (1989).
93 R. P. Andres, R. A. Averback, W. L. Brown, L. E. Brus, W. A. Goddard III, A. Kaldor, S. G. Louie, M. Moskovits, P. S. Peercy, S. J. Riley, R. W. Siegel, F. Spaepen, Y. Wang, J. Mater. Res. 4, 704 (1989).
94 R. W. Siegel, Mater. Sci. Technol., 15, 583 (1991).
95 R. W. Siegel, in *Encyclopedia of Applied Physics*, vol 11, ed. G. L. Trigg, VCH, Weinheim, Germany, pp. 173–200 (1994).
96 M. Kato, Jpn. J. Appl. Phys., part 1, 15, 757 (1976).
97 K. Ogawa, T. Vogt, M. Ullman, S. Johnson, S. K. Friedlander, J. Appl. Phys., 87, 63 (2000).
98 G. P. Johnston, R. Muenchausen, D. M. Smith, W. Fahrenholtz, J. Am. Ceram. Soc., 75, 3293 (1992).
99 T. Sasaki, S. Terauchi, N. Koshizaki, H. Umehara, Appl. Surf. Sci., 127, 398 (1998).
100 R. Whitlock, G. Frick, J. Mater. Res., 9, 2868 (1994).
101 E. H. Hu, D. T. Shaw, "Synthesis and Assembly," in *WTEC Panel Report on Nanostructure Science and Technology: R&D Status and Trends in Nanoparticles, Nanostructured Materials, and Nanodevices*, ed. R. W. Siegel, E. Hu, M. C. Roco (1998).
102 J. Hyeon-Lee, G. Beaucage, S. E. Pratsinis, Chem. Mater., 9, 2400 (1997).
103 M. Kishida, T. Fujita, K. Umakoshi, H. Ishiyama, H. Nagata, K. Wakabayashi, Chem. Commun., 763 (1995).
104 F. Grohn, B. J. Bauer, Y. A. Akpalu, C. L. Jackson, E. J. Amis, Macromolecules, 33, 6042 (2000).
105 M. Benaissa, K. E. Gonsalves, S. P. Rangarajan, Appl. Phys. Lett., 71, 3685 (1997).
106 M. P. Pileni, L. Motte, C. Petit, Chem. Mater., 4, 338 (1992).
107 M. Olshavsky, H. R. Allcock, Chem. Mater., 9, 1367 (1997).
108 V. Pillai, P. Kumar, J. J. Hou, P. Ayyub, D. O. Shah, Adv. Colloid Interface Sci., 55, 231 (1995).
109 L. Spahnhel, M. A. Anderson, J. Am. Chem. Soc., 113, 2826 (1991).
110 L. Guo, S. Yang, C. Yang, P. Yu, J. Wang, W. Ge, G. K. L. Wong, Appl. Phys. Lett., 76, 2901 (2000).
111 K. S. Suslick, T. Hyeon, M. Fang, Chem. Mater., 8, 2172 (1996).
112 J. E. Sunstrom IV, W. R. Moser, B. Marshik-Guerts, Chem. Mater., 8, 2061 (1996).
113 J. Mattsson, J. A. Forrest, L. Börjesson, Phys. Rev. E, 62, 5187 (2000).
114 J. L. Keddie, R. A. L. Jones, R. A. Covy, Europhys. Lett., 27, 59 (1994).

115 G. Reiter, Europhys. Lett., 23, 579 (1993).
116 K J. A. Forrest, K. Dalnoki-Veress., J. R. Stevens, J. R. Ducher, Phys. Rev. Lett., 77, 2002 (1996).
117 J. L. Keddie, R. A. L. Jones, R. A. Cory, Faraday Discuss. Chem. Soc. 98, 219 (1994).
118 J. H. van Zanten, W. E. Wallace, W.-L. Wu, Phys. Rev. E., 53 R2053 (1996).
119 K. F. Mansfield, D. N. Theodorou, Macromolecules, 24, 6283, (1991).
120 J. Baschnagel, K. Binder, MRS Symp. Proc., 543, 157 (1999).
121 K. Kendall, F. R. Sherliker, Br. Polym. J., 12, 85 (1980).
122 M. Y. Boluk, H. P. Schreiber, Polym. Compos., 7(5), 295 (1986).
123 W. Hergeth, U. Steinau, H. Bittrich, G. Simon, K. Schmutlzer, Polymer, 30, 254 (1989).
124 G. Tsagaropoulos, A. Eisenberg, Macromolecules, 28, 6067 (1995).
125 X. Zheng, M. H. Rafailovich, J. Sokolov, Y. Strzhemechny, S. A. Schwarz, B. B. Sauer, M. Rubinstein, Phys. Rev. Lett., 79, 241 (1997).
126 J. Zhu, S. S. Sternstein, MRS Symp. Proc., 661, KK4.3.1 (2001).
127 B. J. Ash, J. Stone, D. F. Rogers, L. S. Schadler, R. W. Siegel, B. C. Benicewicz, T. Apple, MRS Symp. Proc., 661, KK2.10.1 (2001).
128 C. Becker, H. Krug, H. Schmidt, MRS Symp. Proc., 435, 237 (1996).
129 C. Becker, P. Mueller, H. Schmidt, SPIE, 3469, 88 (1998).
130 G. Carotenuto, L. Nicolais, X. Kuang, Z. Zhu, Appl. Comp. Mater., 2, 385 (1995).
131 R. Krishnamoorti, R. A. Vaia, E. P. Giannelis, Chem. Mater., 8, 1728 (1996).
132 K. Gautam, A. Dhinojwala, Macro molecules, vol. 34, 1137 (2001).
133 K. Gautam, A. D. Schwab, A. Dhinojwala, D. Zhang, S. M. Dougal, M. S. Yeganeh, Phys. Rev. Lett., 85, 3854 (2000).
134 M. Vacatello, Macromolecules, 34, 1946 (2001).
135 P. Harder, M. Grunze, R. Dahint, G. M. Whitesides, P. E. Laibinis, J. Phys. Chem. B., 102, 426 (1998).
136 T. J. Webster, C. Ergun, R. H. Doremus, R. W. Siegel, R. Bizios, Biomaterials, 21, 1803 (2000).
137 T. J. Webster, C. Ergun, R. H. Doremus, R. W. Siegel, R. Bizios, J. Biomed. Mater. Res., 51, 475 (2000).
138 T. J. Webster, L. S. Schadler, R. W. Siegel, R. Bizios, Tissue Eng., vol. 7, 299–301 (2001).
139 E. Assouline, S. Pohl, R. Fulchiron, J.-F. Gerard, A. Lustiger, H. D. Wagner, G. Marom, Polymer, 41, 7843 (2000).
140 Y. Kojima, A. Usuki, M. Kawasumi, A. Okada, T. Kurauchi, O. Kamigaito, K. Kaji, J. Polym. Sci., Part B: Polym. Phys., 32, 625 (1994).
141 C. Saujanya, S. Radhakrishnan, Polymer, 42, 6723 (2001).
142 E. Petrovicova, R. Knight, L. S. Schadler, T. Twardowski, J. Appl. Polym. Sci., 77, 1684 (2000).
143 F.-D. Kuchta, P. J. Lemstra, A. Kellar, L. F. Batenburg, H. R. Fischer, MRS Symp. Proc., 576, 363 (1999).
144 Y. Kojima, A. Usuki, M. Kawasumi, A. Okada, Y. Fukushima, T. Kurauchi, O. Kamigaito, J. Mater. Res. 8, 1185 (1993).
145 Y. Kojima, T. Matsuoka, H. Takahashi, T. Kurauchi, J. Appl. Polym. Sci. 51, 683 (1994).
146 J. L. Kardos, Trans. NY Acad. Sci., 35, 136 (1973).
147 C. B. Ng, B. J. Ash, L. S. Schadler, R. W. Siegel, Polym. Composites, 10, 101 (2001).
148 D. Qian, E. C. Dicky, R. Andrews, T. Rantell, Appl. Phys. Lett., 76, 2868 (2000).
149 R. W. Siegel, S. K. Chang, B. J. Ash, J. Stone, P. M. Ajayan, R. W. Doremus, L. S. Schadler, Scripta Materialia, 44, 2061 (2001).
150 J. Liu, A. G. Rinzler, H. J. Dai, J. H. Hafner, R. K. Bradley, P. J. Boul, A. Lu, T. Iverson, K. Shelimov, C. B. Huffman, F. Rodriquez-Macias, Y. S. Shon, T. R. Lee, D. T. Colbert, R. E. Smalley, Science, 280, 1253 (1998).
151 J. Chen, M. A. Hamon, H. Hu, Y. Chen, A. M. Rao, P. C. Eklund, R. C. Haddon, Science, 282, 95 (1998).
152 E. T. Mickelson, I. W. Chiang, J. L. Zimmerman, P. J. Boul, J. Lozano, J. Liu, R. E. Smalley, R. H. Hauge, J. L. Margrave, J. Phys. Chem. B., 103, 4318 (1999).
153 P. J. Boul, J. Liu, E. T. Mickelson, C. B. Huffman, L. M. Ericson, I. W. Chiang, K. A. Smith, D. T. Colbert, R. H. Hauge, J. L. Margrave, R. E. Smalley, Chem. Phys. Lett., 310, 367 (1999).

154 K. D. Ausman, R. Piner, O. Lourie, R. S. Ruoff, M. Korobov, J. Phys. Chem. B., 104, 8911 (2000).

155 O. Lourie, D. M. Cox, H. D. Wanger, Phys. Rev. Lett., 81, 1638 (1998).

156 O. Lourie, H. D. Wagner, Comp. Sci. Technol., 59, 975 (1999).

157 O. Lourie, H. D. Wagner, J. Mater. Res., 13, 2418 (1998).

158 O. Lourie, H. D. Wagner, Appl. Phys. Lett., 72(24), 1 (1998).

159 X. Gong, J. Liu, S. Baskaran, R. D. Voise, J. S. Young, Chem. Mater., 12, 1049 (2000).

160 Q. Zhao, J. R. Wood, H. D. Wagner, J. Polym. Sci., Part B: Polym. Phys., 39, 1492 (2001).

161 Z. Jia, Z. Wang, C. Xu, J. Liang, B. Wei, D. Wu, S. Zhu, Mater. Sci. Eng., A271, 395 (1999).

162 L. S. Schadler, S. C. Giannaris, P. M. Ajayan, Appl. Phys. Lett., 73(26), 3842 (1998).

163 J. Scobbo, D. Grimes, T. Lemmen, V. Umamaheswaren, "Conductive thermoplastic resin for electrostatically painted applications," Proc. 1998 SAE Int. Cong. & Exposition (1998).

164 R. Andrews, D. Jacques, A. M. Rao, T. Rantell, F. Derbyshire, Appl. Phys. Lett., 75(9), 1329 (1999).

165 US Patent 2,951,087 (1960).

166 H. Z. Friedlander, Polym. Prepr., 4, 301 (1963).

167 US Patent 4,739007 (19 Apr 1988).

168 A. Okada, A. Usuki, T. Kurauchi, O. Kamigaito, Chapter 6 in *Hybrid Organic–Inorganic Composites*, ed. J. E. Marck, C. Y.-C. Lee, P. A. Bianconi, ACS Symp. series 585.

169 D. C. Lee, L. W. Jan, J. Appl. Polym. Sci., 61, 1117 (1996).

170 S. Bandyopadhyay, A. Hsieh, E. P. Giannelis, in *Polymer Nanocomposites*, ed. R. A. Vaia, R. Krishnamoorti, American Chemical Society, Washington, DC, USA (2001).

171 A. Okada, M. Kawasumi, A. Usuki, K. Yoshitsugu, T. Kurauchi, O. Kamigaito, MRS Symp. Proc., 171, 45 (1990).

172 M. G. Kanatzidis, L. M. Tonge, R. J. Marks, M. O. Marcy, C. R. Kannewurf, J. Am. Chem. Soc., 109, 3797 (1987).

173 M. W. Weiner, H. Chen, E. P. Giannelis, D. Y. Sogan, J. Am. Chem. Soc., 121, 1615 (1999).

174 E. Manias, H. Chen, R. Krishnamoorti, J. Genzer, E. J. Kramer, E. P. Giannelis, Macromolecules, 33, 7955 (2000).

175 J. Y. Lee, A. R. C. Baljon, R. F. Loring, A. Z. Panagiotopoulos, J. Chem. Phys., 102, 10321 (1998); J. Y. Lee, A. R. C. Baljon, R. F. Loring, J. Chem. Phys., 111, 9068 and 9754 (1999).

176 R. Bharadwaj, B. F. Farmer, R. A. Vaia, J. Chem. Phys., in press.

177 V. V. Ginzburg, O. V. Gendelman, L. I. Manevitch, Phys. Rev. Lett., 86, 5073 (2001).

178 R. A. Vaia, E. P. Giannelis, Macromolecules, 30, 8000 (1997).

179 R. A. Vaia, E. P. Giannelis, Macromolecules, 30, 7990 (1997).

180 N. Hasegawa, H. Okamoto, M. Kawasumi, A. Usuki, J. Appl. Poly. Sci., 74, 3359 (1999).

181 J. S. Shelly, P. T. Mather, K. L. DeVries, Polymer, 42, 5849 (2001).

182 A. Usuki, A. Koiwai, Y. Kojima, M. Kawasumi, A. Okada, T. Kurauchi, O. Kamigaito, J. Appl. Polym. Sci., 55, 119 (1995).

183 Y. Kojima, A. Usuki, M. Kawasumi, A. Okada, T. Kurauchi, O. Kamigaito, K. Kaji, J. Polym. Sci., Part B: Polym. Phys., 33, 1039 (1995).

184 M. Okamoto, P. H. Nam, P. Maiti, T. Kotaka, N. Hasegawa, A. Usuki, Nano Lett., 1, 295 (2001).

185 Y. Kojima, A. Usuki, M. Kawasumi, A. Okada, T. Kurauchi, O. Kamigaito, J. Polym. Sci., Part A: Polym. Chem., 31, 983 (1993).

186 L. Liu, A. Qi, X. Zhu, J. Appl. Poly. Sci., 71, 1133 (1999).

187 K. Yano, A. Usuki, A. Okada, T. Kuraychi, O. Kamigaito, Polym. Prepr. (Am. Chem. Soc., Div. Polym. Chem.), 32, 65 (1991).

188 K. Yano, A. Usuki, A. Okada, J. Polym. Sci., Part A: Polym. Chem., 35, 2289 (1997).

189 T. Lan, P. D. Kaviratna, T. J. Pinnavaia, Chem. Mater., 6, 573 (1994).

190 H.-L. Tyan, Y.-C. Liu, K.-H. Wei, Polymer, 40, 4877 (1999).

191 M. Kawasumi, N. Hasegawa, M. Kato, A. Usuki, A. Okada, Macromolecules, 30, 6333 (1997).

192 M. Kato, A. Usuki, A. Okada, J. Appl. Polym. Sci., 66, 1781 (1997).
193 M.Kawasumi, A. Usuki, A. Okada, T. Kurauchi, Mol. Cryst. Liq. Cryst., 281, 91 (1996).
194 M. Kawasumi, N. Hasegawa, A. Usuki, A. Okada, T. Kurauchi, MRS Symp., 425, 311 (1996).
195 D. C. Lee, J. W. Lee, J. Appl. Polym. Sci., 61, 1117 (1996).
196 M. Okamoto, S. Morita, H. Taguchi, Y.H. Kim, T. Kotaka, H. Tateyama, Polymer, 41, 3887 (2000).
197 G. Chen, X. Chen, S. Lin, W. Ye, J. Mater. Sci. Lett., 18, 1761 (1999).
198 X. Fu, S. Qutubuddin, J. Mater. Lett., 42, 12 (2000).
199 F. Dietsche, Y. Thomann, R. Thomann, R. Mulhaupt, J. Appl. Polym. Sci., 75, 396 (2000).
200 X. Fu, S. Qutubuddin, Mater. Lett., 42, 12 (2000).
201 R. Vaia, H. Ishii, E. Giannelis, Chem. Mater., 5, 1694 (1993).
202 T. Lan , T. J. Pinnavaia, Chem. Mater., 6, 2216 (1994).
203 Z. Wang, T. Lan, T. J. Pinnavaia, Chem. Mater., 8, 2200 (1996).
204 J. Massam, T. J. Pinnavaia, MRS Symp. Proc., 20, 223 (1998).
205 I. J. Chin, T. Thurn-Albrecht, H.-C. Kim, T. P. Russell, J. Wang, Polymer, 42, 5947 (2001).
206 T. Lan, P. D. Kaviratna, T. J. Pinnavaia, Chem. Mater., 7, 2144 (1995).
207 Z. Wang, T. J. Pinnavaia, Chem. Mater., 10, 1820 (1998).
208 Z. Wang, T. J. Pinnavaia, Chem. Mater., 10, 3769 (1998).
209 P. Aranda, E. Ruiz-Hitzky, App. Clay Sci., 15, 119 (1999).
210 K. G. Fournaris, M. A. Krakassides, D. Petridis, K. Yiannakopoulou, Chem. Mater., 11, 2372 (1999).
211 W. Chen, Q. Xu, .Z. Yuan, J. Mater. Sci. Lett., 18, 711 (1999).
212 R. A Vaia, S. Vasudevan, W. Krawwiec, L. G. Scanlon, E. P. Giannelis, Adv. Mater., 7, 154 (1995).
213 Y. Kojima, K. Fukumori, A. Usuki, T. Kurauchi, J. Mater. Sci. Lett., 12, 889 (1993).
214 E. N. Kresge, D. J. Lohse, US Patent 5,576,372 (1996).
215 M. Laus, O. Francescangeli, F. Sandrolini, J. Mater. Res., 12, 3134 (1997).
216 S. D. Burnside, E. P. Giannelis, Chem. Mater., 7, 1597 (1995).
217 S. Wang, C. Long, X. Wang, Q. Li, Z. Qi, J. Appl. Poly. Sci., 69, 1557 (1998).
218 Y. Wang, L. Zhang, C. Tan, D. Yu, J. Appl. Polym. Sci., 78, 1879 (2000).
219 C. O. Oriakhi, X. Zhang, M. M. Lerner, Appl. Clay Sci., 15, 109 (1999).
220 X. Huang, S. Lewis, W. J. Brittain, R. A. Vaia, Macromolecules, 33, 2000 (2000).
221 Y. Ke, C. Long, Z. Qi, J. Appl. Poly. Sci., 71, 1139 (1999).
222 Q. Wu, Z. Xue, Z. Qi, F. Wang, Polymer, 41, 2029 (2000).
223 M. Z. Rong, M. Q. Zhang, Y. X. Zheng, H. M. Zeng, K. Friedrich, Polymer, 42, 3301 (2001).
224 J. I. Hong, K. S. Cho, C. I. Chung, L. S. Schadler, R. W. Siegel, J. Mater. Res., 17(5), 940 (2002).
225 L. S. Schadler, personal communication.
226 G. Carotenuto, Y.-S. Her, E. Matijevic, Ind. Eng. Chem. Res., 35, 2929 (1996).
227 F. Yang, Y. Ou, Z. Yu, J. Appl. Poly. Sci., 69, 355 (1998).
228 Y. Ou, F. Yang, Z.-Z. Yu, J. Polym. Sci., Part B: Polym. Phys., 36, 789 (1998).
229 P. Hajji, L. David, J. F. Gerard, H. Kaddami, J. P. Pascault, G. Vigier, MRS Symp. Proc., 576, 357 (1999).
230 B. J. Ash, L. S. Schadler, R. W. Siegel, Polym. Prepr., 42, 52 (2001).
231 Y. Zhang, G. Zhou. L. Li, Y. Zhang, Chin. J. Mater. Res., 12 (1998).
232 M. Avella, M. E. Errico, E. Martuscelli, Nano Lett., 1, 213 (2001).
233 G.-H. Hsiue, W.-J. Kuo, Y.-P. Huang, R.-J. Jen, Polymer, 41, 2813 (2000).
234 S. Wang, M. Wang, Y. Lei, L. Zhang, J. Mater. Sci. Lett., 18, 2009 (1999).
235 P. Judeinstein, C. Sanchez, J. Mater. Chem, 6, 511 (1996).
236 K. A. Mauritz, P. R. Start, Polym. Prepr., 40, 2, 717 (1999).
237 C. J. T. Landry, B. K. Coltrain, M. R. Landry, J. J. Fitzgerald, V. K. Long, Macromolecules, 26, 3702 (1993).
238 S. P. Nunes, K. V. Peinemann, K. Ohlrogge, A. Alpers, M. Keller, A. T. N. Pires, J. Membr. Sci., 157, 219 (1999).

239 K. F. Silveira, I. V. Yoshida, S. P. Nunes, Polymer, 36, 1452 (1995).

240 D. W. McCarthy, J. E. Mark, D. W. Schaeffer, J. Polym. Sci., Part B: Polym. Phys., 36, 1167 (1998).

241 J. M. Breiner, J. E. Mark, G. Beaucage, J. Polym. Sci., Part B: Polym. Phys., 37, 1421 (1999).

242 Y. Wei, D. Yang, L. Tang, M. K. Hutchins, J. Mater. Res., 8, 1143 (1993).

243 B. M. Novak, Adv. Mater., 5, 422 (1993).

244 P. Gomez-Romero, Adv. Mater., 13, 163 (2001).

245 J. J. Senkevich, S. B. Desu, Chem. Mater., 11, 1814 (1999).

246 D. E. Collins, E. B. Slamovich, Chem. Mater., 11, 2319 (1999).

247 J. W. Burdon, P. Calvert, MRS Symp., 218, 203 (1991).

248 C. Saujanya, P. S. Ashamol, S. Radhakrishnan, Polymer, 42, 2255 (2000).

249 S. T. Selvan, T. Hayakawa, M. Nogami, M. Moller, J. Phys. Chem. B., 103, 7441 (1999).

250 A. B. R. Mayer, Mater. Sci. Eng. C,. 6, 155 (1998).

251 A. Roescher, M. Moller, PMSE Prep., 72, 283 (1995).

252 M. Antonietti, E. Wenz, L. M. Bronstein, M. Seregina, Adv. Mater., 7, 1000 (1995).

253 M. Seregina, L. M. Bronstein, O. A. Platonova, D. M. Chernyshov, P. M. Valetsky, E. Wenz, M. Antonietti, Chem. Mater., 9, 923 (1997).

254 M. Antonietti, C. Goltner, Angew. Chem. Int. Ed. Engl., 36, 910 (1997).

255 M. Antonietti, F. Grohn, J. Hartmann, L. Bronstein, Angew. Chem., 109, 2170 (1997).

256 A. B. R. Mayer, J. E. Mark, R. E. Morris, Polym. J., 30, 197 (1998).

257 E. Wenz, M. Antonietti, H. Weller, unpublished

258 U. Kriebig, M. Vollmer, *Optical Properties of Metal Clusters*, Springer-Verlag, Berlin, Germany, 1995.

259 V. M. Rudoy, I. V. Yaminskii, O. V. Dement'eva, V. A. Ogarev, Colloid J., 61, 800 (1999).

260 J. A. Becker, R. Schafer, R. Festag, W. Ruland, J. H. Wendorff, J. Pebler, S. A. Qaiser, W. Helbig, M. T. Reetz, J. Chem. Phys., 103, 2520 (1995).

261 D. L. Carroll, Phys. Rev. Lett., 81, 2332 (1998).

262 X. Blasé, Phys. Rev. Lett., 83, 5078 (1999)

263 R. Czerw, M. Terrones, J.-C. Charlier, X. Blasé, B. Foley, R. Kamalakran, N. Grobert, H. Terrones, D. Tekleab, P. M. Ajayan, W. Blau, W. Ruhle, D. L. Carroll, Nanolett. (2001).

264 A. Eitan, L. S. Schadler, J. Hansen, P. M. Ajayan, R. W. Siegel, M. Terrones, R. Andrews, Proc. Japan – US Conf. Composites Mater., San Jose, CA, USA, September, 2002

265 A. Eitan, K. Jiang, R. Andrews, L. S. Schadler, submitted Chem. Mater. (2002).

266 K. Jiang, A. Eitan, L. S. Schadler, P. M. Ajayan, R. W. Siegel, N. Grobert, M. Mayne, M. Reyes-Reyes, H. Terrones, M. Terrones, submitted Nano Lett. (2002)

267 J. Chen. M. A. Hamon, H. Hu, Y. Chen, A. M. Rao, P. R. Eklund, R. C. Haddon, Science, 282, 95 (1998).

268 C. N. R Rao, A. Govindaraj, B. C. Satishkumar, Chem. Commun., 1525 (1996).

269 S. S. Wong, E. Joselvich, A. T. Woolley, C. L. Cheung, C. M. Lieber, Nature, 394, 52 (1998).

270 J. Liu, A. G. Rinzler, H. Dai, J. Hafner, R. K. Bradley, P. Boul, A. Lu, T. Iverson, K. Shelimov, C. B. Huffman, F. Rodriquez-Macias, Y.-S. Shon, T. R. Lee, D. T. Colbert, R. E. Smalley, Science, 280, 1253 (1998).

271 J. L. Bahr, J. Yang, D. V. Kosynkin, M. J. Bronikowski, R. E. Smalley, J. M. Tour, J. Am. Chem. Soc., 123, 6536 (2001).

272 E. T. Mickelson, I. W. Chiang, J. L. Zimmerman, P. J. Boul, J. Lozano, J. Liu, R. E. Smalley, R. H. Hauge, J. L. Margrave, J. Phys. Chem. B, 103, 4318 (1999).

273 P. Allongue, M. Delamar, B. Desbat, O. Fagebaume, R. Hitmi, J. Pinson, J.-M. Salvetat, J. Am. Chem. Soc., 119, 201 (1997).

274 B. Ortiz, C. Saby., G. Y. Champagne, D. Belanger, J. Electroanal. Chem., 455, 75 (1998).

275 J. Chen, A. M. Rao, S. Lyuksyutov, M. E. Itkis, M. A. Hamon, H. Hu, R. W. Cohn, P. C. Eklund, D. T. Colbert, R. E. Smalley, R. C. Haddon, J. Phys. Chem. B, 105, 2525 (2001).

276 J.-M. Bonnard, T. Stora, J.-P. Salvetat, F. Maier, T. Stockli, C. Duschl, L. Forro, W. A.

De Herr, A. Chatelain, Adv. Mater., 9, 827 (1997).
277 A. Koshio, M. Yudaska, M. Zhang, S. Iijima, Nanolett. (2001).
278 Q. Chen, L. Dia, M. Gao, S. Huang, A. Mau, J. Phys. Chem. B., 105, 618 (2001).
279 J. Chen, M. A. Hamon, H. Hu, Y. Chen, A. M. Rao, P. C. Eklund, R. C. Haddon, Science, 282, 95 (1998).
280 R. J. Chen, Y. Zhang, D. Wang, H. Dai, J. Am. Chem. Soc., 123, 3838 (2001).
281 R. Czerw, Z. Guo, P. M. Ajayan, Y.-P. Sun, D. L. Carroll, Nano Lett. (2001).
282 F. Caruso, Adv. Mater., 13, 11 (2001).
283 O. Makarova, T. Rajh, M. C. Thurnauer, A. Martin, P. A. Kemme, D. Cropek, Environ. Sci. Technol., 34, 4797 (2000).
284 T. Konovalova, L. D. Kispert, V. V. Konovalov, J. Phys. Chem. B, 103 4672 (1999).
285 Paul Braun, personal communication
286 J. Wang, S. Kara, T. E. Long, T. C. Ward, J. Polym. Sci., Part A: Polym. Chem., 38, 3742 (2000).
287 C. H. M. Hofman-Caris, New. J. Chem., 18, 1087 (1994).
288 L. Quaroni, G. Chumanov, J. Am. Chem. Soc., 121, 10642 (1999).
289 N. Tsubokawa, A. Kogure, K. Maruyama, Y. Sone, M. Shimomura, Polym. J., 22, 827 (1990).
290 M. Z. Rong, M. Q. Zhang, Y. X. Zheng, H. M. Zeng, R. Walter, K. Friedrich, Polymer, 42, 167 (2001).
291 Y. Mao, B. M. Fung, Chem. Mater., 10, 509 (1998).
292 T. VonWerne, T. E. Patten, J. Am. Chem. Soc., 121, 7409 (1999).
293 F. Caruso, Chem. Eur. J., 6, 413 (2000).
294 O. Kalinina, E. Kumacheva, Macromolecules, 32, 4122 (1999).
295 M. Ohmori, E. Matijevic, J. Colloid Interface Sci., 150, 594 (1992).
296 H. Giesche, E. Matijevic, J. Mater. Res., 9, 436 (1994).
297 A. Hanprasopwattana, S. Srinivasan, A. G. Sault, A. K. Datye, Langmuir, 12, 3173 (1996).
298 R. Partch, Y. Xie, S. T. Oyama, E. Matijevic, J. Mater. Res., 8, 2014 (1993).
299 R. C. Stephenson, R. E. Partch, Proc. Mater. Res. Soc., 458, 435 (1996).
300 N.A. Dhas, A. Zaban, A. Gedanken, Chem. Mater., 11, 806 (1999).
301 C. Brinson, personal communication.
302 R. M. Christensen, *Mechanics of Composite Materials*, reprinted by Krieger, Malabar, FL, USA (1991), orig. pub. Wiley, New York, NY, USA (1979).
303 A.Oya, Y. Kurokawa, H. Yasuda, J. Mater. Sci., 35, 1045 (2000).
304 N. Hasegawa, H. Okamoto, M. Kato, A. Usuki, J. Appl. Polym. Sci., 78, 1918 (2000).
305 Y. T. Lim, O. O. Park, Macromol. Rapid Commun., 21, 231 (2000).
306 H. Shi, T. Lan, T. J. Pinnavaia, Chem. Mater., 8, 1584 (1996).
307 N. Hasegawa, M. Kawasumi, M. Kato, A. Usuki, A. Okada, J. Appl. Polym. Sci., 67, 87 (1998).
308 T. Agag, T. Koga, T. Takeichi, Polymer, 42, 3399 (2001).
309 C. B. Bucknall, "Deformation mechanisms in rubber-toughened polymers" in *Polymer Blends, Vol. 2: Performance*, ed D. R. Paul, C. B. Bucknall. Wiley, New York, NY, USA (2000).
310 S. Wu, Polymer, 26, 1855 (1985).
311 J. M. Gloagun, J. M. Lefebvre, Polymer, 42, 5841 (2001).
312 T.-K. Chen, Y.-I. Tien, K. Wei, Polymer, 41, 1345 (2000).
313 D. B. Zax, D.-K. Yang, R. A. Santos, H. Hegemann, E. P. Giannelis, E. Manias, J. Chem. Phys., 112, 2945 (2000).
314 E. Hackett, E. Manias, E. P. Giannelis, Chem. Mater., 12, 2161 (2000); M. R. Nyden, J. Gilman, Comp. Theor. Polym. Sci., 7, 191 (1997).
315 D. Cole, K. R. Shull, P. Baldo, L. Rehn, Macromolecules, 32, 771 (1999).
316 B. J. Ash, L. S. Schadler, R. W. Siegel, Mater. Lett., 53, 83–87 (2002).
317 R. Krishnamoorti, E. P. Giannelis, Macromolecules, 30, 4097 (1997).
318 S. S. Sternstein, A.-J. Zhu, Macromolecules, 35, 7262 (2002).
319 E. Petrovicova, R. Knight, L. S. Schadler, T. Twardowski, J. Appl. Polym. Sci., 78, 2272 (2000).
320 Q. Wang, J. Xu, S. Weichang, Q. Xue, Wear, 209, 316 (1997).
321 Q. Wang, J. Xu, S. Weichang, Tribology Int., 30, 193 (1997).
322 Q. Wang, Q. Xue, H. Liu, S. Weichang, J. Xu, Wear, 198, 216 (1996).

323 Q. Wang, J. Xu, S. Weichang, L. Weimin, Wear, 196, 82 (1996).
324 D. E. George, J. S. Bloom, T. P. Feist, US Patent 5,789,523 (1996).
325 L. Nielsen, J. Macromol. Sci. Chem., A1, 929 (1967).
326 E. L. Cussler, S. E. Hughes, W. J. Ward III, R. Aris, J. Membr. Sci., 38, 161 (1988).
327 Modern Plastics, February, 1998.
328 Y. Kojimoto, A. Usuki, M. Kawasumi, A. Okada, T. Kurauchi, O. Kamigaito, J. Appl. Poly. Sci., vol. 49, 1259-1264 (1993).
329 Modern Plastics, February, 1999.
330 Y. Kojima, A. Usuki, M. Kawasumi, A. Okada, T. Kurauchi, O. Kamigaito, J. Appl. Polym. Sci., 49, 1259 (1993).
331 G. Kraus, *Reinforcement of Elastomers*, Interscience, New York, NY, USA (1965).
332 S. S. Sternstein, J. Macromol. Sci., Phys., B6/1, 243 (1972).
333 N. Salahuddin, M. Shehata, Polymer, 42, 8379 (2001).
334 A. Blumstein, J. Polym. Sci., Part A: Polym. Chem., 3, 2665 (1965).
335 J. Lee, E. Giannelis, Polym. Prepr., 38, 688 (1997).
336 J. Gilman, T. Kashiwagi, J. Lichtenhan, SAMPE J., 33, 40 (1997).
337 J. Gilman, T. Kashiwagi, J. E. T. Brown, S. Lomakin, "Flammability studies of polymer layered silicate nanocomposites", Proc. 43rd Int. SAMPE Symp., 1053 (1998).
338 J. Gilman, Appl. Clay Sci., 15, 31 (1999).
339 S. Bourbigot, M. Le Bras, F. Dabrowski, "Intumescence and polymer blending: an approach for flame retardancy?" Proc. Annu. Conf. Fire Res., NISTIR 6242, 43 (1998).
340 H. Inoue, T. Hosokawa, Japanese Patent JP 10 81,510 (98 81,510) (1998).
341 R. A. Vaia, G. Price, P. N. Ruth, H. T. Nguyen, J. Lichtenhan, Appl. Clay Sci., 15, 67 (1999).
342 H. Fong, R. A. Vaia, J. H. Sanders, D. Lincoln, P. J. John, A. J. Vreugdenhil, J. Bultman, C. A. Cerbus, H. G. Jeon, Polym. Prepr., 42, 354 (2001).
343 D. Barber, C. R. Pollock, L. L. Beecroft, C. K. Ober, Opt. Lett., 22, 1247 (1997).
344 J. I. Hong, L. S. Schadler, E. Martensson, personal communication.
345 H. Sabuni, J.K. Nelson, J. Mater. Sci., 11, 1574 (1976).
346 S. M. H. Sabuni, J. K. Nelson, J. Mater. Sci., 14, 2791 (1979).
347 J. Coleman, A. Dalton, S. Curran, A. Rubio, A. Davey, A. Drury, B. McCarthy, B. Lahr, P. Ajayan, S. Roth, R. Barklie, W. Blau. Adv. Mater., 12, 213 (2000).
348 C. Brinker, E. Giannelis, R. Laine, C, Sanchez (ed), *Hybrid Materials*, Proc. MRS Symp. Proc. Series, 519 (1999).
349 M. Kerker, *The Scattering of Light*, Academic, New York, NY, USA (1969), p. 414.
350 T. Li, Q. Chen, L. S. Schadler, R. W. Siegel, J. Mendel, G. C. Irvin, Polym. Composites, in press.
351 L. Zimmerman, M. Weibel, W. Caseri, U. Suter, J. Mater. Res., 8, 1742 (1993).
352 T. Kyprianidou-Leodidou, W. Caseri, U. W. Suter, J. Phys. Chem., 98, 8992 (1994).
353 T. Kyprianidou-Leodidou, H.-J. Althaus, Y. Wyser, D. Vetter, M. Buchler, W. Caseri, U. W. Suter, J. Mater. Res., 12, 2198 (1997).
354 H. Ago, M. S. P. Shaffer, D. S. Ginger, A. H. Windle, R. H. Friend, Phys. Rev. B, 61, 2286 (2000).
355 H. S. Woo, R. Czerw, S. Webster, D. L. Carroll, J. Ballato, A. E. Strevens, D. O'Brien, W. J. Blau, Appl. Phys. Lett., 77, 1393 (2000).
356 C. O. Oriahkhi, X. Zhang, M. M. Lerner, Appl. Clay Sci., 15, 109 (1999).
357 T.-W. Lee, O. O. Park, J. Yoon, J.-J. Kim, Adv. Mater., 13, 211 (2001).
358 S. A. Carter, J. C. Scott, P. J. Brock, Appl. Phys. Lett., 71, 1145 (1997).
359 B. A. Dabbousi, M. G. Bawendi, O. Onitduka, M. F. Rubner, Appl. Phys. Lett., 66, 1316 (1996).
360 F. Zimmerman, A. Wokaun, Mol. Phys., 73, 959 (1991).
361 M. Lin, D. G. Ast, Adv. Mater., 13, 719, 2001.
362 Y. Dirix, C. Bastiaansen, W. Caseri, P. Smith, J. Mater. Sci., 34 3859 (1999).
363 B. Z. Tang, H. Xu, Macromolecules, 32, 2569 (1999).